Spring 5-2021

Lateral Torsional Buckling Resistance of Continuous Steel Stringers in Existing Bridges

Dinesha Malky Kuruppuarachchi Kuruppuarachchi Appuhamilage Don

LATERAL TORSIONAL BUCKLING RESISTANCE OF CONTINUOUS STEEL STRINGERS IN EXISTING BRIDGES

by

Kuruppuarachchi Appuhamilage Don
Dinesha Malky Kuruppuarachchi, B.S., M.S.

A Dissertation Presented in Partial Fulfillment
of the Requirements of the Degree
Doctor of Philosophy

COLLEGE OF ENGINEERING AND SCIENCE
LOUISIANA TECH UNIVERSITY

May 2021

LOUISIANA TECH UNIVERSITY

GRADUATE SCHOOL

January 29, 2021
Date of dissertation defense

We hereby recommend that the dissertation prepared by

Kuruppuarachchi Appuhamilage Don Dinesha Malky Kuruppuarachchi, B.S., M.S.

entitled **LATERAL TORSIONAL BUCKLING RESISTANCE OF CONTINUOUS STEEL STRINGERS IN EXISTING BRIDGES**

be accepted in partial fulfillment of the requirements for the degree of

Doctor of Philosophy in Engineering, Materials & Infrastructure Systems Conc.

C. Shawn Sun
Supervisor of Dissertation Research

Jay Xingran Wang
Head of Engineering

Doctoral Committee Members:
Jay Xingran Wang
Shaurav Alam
John C. Matthews
Elizabeth Matthews

Approved:

Hisham Hegab
Dean of Engineering & Science

Approved:

Ramu Ramachandran
Dean of the Graduate School

GS Form 13a
(01/20)

ABSTRACT

Some of the Louisiana's bridges built in the 1950s and 1960s used two-girder or truss systems, in which floorbeams are carried by main members and the continuous (spliced) stringers are supported by the floorbeams. The main members are either two edge (fascia) girders or trusses. When the flexural capacity of continuous stringers is calculated, the moment gradient factor (C_b) is not accurately calculated considering the lateral torsional buckling (LTB) at the negative moment section. In particular, the bracing effect of the non-composite concrete deck is not accounted for, and as a result, the current practice has underestimated the LTB strength of continuous stringers significantly, which would cause either expensive bridge rehabilitation or unnecessary bridge postings. This dissertation presents the re-assessment of methodology behind flexural capacity of continuous stringers with the effort focusing on more realistic values for C_b. Theoretical solution and finite element analyses were addressed to examine C_b in continuous stringers. The analysis results were also calibrated using the lab testing data. Recommendations were provided on how to determine C_b more accurately and load rate the continuous stringers more reasonably.

Chapter 1 presents a literature review including various codes and specifications, and relevant work by several researchers. Chapter 2 addresses a theoretical solution for the LTB resistance of continuous stringers. Chapter 3 illustrates the finite element analyses of the continuous stringers accounting for various bracing conditions and load

cases. Chapter 4 addresses the lab testing findings and discusses the bracing effect due to various types of bracings, including the intermediate steel diaphragms, timber ties, and non-composite concrete deck. Chapter 5 presents the conclusions and recommendations on load ratings of continuous stringers with non-composite deck.

APPROVAL FOR SCHOLARLY DISSEMINATION

The author grants to the Prescott Memorial Library of Louisiana Tech University the right to reproduce, by appropriate methods, upon request, any or all portions of this Dissertation. It is understood that "proper request" consists of the agreement, on the part of the requesting party, that said reproduction is for his personal use and that subsequent reproduction will not occur without written approval of the author of this Dissertation. Further, any portions of the Dissertation used in books, papers, and other works must be appropriately referenced to this Dissertation.

Finally, the author of this Dissertation reserves the right to publish freely, in the literature, at any time, any or all portions of this Dissertation.

Author _Kuruppuarachchi Appuhamilage Don Dinesha Malky Kuruppuarachchi__

Date _____4/19/2021_____

DEDICATION

To my parents

TABLE OF CONTENTS

LIST OF FIGURES

LIST OF TABLES

ACKNOWLEDGMENTS

First and foremost, I wish to express my gratitude to my supervisor, Dr. Shawn Sun, for his constant support, advice, and encouragement during the entire time of this research. I consider myself very fortunate to have studied under his supervision. A special thank you goes to Dr. Daniel Linzell and Dr. Jay Puckett for their leadership and guidance in performing lab testing at the University of Nebraska-Lincoln. Furthermore, I am deeply grateful to Dr. Jay Wang for his interest in my subject and his ideas during the progress of my research. I would specially like to thank Dr. Shaurav Alam for his continuous support and motivation. I am grateful to Dr. John Matthews for his encouragement and guidance. Furthermore, I would like to thank Dr. Elizabeth Matthews for her much appreciated input. Special thanks go to Dr. Ramu Ramachandran and Dr. Collin Wick for their leadership during the course of my study.

I am grateful to my colleagues Tobi and Nahid for making this research possible. Thank you for your support, friendship and encouragement during that challenging time. I would also like to thank to Greta, Shams Arafat, Yemi, Arafat, Roksana, Sevda, Ishani and Christy for their moral support, friendship, and all the memories we have shared. Finally, my biggest gratitude goes to my parents, siblings, and their family, and whole extended family for always being there for me.

CHAPTER 1

INTRODUCTION

Some of the bridges in Louisiana built in the 1950s and 1960s used two-girder or truss systems, in which the main members carried floorbeams, and the floorbeams supported continuous (spliced) I-stringers. The main members are either two edge (fascia) girders **Figure 1-1** or trusses **Figure 1-2**.

The focus of this research is on flexural capacity of continuous stringers using a non-composite concrete deck. In accordance with American Association of State Highway Officials (AASHTO) LRFD Bridge Design Specifications (AASHTO LRFD Specifications) [1], when the flexural resistance of an I-beam is determined, both local buckling and LTB are accounted for. LTB of the continuous stringers often controls the flexural strength when bridges are load rated. The AASHTO LRFD Specifications provide LTB resistance derived for uniform major-axis bending moment. A moment gradient factor, C_b, is applied to account for the effects of variable moment along an unbraced length. The LTB resistance is capped at F_{max} or M_{max}, as illustrated by the dashed line in **Figure 1-3**, R_n is given by the following equation, where F_{nc} represents the nominal flexural resistance of a member:

$$F_{nc} = C_b \left[1 - \left(1 - \frac{F_{yr}}{R_h F_{yc}}\right)\left(\frac{L_b - L_p}{L_r - L_p}\right)\right] R_b R_h F_{yc} \leq R_b R_h F_{yc} \qquad \textbf{Eq. 1-1}$$

As shown in this equation, C_b directly affects the flexural strength of the stringer. As specified in AASHTO LRFD Specifications Appendix A6 [1], when flexural resistance of non-composite I-sections is calculated, the contribution from the concrete deck and longitudinal reinforcement is neglected at the negative moment section. This underestimates the flexural capacity of the continuous stringer. The objective of this research is to re-assess the flexural strength of a continuous stringer with a non-composite deck and propose a reasonable approach to determine C_b.

Figure 1-1: Sample floor system, edge girder

Figure 1-2: Sample floor system, truss

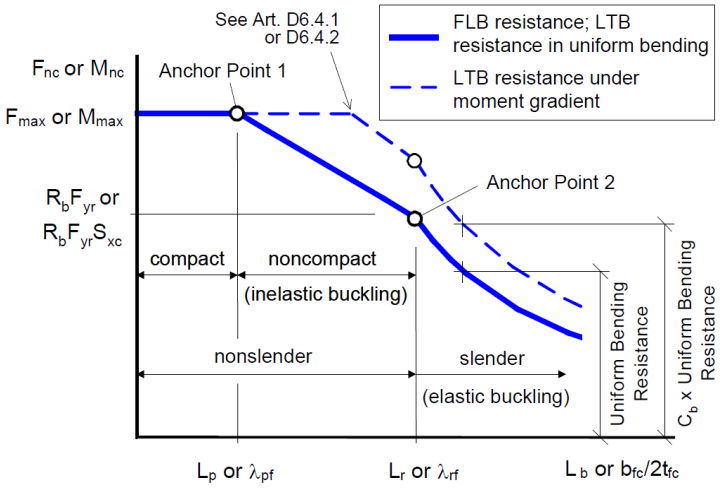

Figure 1-3: Basic form of I-section compression-flange flexural resistance equations [1]

This chapter presents a literature review of C_b in accordance with a variety of codes and specifications. Also presented is the significant work by several researchers. In addition, there are reference summaries on the bracing effect of the bridge decks.

1.1 Moment Gradient Factor

The focus of this research is related to I-shaped stringers having doubly symmetric sections and primarily subject to vertical loading. Several significant references associated with the development of C_b and lateral bracing provided by bridge decks are discussed herein. A number of specifications and codes are presented, including the *AASHTO LRFD Bridge Design Specifications*, the *AISC Steel Construction Manual*, the *Canadian Highway Bridge Design Code*, the *Australian Steel Code*, the *British Standards Structural Use of Steelwork in Building*, and the *Japanese Standard Specifications for Steel and Composite Structures*. In addition, works by several significant researchers are included. Each section presents relevant background

discussions and equations for the moment gradient factor followed by definitions of the primary parameters.

1.1.1 AASHTO LRFD Bridge Design Specifications, Seventh Edition, 2014 [1]

The LTB resistance equations in the *AASHTO LRFD Bridge Design Specifications* provide predictions close to mean LTB resistances from uniform bending experimental tests conducted by Galambos and Ravindra in 1978 [2]. For members subject to a moment gradient, the factor is included primarily following research work performed by Salvadori [3]. For continuous stringers supported by floorbeams, C_b can be greater than 1.0 using **Eq. 1-2.**

$$C_b = 1.75 - 1.05\left(\frac{f_1}{f_2}\right) + 0.3\left(\frac{f_1}{f_2}\right)^2 \leq 2.3 \qquad \textbf{Eq. 1-2}$$

where

f_1 = stress without consideration of lateral bending at the brace point opposite to the one corresponding to f_2, calculated as the intercept of the most critical assumed linear stress variation passing through f_2 and either f_{mid} or f_0, whichever produces the smaller value of C_b. When variations in the moment along the entire length between the brace points are concave in shape, then $f_1 = f_0$; otherwise, $f_1 = 2f_{mid} - f_2 \geq f_0$.

f_2 = largest compressive stress without consideration of lateral bending at either end of the unbraced length of the flange under consideration, calculated from the critical moment envelope value. Due to the factored loads, f_2 shall be positive. If the stress is zero or the tensile in the flange under consideration at both ends of the unbraced length, f_2 is zero.

1.1.2 AISC Steel Construction Manual, 2016 [4]

The *AISC Steel Construction Manual* provides the lateral-torsional buckling modification factor, C_b, for non-uniform moment diagrams primarily based on the research work by Kirby and Nethercot with slight modifications [5]. C_b is determined as follows:

$$C_b = \frac{12.5M_{max}}{2.5M_{max} + 3M_A + 4M_B + 3M_c} \quad \textbf{Eq. 1-3}$$

where

M_{max} = the absolute value of maximum moment in the unbraced segment;

M_A = the absolute value of moment at the quarter point of the unbraced segment;

M_B = the absolute value of moment at the center of the unbraced segment; and

M_C = the absolute value of moment at the three-quarter point of the unbraced segment.

1.1.3 Canadian Highway Bridge Design Code, S6-14 [6]

In accordance with the *Canadian Highway Bridge Design Code*, structural sections shall be designated as Class 1, 2, 3, or 4, depending on width-to-thickness ratios of the elements that make up the cross-section and on loading conditions. A Class 1 section is one that will attain the plastic moment capacity, adjusted for the presence of axial force if necessary, and permit subsequent redistribution of bending moment. A Class 2 section is one that will attain the plastic moment capacity, adjusted for the presence of axial force if necessary, but not necessarily permit subsequent moment redistribution. A Class 3 section is one that will attain the yield moment capacity, adjusted for the presence of axial force if necessary. A Class 4 section is one in which the slenderness of the elements making up the cross-section exceeds the limits of Class 3.

The moment gradient factor is calculated as:

$$w_2 = \frac{4M_{max}}{\sqrt{M_{max}^2 + 4M_a^2 + 7M_b^2 + 4M_c^2}} \leq 2.5 \qquad \textbf{Eq. 1-4}$$

where

M_{max} = maximum absolute value of factored moment in the unbraced segment;

M_a = factored bending moment at one-quarter point of the unbraced segment;

M_b = factored bending moment at midpoint of the unbraced segment; and

M_c = factored bending moment at three-quarter point of the unbraced segment.

1.1.4 Australian Steel Code AS4100 [7]

AS4100 provides **Eq. 1-5** to determine an equivalent uniform moment factor or moment modification factor, α_m, for stringers where β is the ratio of the two end moments. It also allows simple approximation using **Eq. 1-6** that applies to any bending moment distribution:

$$\alpha_m = 1.75 + 1.05\beta + 0.3\beta^2 \leq 2.5 \qquad \textbf{Eq. 1-5}$$

$$\alpha_m = \frac{1.7M_m}{\sqrt{(M_2)^2 + (M_3)^2 + (M_4)^2}} \leq 2.5 \qquad \textbf{Eq. 1-6}$$

where

M_m = maximum design bending moment;

M_2, M_4 = design bending moments at the quarter points; and

M_3 = design bending moment at the midpoint of the segment.

1.1.5 British Standards Institution (BSI), Structural Use of Steelwork in Building, BS 5950-1:2000 [8]

In the British code, the moment gradient factor of I-stringers with equal flanges should satisfy the following:

$$m_{LT} = 0.2 + \frac{0.15M_2 + 0.5M_3 + 0.15M_4}{M_{max}} \geq 0.44 \qquad \textbf{Eq. 1-7}$$

Where, all moments are taken as positive. The moment M_2 and M_4 are the values at the quarter points, M_3 is the value at mid-length and M_{max} is the maximum moment in the segment.

1.1.6 Research by Lopez et al. [9]

Lopez et al. proposed a closed form expression for the equivalent uniform moment factor, C_1, applicable to any moment distribution. The proposed formula incorporates end support conditions through a parameter related to the lateral torsional buckling length of the stringer. For a general moment diagram, the coefficient C_1 may be obtained by:

$$C_1 = \frac{\sqrt{\sqrt{k}A_1 + \left[\frac{(1-\sqrt{k})A_2}{2}\right]^2} + \frac{(1-\sqrt{k})A_2}{2}}{A_1} \qquad \textbf{Eq. 1-8}$$

where

k depends on the lateral bending and warping condition coefficients k_1 and k_2 :

$$k = \sqrt{k_1 k_2} \qquad \textbf{Eq. 1-9}$$

and A_1 and A_2 are given by:

$$A_1 = \frac{M_{max}^2 + \alpha_1 M_1^2 + \alpha_2 M_2^2 + \alpha_3 M_3^2 + \alpha_4 M_4^2 + \alpha_5 M_5^2}{(1 + \alpha_1 + \alpha_2 + \alpha_3 + \alpha_4 + \alpha_5) M_{max}^2} \qquad \textbf{Eq. 1-10}$$

$$A_2 = \left|\frac{M_1 + 2M_2 + 3M_3 + 2M_4 + M_5}{9M_{max}}\right| \qquad \textbf{Eq. 1-11}$$

where

$$\alpha_1 = 1 - k_2; \quad \alpha_2 = 5\frac{k_1^3}{k_2^2}\ ; \quad \alpha_3 = 5\left(\frac{1}{k_1} + \frac{1}{k_2}\right)\ ;$$

$$\alpha_4 = 5\frac{k_2^3}{k_1^2}\ ;\ \alpha_5 = 1 - k_1 \qquad \textbf{Eq. 1-12}$$

In **Eq. 1-10** and **Eq. 1-11**, M_{max} is the maximum moment, and M_1, M_2, M_3, M_4, and M_5 are the values of the moment at different sections of the stringer, each of them with the corresponding sign.

1.1.7 Research by Subramanian and White [10]

The LTB curves in AASHTO and AISC are based in large part on unified provisions proposed by White [11], which were in turn based largely on experimental data compiled by White and Jung [12] and White and Kim [13]. A recent study by Subramanian *et al*. demonstrated that rolled I-stringers may exhibit an inelastic C_b effect. This essentially means that, when the inelastic LTB strength is scaled by the modification factor C_b (where C_b is developed based on elastic buckling formulations), strength estimates tend to be higher than the true inelastic LTB strength under a moment gradient. Subramanian *et al*. concluded that when the maximum moment in a span occurs at a braced location, the proposed LTB model for uniform moment, along with current handling of C_b in the AASHTO and AISC, is satisfactory, and no modifications were proposed for such cases. When the maximum moment occurs within an unbraced segment of the stringer, the current AISC specification moment modifier in the inelastic LTB region could be as much as 20% un-conservative. The SABRE2 computational tool was developed to implicitly and rigorously capture moment gradient effects based on applied loading as well as any unbraced length end-restraint effects.

1.1.8 Research by Helwig et al. [14]

Helwig *et al*. suggested multiplying the original equation for C_b from Kirby and Nethercot [5] by the terms $1.4^{2y/h}$ to account for the effects of load height within the cross-section and by R to account for the effects of I-section monosymmetry and reverse curvature bending in prismatic members. The term $1.4^{2y/h}$ considers destabilizing or the tipping effect of the loads applied transversely to the top flange, or the stabilizing or the restoring effect of loads applied transversely to the bottom flange. If one or more intermediate braces are provided within an ordinary or cantilever span in which the ends are prevented from twisting, the load height effects do not need to be considered in the calculation of C_b:

$$C_b = \frac{12.5M_{max}}{2.5M_{max} + 3M_A + 4M_B + 3M_c}\left(1.4^{2y/h}\right)R \qquad \textbf{Eq. 1-13}$$

where

M_{max} = the absolute value of the maximum moment within the unbraced length;

M_A, M_B, and M_C = the absolute values of the moments at the 1/4, middle, and 3/4 points of the unbraced segment;

y = the distance from the mid-depth of the cross section to the point of the load application, which is taken as negative for downward loads applied above mid-depth and positive for downward loads applied below mid-depth;

h = the distance between the compression and tension flange centroids; and

R = 1.0 for beams with single-curvature bending.

For reverse-curvature bending,

$$R = 0.5 + 2\left(\frac{I_{y\,Top}}{I_y}\right)^2 \qquad \textbf{Eq. 1-14}$$

where

$I_{y\,Top}$ = moment of inertia of the top flange on an axis in the plane of the web; and

I_y = moment of inertia of the entire section about an axis in the plane of the web.

1.1.9 Research by Salvadori [15]

Beginning with the 1961 AISC Manual and continuing through the 1986 AASHTO LRFD Specifications, **Eq. 1-15** was used to adjust lateral-torsional buckling equations for variations in the moment diagram within an unbraced length:

$$C_b = 1.75 + 1.05\left(\frac{M_1}{M_2}\right) + 0.3\left(\frac{M_1}{M_2}\right)^2 \leq 2.3 \qquad \textbf{Eq. 1-15}$$

where

M_1 = smaller moment at end of unbraced lengths;

M_2 = larger moment at end of unbraced lengths; and

(M_1/M_2) is positive when moments cause reverse curvature and negative for single curvature.

1.1.10 Research by Wong and Driver [16]

Wong and Driver reviewed several approaches and recommended the following quarter-point equation for use with doubly symmetric I-shaped members:

$$C_b = \frac{4M_{max}}{\sqrt{{M_{max}}^2 + 4{M_A}^2 + 7{M_B}^2 + 4{M_c}^2}} \qquad \textbf{Eq. 1-16}$$

The equation gives improved predictions for several important cases, including cases with moderately nonlinear moment diagrams. Also, the length between braces, not the distance to inflection points, is used in all cases.

1.1.11 Research by Yura and Helwig [17] [18]

Many situations arise where a stringer is subjected to reverse curvature bending with one of the flanges continuously braced laterally by closely spaced joists and/or light gauge decking normally used for roofing or flooring systems. Although this type of lateral bracing provides significant restraint to one of the flanges, the other flange can still buckle laterally due to compression caused by the reverse curvature bending. For gravity loaded, rolled I–section stringers with the top flange laterally restrained, the following expression is applicable:

$$C_b = 3.0 - \frac{2}{3}\left(\frac{M_1}{M_0}\right) - \frac{8}{3}\left[\frac{M_{CL}}{(M_1 + M_0)^*}\right] \qquad \textbf{Eq. 1-17}$$

where

M_0 = moment at the end of the unbraced length that gives the largest compressive stress in the bottom flange;

M_1 = moment at the other end of the unbraced length;

M_{CL}= moment at the middle of the unbraced length; and

$(M_0 + M_1)^* = M_0$, if M_1 is positive, causing tension on the bottom flange.

1.1.12 Research Findings in Other References [19] to [53]

Additional references on the flexural strength accounting for lateral torsional buckling and moment gradient factor were studied. Because the research findings in these publications are similar or comparable to those listed above, they are not described individually for brevity.

1.2 Lateral Bracing Effect of Bridge Decks

Bracing members are commonly classified as torsional (diaphragms or cross frames) or lateral (top chord, upper and lower laterals or bridge decks). Both tests and

theoretical solutions have shown that cross section distortion has a significant effect on torsional brace effectiveness [54]. A bridge deck has the potential to act as a lateral and/or torsional brace. The friction that may be mobilized at the deck-stringer interface acts as a lateral brace because it restrains lateral movement of the stringer top flange. A number of researchers concluded that even if there is no mechanical connection between the deck and the stringers, friction may still be adequate to develop the required deck stiffness to act as a lateral brace at the contact area of the wheel load. Therefore, if a stringer is non-composite and it is subject to positive moment, it might be considered laterally supported at the wheel load location near the mid-span [55].

A full-size test on a five-girder short-span bridge conducted by Yura *et al*. showed that timber decks not positively attached to the stringers can provide lateral bracing at wheel load locations through friction [56]. Common timber decks have enough lateral bracing stiffness to permit the stringers to reach yield without buckling. It can be inferred that concrete decks provide greater lateral stiffness and have better friction resistance than timber decks.

Kissane completed another study of bracing effects provided by bridge decks for the New York State Department of Transportation in 1985 [57]. The objective was to determine the effectiveness of a non-composite concrete bridge deck as a lateral brace for the compression flange of the supporting stringers without any positive shear connections. To complete the comparison, we conducted tests where the physical or chemical bond between the concrete deck and the stringers was intentionally eliminated. Kissane concluded that friction resistance between the concrete deck and the stringers was sufficient to use the deck as a brace and allow the stringers to reach their full bending

capacity without buckling laterally. In addition, Linzell *et al*. conducted field-testing of a riveted through-girder bridge in Pennsylvania and identified unintended composite action under live loads [58].

When a stringer is made composite with a concrete deck slab or the top flange is fully embedded in the deck slab, the top flange is considered to be fully braced if the subject is connected to the positive moment (compression on top), and therefore, LTB is not applicable. In the negative moment region, the bottom flange of the stringers is in compression and shall be evaluated for LTB resistance. In past practices, points of contra flexure sometimes have been considered as the brace points when the influence of moment gradient is not included in LTB resistance equations. However, this practice sometimes can lead to a substantially un-conservative estimate of the flexural resistance [1]. The influence of moment gradient may be correctly accounted for using C_b and the effect of restraint from adjacent unbraced segments may be accounted for by using an effective length factor less than 1.0. Multiple researchers have proposed using a braced column monograph as an acceptable analogy for obtaining the effective length of the critical stringer [58, 59].

CHAPTER 2

THEORY BACKGROUND

This chapter presents the theory background of steel beams' LTB resistance. It summarizes different approaches of solving the LTB problem, including the finite difference method (FDM). Several studies have been conducted to evaluate the LTB of simple-span beams and different loading cases. This chapter discusses a theoretical solution for C_b for continuous beams and addresses a comparison with the existing methods.

Prandtl and Mitchell developed the first documentation about LTB in 1899, accounting for a thin rectangular cross section. Timoshenko included the effect of warping to Prandtl's work in 1905, and introduced a fourth order differential equation for LTB in 1961 [60] (See **Eq. 2-1**).

$$EC_w \frac{d^4\Phi}{dz^4} - \frac{GJd^2\Phi}{dz^2} - \frac{{M_o}^2\Phi}{EI_y} = 0 \qquad \textbf{Eq. 2-1}$$

where

E - modulus of elasticity

G - shear modulus

C_w - warping constant

M_o - bending moment in strong axis

J - torsional constant

I_y - moment of inertia in weak axis

Φ - twisting angle

LTB is affected by material properties (shear modulus and Young's modulus), cross-section properties (torsional constant, warping constant, second moment of inertia about weak axis), geometric properties (unbraced length of the beam), boundary conditions, load type (distributed versus concentrated loads) and point of load application (top flange, shear center, bottom flange, etc.). LTB is likely to occur when the torsional stiffness (GI_t), warping stiffness(EI_w), and flexural stiffness in weak axes are low. A larger unbraced length and a higher loading position along the beam height (e.g., beam top flange) also increase the risk of LTB. **Eq. 2-1** is based on the following assumptions [61]:

1. Beam has no initial geometric imperfections or residual stresses.
2. The beam is within the linear elastic range and has no distortion in the cross section while loading.
3. Load acts in plane of the web.

2.1 Finite Difference Method for Simple Beam

Suryaatmono *et al.* (2002) [62] investigated the use of FDM considering a few load cases using a simple-span beam. **Figure 2-1** shows a beam subjected to a constant bending moment *(M_o)*. Since the top flange of the beam is in compression, it tends to displace laterally and rotate with a twisting angle of Φ. The major axis is indicated in the x-direction and the minor axis in the y-direction.

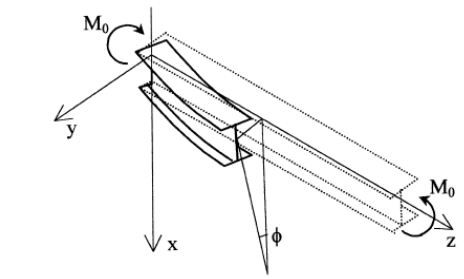

Figure 2-1: LTB for a simple-span beam [63]

2.1.1 Taylor Series

As shown in **Figure 2-2**, a beam is divided into n discrete segments where the nodes are indexed from 0 to n. Δz (= L/n) is the distance between adjacent grid points. A fourth order differential equation can be transformed to a first order differential equation by using Taylor series. In this study, the first term of the Taylor series of each derivative is used (See **Eq. 2-2** to **Eq. 2-5**).

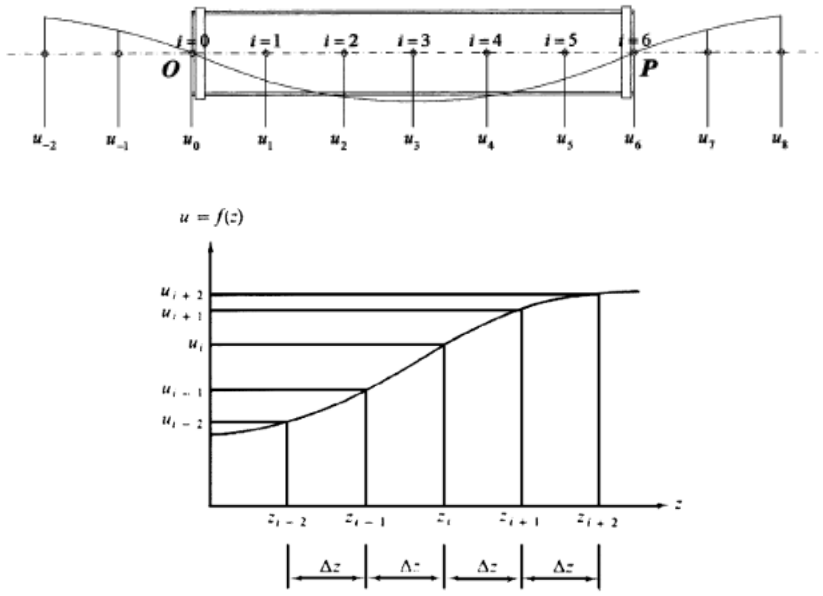

Figure 2-2: Equally spaced grid points in finite difference approximation [62]

$$\Phi_i' = \frac{1}{2\Delta z}(-\Phi_{i-1} + \Phi_{i+1}) \quad \textbf{Eq. 2-2}$$

$$\Phi_i'' = \frac{1}{\Delta z^2}(\Phi_{i-1} - 2\Phi_i + \Phi_{i+1}) \quad \textbf{Eq. 2-3}$$

$$\Phi_i''' = \frac{1}{2\Delta z^3}(-\Phi_{i-2} + 2\Phi_{i-1} - 2\Phi_{i+1} + \Phi_{i+2}) \quad \textbf{Eq. 2-4}$$

$$\Phi_i'''' = \frac{1}{\Delta z^4}(\Phi_{i-2} - 4\Phi_{i-1} + 6\Phi_i - 4\Phi_{i+1} + \Phi_{i+2}) \quad \textbf{Eq. 2-5}$$

The transformed equation of **Eq. 2-1** is as follows:

$$\frac{EC_w}{\Delta z^4}(\Phi_{i-2} - 4\Phi_{i-1} + 6\Phi_i - 4\Phi_{i+1} + \Phi_{i+2}) + \frac{GJ}{\Delta z^2}(\Phi_{i-1} - 2\Phi_i + \Phi_{i+1}) + \frac{{M_o}^2}{EI_y}\Phi_i = 0 \quad \textbf{Eq. 2-6}$$

2.1.2 Boundary Conditions

Figure 2-3 shows boundary conditions for simply supported, warping fixed, lateral bending fixed, and completely fixed conditions [64]. Timoshenko equation is created for simply supported case

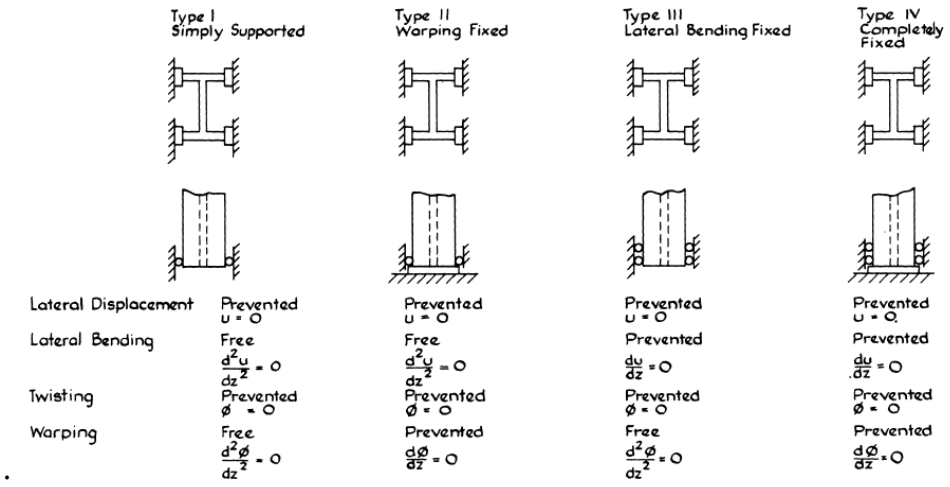

Figure 2-3: Boundary conditions [64]

Using Taylor series these boundary conditions can be written as below

$$\Phi = 0 \rightarrow \Phi_i = 0 \qquad \textbf{Eq. 2-7}$$

$$\frac{d^2\Phi}{dz^2} = 0 \ \rightarrow \ \Phi_{i-1} - 2\Phi_i + \Phi_{i+1} = 0 \qquad \textbf{Eq. 2-8}$$

$$\frac{d\Phi}{dz} = 0 \ \rightarrow -\Phi_{i-1} + \Phi_{i+1} = 0 \qquad \textbf{Eq. 2-9}$$

2.1.3 Creating a Matrix

For example, if a beam has five grid points (i = 1,2,3,4 and 5), equations for each node can be written as below. Boundary conditions introduce two equations at the beginning and the ending nodes. There are nine unknowns and nine equations can solve this matrix. Large number of nodes are suggested to achieve accurate results.

$i=1 \rightarrow \Phi_1 = 0$ **Eq. 2-10**

$i=1 \rightarrow \Phi_0 - 2\Phi_1 + \Phi_2 = 0$ **Eq. 2-11**

$i=1 \rightarrow \frac{EC_w}{\Delta z^4}(\Phi_{-1} - 4\Phi_0 + 6\Phi_1 - 4\Phi_2 + \Phi_3) + \frac{GJ}{\Delta z^2}(\Phi_0 - 2\Phi_1 + \Phi_2) + \frac{{M_o}^2}{EI_y}\Phi_1 = 0$ **Eq. 2-12**

$i=2 \rightarrow \frac{EC_w}{\Delta z^4}(\Phi_0 - 4\Phi_1 + 6\Phi_2 - 4\Phi_3 + \Phi_4) + \frac{GJ}{\Delta z^2}(\Phi_1 - 2\Phi_2 + \Phi_3) + \frac{{M_o}^2}{EI_y}\Phi_2 = 0$ **Eq. 2-13**

$i=3 \rightarrow \frac{EC_w}{\Delta z^4}(\Phi_1 - 4\Phi_2 + 6\Phi_3 - 4\Phi_4 + \Phi_5) + \frac{GJ}{\Delta z^2}(\Phi_2 - 2\Phi_3 + \Phi_4) + \frac{{M_o}^2}{EI_y}\Phi_3 = 0$ **Eq. 2-14**

$i=4 \rightarrow \frac{EC_w}{\Delta z^4}(\Phi_2 - 4\Phi_3 + 6\Phi_4 - 4\Phi_5 + \Phi_6) + \frac{GJ}{\Delta z^2}(\Phi_3 - 2\Phi_4 + \Phi_5) + \frac{{M_o}^2}{EI_y}\Phi_4 = 0$ **Eq. 2-15**

$i=5 \rightarrow \frac{EC_w}{\Delta z^4}(\Phi_3 - 4\Phi_4 + 6\Phi_5 - 4\Phi_6 + \Phi_7) + \frac{GJ}{\Delta z^2}(\Phi_4 - 2\Phi_5 + \Phi_6) + \frac{{M_o}^2}{EI_y}\Phi_5 = 0$ **Eq. 2-16**

$i=5 \rightarrow \Phi_4 - 2\Phi_5 + \Phi_6 = 0$ **Eq. 2-17**

$i=5 \rightarrow \Phi_5 = 0$ **Eq. 2-18**

2.1.4 Smallest Positive Eigenvalue λ

The matrix is created by rearranging nodes and simplifying boundary conditions according to Kaminski *et al.* (2016) [65]. In this example, five nodes (n =5) are used for

the simply supported beam. All the elements are located on the main diagonal of the matrix. The smallest positive eigenvalue (λ) that derives from **Eq. 2-19** corresponds to the critical buckling moment or force, depending on the load case.

$$[A-\lambda I]\,\Phi = 0 \qquad \textbf{Eq. 2-19}$$

Constant Moment

Matrix A is written for a simple span subjected to a constant moment. λ is the unknown, and M is the critical buckling moment. Simple support boundary condition is applied.

$$A = \begin{pmatrix} 6EIw/\Delta x^4+2GIt/\Delta x^2 & -4EIw/\Delta x^4-GIt/\Delta x^2 & EIw/\Delta x^4 & & & \\ -4EIw/\Delta x^4-GIt/\Delta x^2 & 6EIw/\Delta x^4+2GIt/\Delta x^2 & -4EIw/\Delta x^4-GIt/\Delta x^2 & EIw/\Delta x^4 & \dots & 0 \\ EIw/\Delta x^4 & -4EIw/\Delta x^4-GIt/\Delta x^2 & 6EIw/\Delta x^4+2GI/\Delta x^2 & -4EIw/\Delta x^4-GIt/\Delta x^2 & EIw/\Delta x^4 & \\ \dots & & \dots & & \dots & \\ & EIw/\Delta x^4 & -4EIw/\Delta x^4-GIt/\Delta x^2 & 6EIw/\Delta x^4+2GIt/\Delta x^2 & -4EIw/\Delta x^4-GIt/\Delta x^2 & EIw/\Delta x^4 \\ 0 & \dots & EIw/\Delta x^4 & -4EIw/\Delta x^4-GIt/\Delta x^2 & 6EIw/\Delta x^4+2GIt/\Delta x^2 & -4EIw/\Delta x^4-GIt/\Delta x^2 \\ & & & EIw/\Delta x^4 & -4EIw/\Delta x^4-GIt/\Delta x^2 & nEIw/\Delta x^4+2GIt \end{pmatrix}$$

$$\lambda = \frac{M^2}{EI_y} \qquad \textbf{Eq. 2-20}$$

Point Load at Midspan

Matrix B is written for a beam subjected to a point load at the midspan. Simple support boundary conditions are applied. λ is arranged in a way that P, critical buckling load, is the only unknown variable (See **Eq. 2-21 and 2-22**). The first half of the span is shown in **Eq. 2-23,** and the other half of the span is shown in **Eq. 2-24** because the bending moment diagram consists of two lines with two slopes. Hence, there is a need for two equations:

$$\Phi[B-\lambda I] = 0 \qquad \textbf{Eq. 2-21}$$

$$\lambda = \frac{P^2}{EI_y} \qquad \textbf{Eq. 2-22}$$

$0 \le z < L/2$ $$\frac{EC_w d^4\Phi}{dz^4} - \frac{GJd^2\Phi}{dz^2} - \frac{(Pz/2)^2\Phi}{EI_y} = 0$$ **Eq. 2-23**

$L/2 \le z \le L$ $$\frac{EC_w d^4\Phi}{dz^4} - \frac{GJd^2\Phi}{dz^2} - \frac{(\frac{P(L-z)}{2})^2\Phi}{EI_y} = 0$$ **Eq. 2-24**

$$B = \begin{bmatrix} \frac{5EIw/\Delta x4+2GIt/\Delta x2}{z^2} & \frac{4EIw/\Delta x4-GIt/\Delta x2}{z^2} & \frac{EIw/\Delta x4}{z^2} & & & & & & \\ \frac{-4EIw/\Delta x4-GIt/\Delta x2}{z^2} & \frac{6EIw/\Delta x4+2GIt/\Delta x2}{z^2} & \frac{4EIw/\Delta x4-GIt/\Delta x2}{z^2} & \frac{EIw/\Delta x4}{z^2} & & 0 & & & \\ \frac{EIw/\Delta x4}{z^2} & \frac{-4EIw/\Delta x4-GIt/\Delta x2}{z^2} & \frac{6EIw/\Delta x4+2GIt/\Delta x2}{z^2} & \frac{4EIw/\Delta x4-GIt/\Delta x2}{z^2} & \frac{EIw/\Delta x4}{z^2} & & & & \\ & \cdots & & \cdots & & \cdots & & & \\ & \frac{EIw/\Delta x4}{(z-L/2)^2} & \frac{-4EIw/\Delta x4-GIt/\Delta x2}{(z-L/2)^2} & \frac{6EIw/\Delta x4+2GIt/\Delta x2}{(z-L/2)^2} & \frac{4EIw/\Delta x4-GIt/\Delta x2}{(z-L/2)^2} & \frac{EIw/\Delta x4}{(z-L/2)^2} & & & \\ 0 & \frac{EIw/\Delta x4}{(z-L/2)^2} & \frac{-4EIw/\Delta x4-GIt/\Delta x2}{(z-L/2)^2} & \frac{6EIw/\Delta x4+2GIt/\Delta x2}{(z-L/2)^2} & \frac{4EIw/\Delta x4-GIt/\Delta x2}{(z-L/2)^2} & & & & \\ & & \frac{EIw/\Delta x4}{(z-L/2)^2} & \frac{-4EIw/\Delta x4-GIt/\Delta x2}{(z-L/2)^2} & \frac{5EIw/\Delta x4+2GIt/\Delta x2}{(z-L/2)^2} & & & & \end{bmatrix}$$

2.1.5 MatLab Solution

For example, a W16 x31 beam is considered. The span length varied from 12ft to 24ft. Following the steps above, a matrix is created for this beam assuming simply supported and subjected to a uniform moment. The solution is compared with **Eq. 2-25**, which is the smallest moment that satisfies Timoshenko equation (**Eq. 2-1**).

$$M_{ocr} = \frac{\pi}{L}\sqrt{EI_yGJ + (\frac{\pi E}{L})^2 I_y C_w}$$ **Eq. 2-25**

Figure 2-4 shows that Timoshenko solution and FDM solution are in good agreement, which validates the developed Matlab [66] codes and allow the codes to be upgraded for other cases. **Figure 2-4** also shows the buckling moment variation when a point load is applied at the mid-span of a beam.

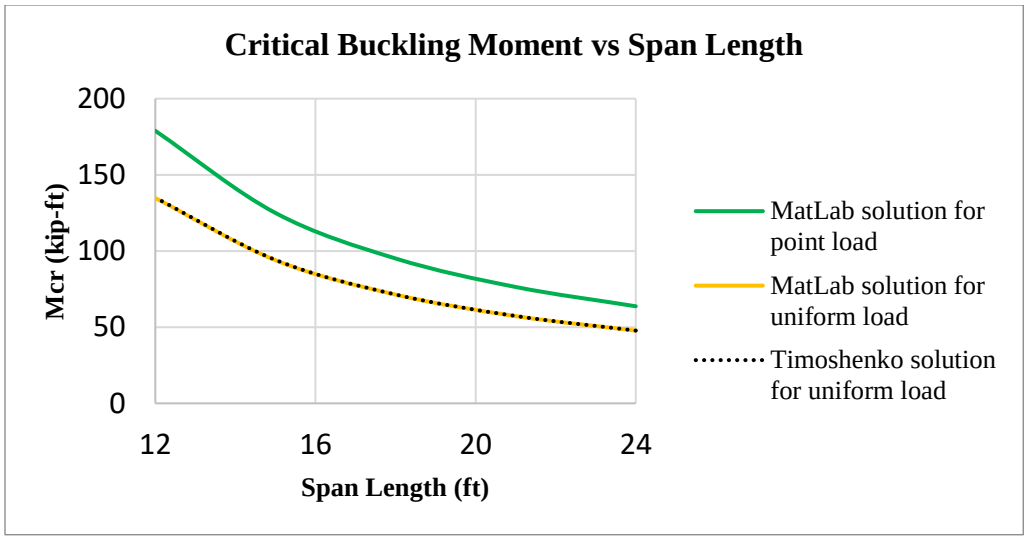

Figure 2-4: Critical buckling moment vs. span length

2.2 Finite Difference Method for Continuous Beam

2.2.1 Boundary Condition

At the interior support, when there is no steel diaphragm bracing, lateral deflection curves of adjacent spans have the same tangent. When the steel diaphragms are present at the interior supports the web restraints twisting, but flanges are free to warp. (See **Figure 2-3** -Type 3). Boundary conditions for continuous beam are as follow:

$$\Phi = 0 \rightarrow \Phi_i = 0 \qquad \textbf{Eq. 2-26}$$

$$\frac{d^2\Phi}{dz^2} = 0 \ \rightarrow \ \Phi_{i-1} - 2\Phi_i + \Phi_{i+1} = 0 \qquad \textbf{Eq. 2-27}$$

2.2.2 One Span Loaded Case

Moment diagram is presented in **Figure 2-6** and Matrix is shown in **Appendix B**. Beam is loaded at one span only; therefore, the equations are as follows:

$0 \leq z < L/2$ $$\frac{EC_w d^4\Phi}{dz^4} - \frac{GJd^2\Phi}{dz^2} - \frac{(\frac{13Pz}{32})^2\Phi}{EI_y} = 0 \qquad \textbf{Eq. 2-28}$$

L/2 ≤ z < L $$\frac{EC_w d^4\Phi}{dz^4} - \frac{GJd^2\Phi}{dz^2} - \frac{[P\frac{13z}{32} - P\left(z-\frac{L}{2}\right)]^2\Phi}{EI_y} = 0$$ **Eq. 2-29**

L ≤ z ≤ 2L $$\frac{EC_w \mathrm{d}^4\Phi}{\mathrm{dz}^4} - \frac{GJ\mathrm{d}^2\Phi}{\mathrm{dz}^2} - \frac{[P\frac{13z}{32} - P\left(z-\frac{L}{2}\right) + \frac{22}{32}P(z-L)]^2\Phi}{EI_y} = 0$$ **Eq. 2-30**

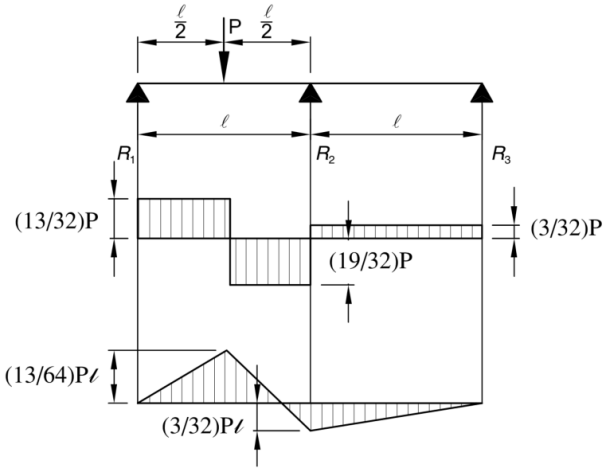

Figure 2-5: A continuous beam with one span loaded

2.2.3 Two Spans Loaded Case

When a continuous beam is loaded at both spans, the equations are updated as follows:

0 ≤ z < L/2 $$\frac{EC_w d^4\Phi}{dz^4} - \frac{GJd^2\Phi}{dz^2} - \frac{(\frac{5}{16}Pz)^2\Phi}{EI_y} = 0$$ **Eq. 2-31**

L/2 ≤ z < L $$\frac{EC_w \mathrm{d}^4\Phi}{\mathrm{dz}^4} - \frac{GJ\mathrm{d}^2\Phi}{\mathrm{dz}^2} - \frac{[P\frac{5}{16}z - P(z-\frac{L}{2})]^2\Phi}{EI_y} = 0$$ **Eq. 2-32**

L ≤ z < 3L/2 $$\frac{EC_w \mathrm{d}^4\Phi}{\mathrm{dz}^4} - \frac{GJ\mathrm{d}^2\Phi}{\mathrm{dz}^2} - \frac{[\mathrm{P}\frac{5}{16}\mathrm{z} - \mathrm{P}\left(\mathrm{z}-\frac{\mathrm{L}}{2}\right) + \mathrm{P}\frac{11}{8}(\mathrm{z}-\mathrm{L})]^2\Phi}{EI_y} = 0$$ **Eq. 2-33**

3L/2 ≤ z < 2L $$\frac{EC_w \mathrm{d}^4\Phi}{\mathrm{dz}^4} - \frac{GJ\mathrm{d}^2\Phi}{\mathrm{dz}^2} - \frac{[\mathrm{P}\frac{5}{16}\mathrm{z} - \mathrm{P}\left(\mathrm{z}-\frac{\mathrm{L}}{2}\right) + \mathrm{P}\frac{11}{8}(\mathrm{z}-\mathrm{L}) - \mathrm{P}\left(\mathrm{z}-\frac{3\mathrm{L}}{2}\right)]^2\Phi}{EI_y} = 0$$ **Eq. 2-34**

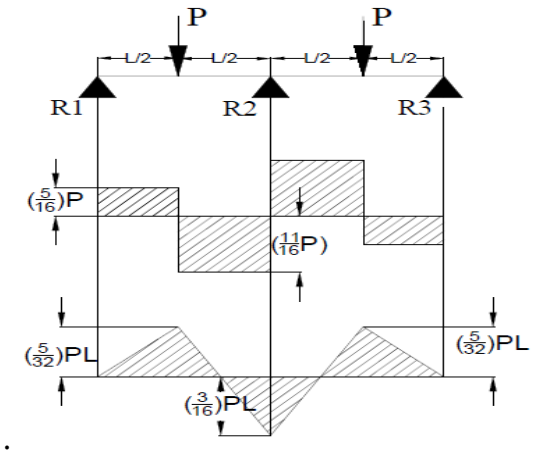

Figure 2-6: A continuous beam with both spans loaded

2.2.4 Numerical Example

For discussion purpose, a two-span continuous beam is analyzed and the analysis results using the FDM are compared with the AASHTO, AISC, and lab test data. The following assumptions are made:

Beam type = W 16 x 31	Torsional constant (I_t) = 0.461 in^4
Modulus elasticity (E) = 29000 ksi	Span length (L) = 288 in
Warping constant (I_w) = 739 in^6	Minor axis inertia (I_y) = 12.4 in^4
Shear modulus (G) = 11154 ksi	

Figure 2-7 and **Figure 2-8** presents buckled shapes from FDM solution. In **Figure 2-8**, "S"-shape is shown for illustration. Another mode can be determined similarly. Lab testing [67] is discussed in Chapter 3. Results of two test runs that include lateral bracing by steel diaphragms (Test Run #19 (one span loaded) and Test Run #20 (two spans loaded)) are presented for comparison purpose. The predicated LTB resistance according to AASHTO, AISC, and lab testing consider point of load application as the beam's top flange. However, FDM considers point of load application

to be beam's shear center. Therefore, FDM results are converted to top flange loading position for comparison purpose.

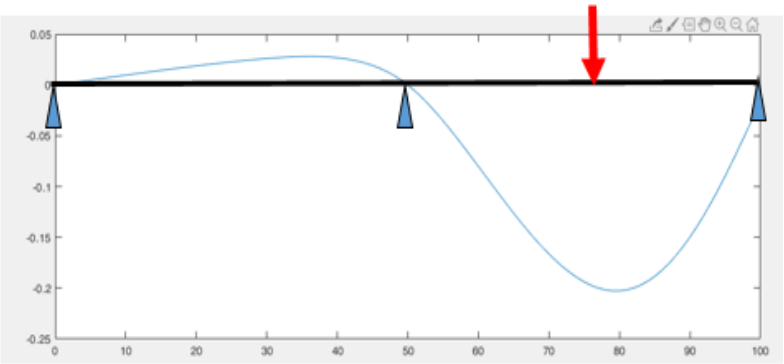

Figure 2-7: Buckled shape: one span loaded

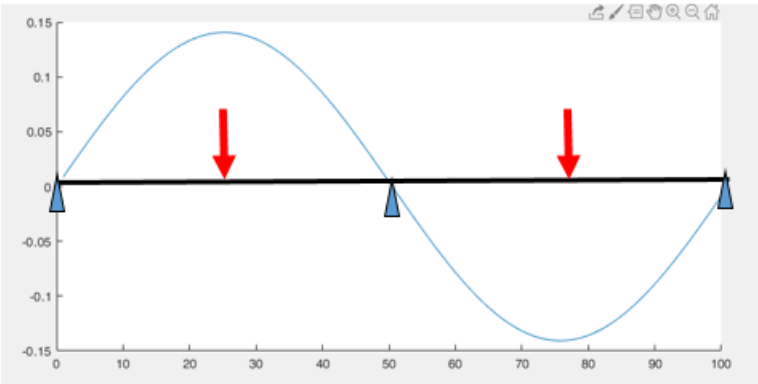

Figure 2-8: Buckled shape: two spans loaded

Figure 2-9 illustrates critical buckling moment for continuous span bridge subjected to a point load at the midspan. The predicted buckling moment values from the FDM are higher than the test data. This difference is attributed to the fact that FDM did not account for geometry imperfections, and residual stresses. C_b in AASHTO and AISC codes are presented in **Eq. 1-1** and **Eq. 1-2** respectively. The resultant C_b is multiplied by **Eq. 2-25** to find critical buckling moments (M_{cr}) that are shown **Figure 2-10**. The FDM results for one span and both spans loaded are multiplied by 0.714 to count for the

loading position. [14]. **Table 2-1** shows C_b results of all cases. FDM results shows a higher critical moment for one span loaded case, and a lower critical moment for two span loaded case. In two span loaded case, FDM results show a "S" buckled shape, however, lab testing demonstrate a symmetric buckled shape. Therefore, buckling modes are not exactly same to compare results.

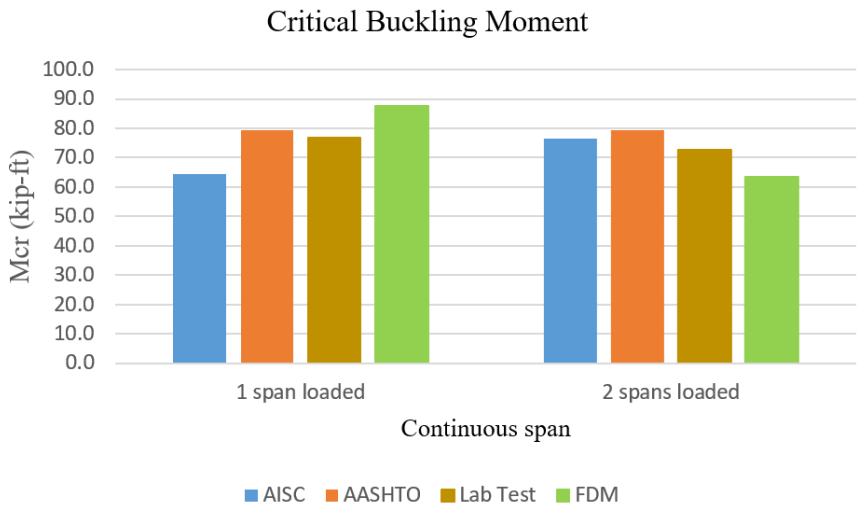

Figure 2-9: Critical buckling moment for continuous span

Table 2-1: C_b for continuous span using codes, lab testing and FDM

	C_b	
	One Span Loaded	Two Spans Loaded
AASHTO	1.75	1.75
AISC	1.42	1.69
Lab Test	1.70	1.62
FDM	1.94	1.41

2.3 Finite Difference Method for Beams with Non-composite Concrete Deck

When a non-composite concrete deck is provided, the bracing effect of the deck does not allow the beam's top flange to move freely along the transverse direction (perpendicular to the beam length). At the negative moment region, the beam's bottom

flange is in compression and tends to buckle. Khelil *et al.* (2008) [68] studied the LTB of beams that were continuously restrained at one flange. Their research used the Galaerkin method in the finite difference method. The matrix consisted of three submatrices that corresponded to rigidity (geometry), boundary conditions, and loading conditions. Additional information on use of FDM for composite beams can be found in Durant (1944), Wirianto (1979) and Ivan *et al*. (2015) [69 -71].

CHAPTER 3

NUMERICAL ANALYSES

As part of the research on the LTB resistance of continuous stringers, full-scale lab testing [67] was conducted at the University of Nebraska – Lincoln. The lab testing results served as a baseline to allow for calibrating the finite element analyses of the continuous stringers, which is the focus of Chapter 3. The analyses matched a variety of test setups accounting for different bracing conditions and load cases. The analysis results were compared with the lab testing data, including the vertical and lateral deflections, and strain readings at the representative sections of the stringers. A more accurate approach was proposed to determine C_b to account for the bracing effect of the concrete deck.

3.1 Lab Testing

This test setup corresponded to a two-span structure, which involved three lines of stringers, steel diaphragms at the ends for support, and a floorbeam as the interior support. Lateral restraints provided three options (i.e. steel diaphragms, timber struts at the top flange, and non-composite concrete deck). To investigate the effect of the floorbeam's relative stiffness for LTB, the floorbeam was supported as rigid and flexible. To analyze variations of the connection restraint for LTB, the bottom of the stringers were connected to the floorbeam with bolts and without bolts. One-span load case and two-span load case were tested on the interior stringer.

Basic setup included a grillage system that involved three lines of 50 ft. long W16 x 31 stringers, one 25-ft-long W24 x 68 floorbeam, and C12 x 20 end diagrams bolted to the stringers. **Figure 3-1** and **Figure 3-2** show the framing plan and a section of the grillage at the floorbeam, respectively. Each span was 24 ft. long and the stringers were spaced at 4 ft. As shown in **Figure 3-3** and **Figure 3-4**, stiff supports underneath the floorbeam differentiated the rigid and flexible support conditions. The deck was 50 ft. long by 10 ft. wide and 6 in. thick. The deck was conventionally reinforced using Grade 60 rebar. **Figure 3-5** and **Figure 3-6** present the deck plan and a typical section.

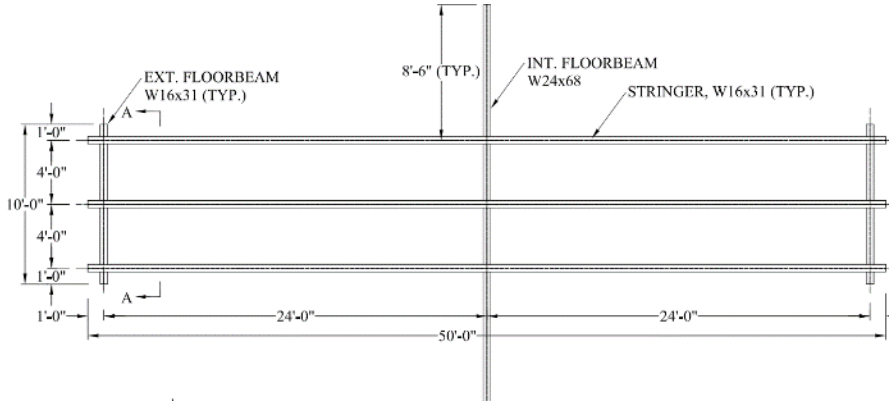

Figure 3-1: Grillage system framing plan

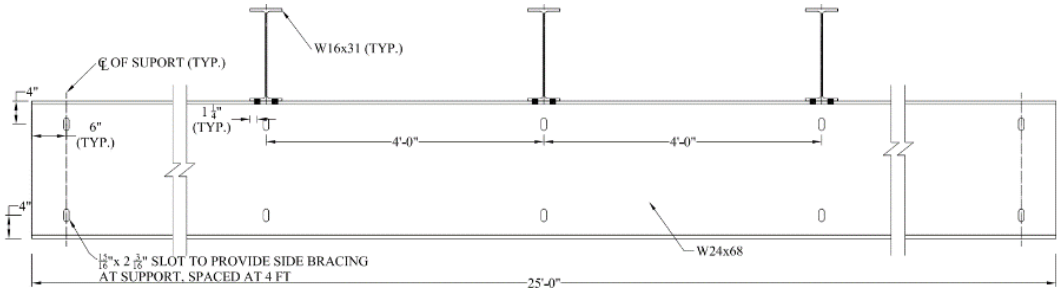

Figure 3-2: Grillage system section at floorbeam

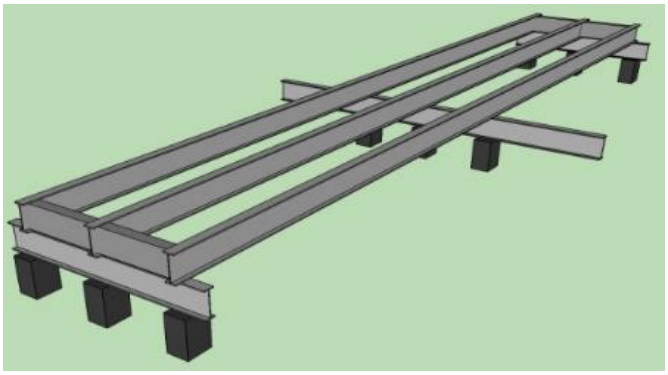

Figure 3-3: Test setup mimicking rigid (stiff) floorbeam

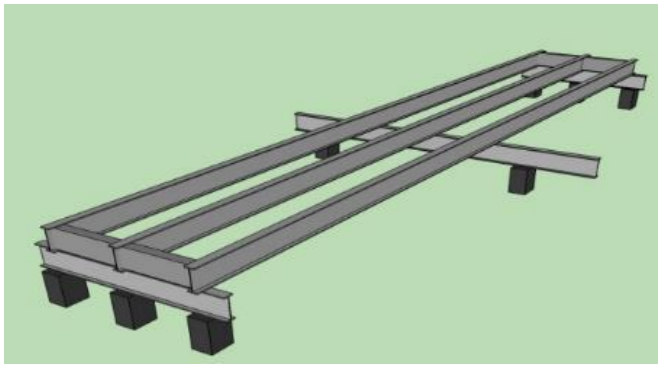

Figure 3-4: Test setup mimicking flexible floorbeam

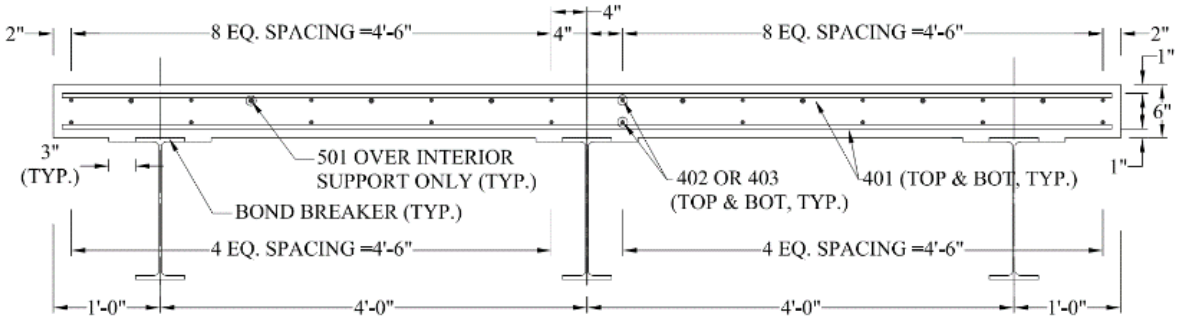

Figure 3-5: Deck reinforcement plan

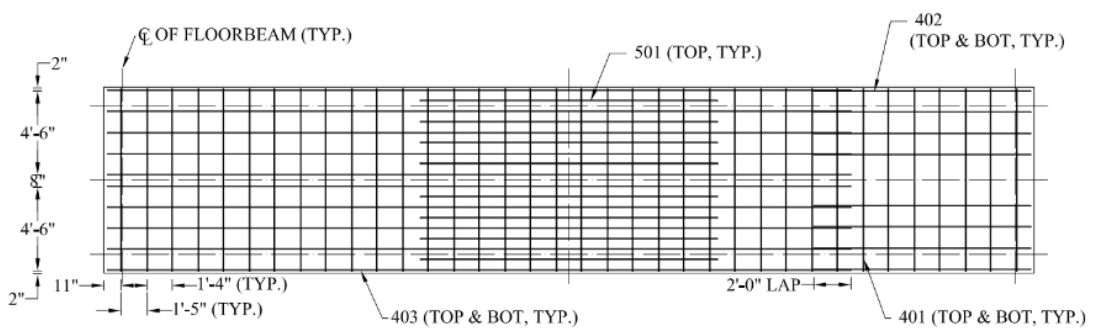

Figure 3-6: Deck reinforcement plan

Table 3-1 provides the complete test matrix including categories; corresponding configurations (i.e., test setups); stringer support conditions (i.e., floorbeam flexural stiffness); loading and bracing conditions, including existence or absence of composite action (i.e., C or NC); and test run identification numbers. Testing is categorized into four general groups as listed below (See **Figure 3-7** to **Figure 3-10**).

Group I

This category included stringers without any restraint at the top flange. Results are shown when the bottom flange was bolted and not bolted, as well as when the floorbeam was flexible and rigid. Spans were loaded either only one span or both spans.

Group II

In this group, intermediate steel diaphragms (C12x20) were placed at various locations including the interior support, and $L/2$, $L/8$, $L/4$, and $3L/8$ away from the interior support (L = span). Bottom flange bolted and not bolted conditions were applied in this group as well.

Group III

This group consisted of test runs where the stringer's top flanges were laterally braced by timber ties (4 x 4) and C-clamps. LTB when braced at L/2, L/3, L/4, and L/5, locations were analyzed.

Group IV

Concrete deck was poured on top of the stringers. The deck was intentionally made non-composite with the stringer by applying de-bonding material in between them. The results of this group help to calculate C_b factor for a non-composite continuous stringer system.

Figure 3-7: Example Group I setup [67]

Table 3-1: Test Matrix

Group	Test setup	NC or C	Description of boundary conditions			Load condition	Test Run #
			Interior support at center stringer	Top flange of stringer	Bottom flange of stringer		
I	No. 1	NC	Rigid	Unbraced	Unbraced	1 point load	1
						2 point loads	2
	No. 1A				Braced laterally by bolts	1 point load	3
						2 point loads	4
	No. 1B		Flexible		Unbraced	1 point load	5
						2 point loads	6
	No. 1C				Braced laterally by bolts	1 point load	7
						2 point loads	8
II	No. 1'	NC	Rigid	Diaphragms @ Int. Support	Unbraced	1 point load	9
						2 point loads	10
				Diaphragms @ L/2		1 point load	11
						2 point loads	12
				Diaphragms @ L/8 from Int. Support		1 point load	13
						2 point loads	14
				Diaphragms @ L/4 from Int. Support		1 point load	15
						2 point loads	16
				Diaphragms @ 3L/8 form Int. Support		1 point load	17
						2 point loads	18
	No. 1'A		Rigid	Diaphragms @ Int. Support	Braced laterally by bolts	1 point load	19
						2 point loads	20
				Diaphragms @ L/2		1 point load	21
						2 point loads	22
				Diaphragms @ L/8 from Int. Support		1 point load	23
						2 point loads	24
				Diaphragms @ L/4 from Int. Support		1 point load	25
						2 point loads	26
				Diaphragms @ 3L/8 form Int. Support		1 point load	27
						2 point loads	28
III	No. 2	NC	Rigid	Timber strut @ L/2, TF	Unbraced	2 point loads	29
				Timber strut @ L/3, TF		2 point loads	30
				TS @ L/4, L/2, L, L/2, L/4		2 point loads	30'
				Timber strut @ L/4, TF		2 point loads	31
				Timber strut @ L/5, TF		2 point loads	32
	No. 2A			Timber strut @ L/2, TF	Braced laterally by bolts	2 point loads	33
				Timber strut @ L/3, TF		2 point loads	34
				TS @ L/4, L/2, L, L/2, L/4		2 point loads	34'
				Timber strut @ L/4, TF		2 point loads	35
				Timber strut @ L/5, TF		2 point loads	36
				TS @ L/8, L/4, L/2, L, L/8, L/4, L/2		2 point loads	36'
	No. 2B		Flexible	Timber strut @ L/2, TF	Unbraced	2 point loads	37
				Timber strut @ L/3, TF		2 point loads	38
				Timber strut @ L/4, TF		2 point loads	39
				Timber strut @ L/5, TF		2 point loads	40
	No. 2C			Timber strut @ L/2, TF	Braced laterally by bolts	2 point loads	41
				Timber strut @ L/3, TF		2 point loads	42
				Timber strut @ L/4, TF		2 point loads	43
				Timber strut @ L/5, TF		2 point loads	44
IV	No. 3	NC Concrete slab cast to stringer top flange	Rigid	No Diaphragms	Unbraced	1 point load	45
						2 point loads	46
	No. 3A				Braced laterally by bolts	1 point load	57
	No. 3B		Flexible	No Diaphragms	Unbraced	1 point load	69
	No. 3C				Braced laterally by bolts	1 point load	81

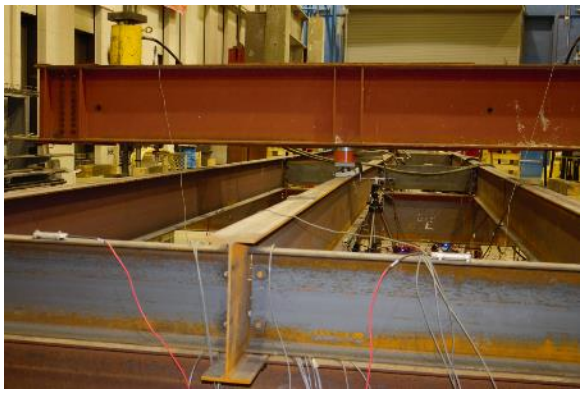

Figure 3-8: Example Group II setup [67]

Figure 3-9: Example Group III setup [67]

Figure 3-10: Example Group IV setup [67]

LVDTs are installed at mid-span of the interior stringer of both spans to capture vertical and lateral deflections. Load and pressure cells were able to measure the force

applied. The strain gauges were able to capture stresses at each location shown in **Figure 3-11**. Testing results are commonly reported at four critical locations herein. Those sections are presented in **Table 3-2**.

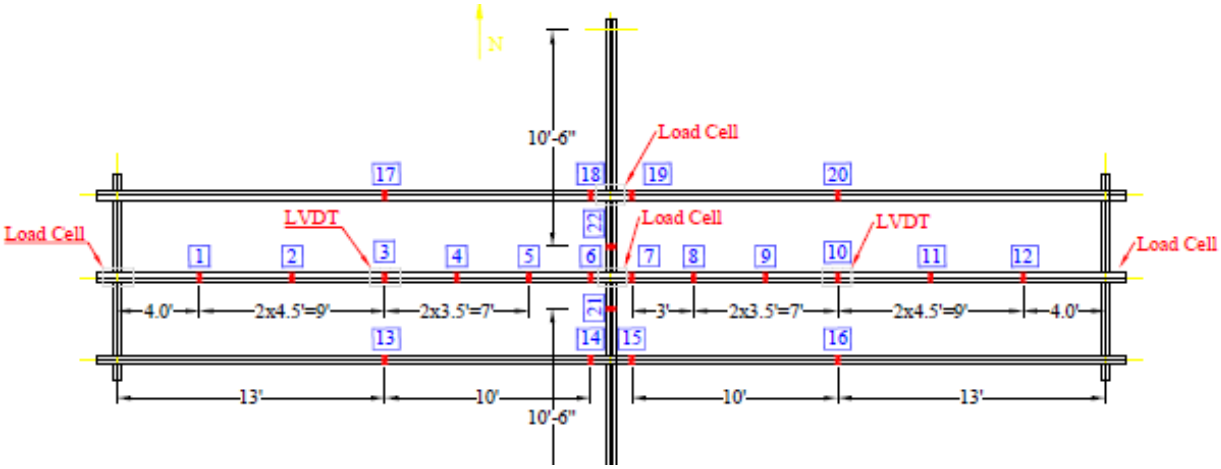

Figure 3-11: Instrumentation plan view

Table 3-2: Four critical locations

Location	Description
3	Mid-span max. +M when loaded at Loc. 3 Mid-span -M when loaded at Loc. 10
6	Critical -M location adjacent to floorbeam
7	Critical -M location adjacent to floorbeam
10	Mid-span max. +M when loaded at Loc. 10 Mid-span -M when loaded at Loc. 3

3.2 Stress Components Corresponding to Strain Gauge Readings

Strain data obtained by the strain gages can be converted to stresses by using the elastic of the modulus. This stress is a collective stress of axial, in-plane (primary) and out-of-plane bending, and warping torsion components. **Figure 3-12** presents stress combinations at the top and bottom flanges of the stringer.

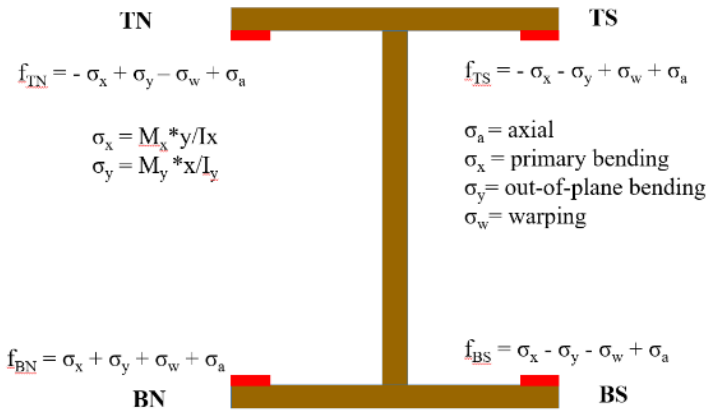

Figure 3-12: Stress components

Figure 3-13 to **Figure 3-16** provide load verses stress plots for each stress component at Loc. 3 for Test Run #1. TN (top-north), TS (top-south), BN (bottom-north) and BS (bottom-south) are the stresses at Location 3, which is 1 ft. from the loading position for Test Run #1. Axial loads are typically zero. Weak axis bending and warping torsion shows a gradual drop after peak load indicating LTB of the stringer. Note how warping stress and weak axis bending moment at the top flange affect the total stress in **Figure 3-13** and **Figure 3-14**. On the other hand, warping and weak axis bending moment at the stringer's bottom flange act on opposite directions and therefore the sum of them barely affects the total stress (See **Figure 3-15** and **Figure 3-16**). The stress plots sof Test Run #1 are provided for illustration purpose. The test results of the other test runs are selectively shown when they are used to calibrate the finite element analyses results.

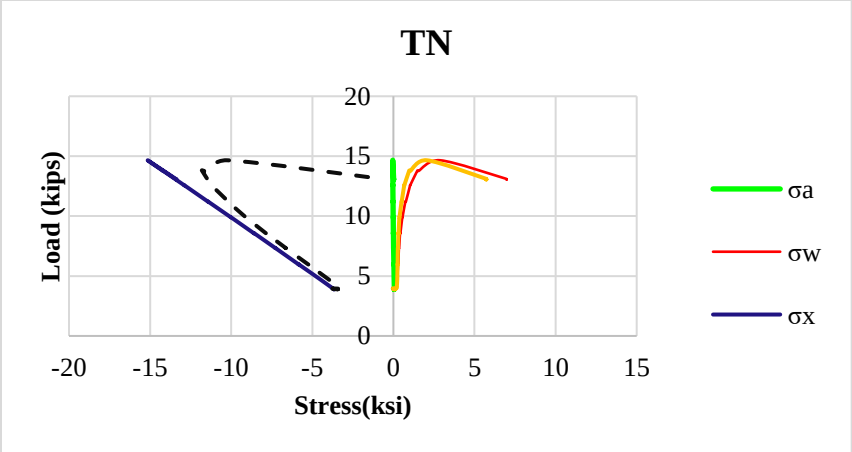

Figure 3-13: Stress components, Loc. 3 TN, Test Run #1

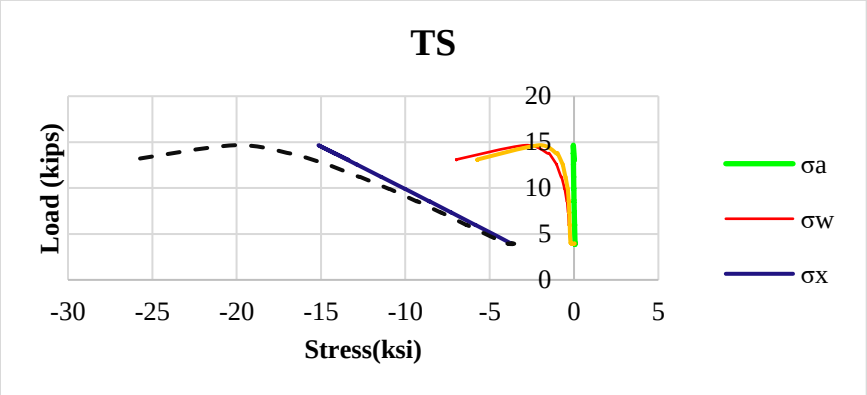

Figure 3-14: Stress components, Loc. 3 TS, Test Run #1

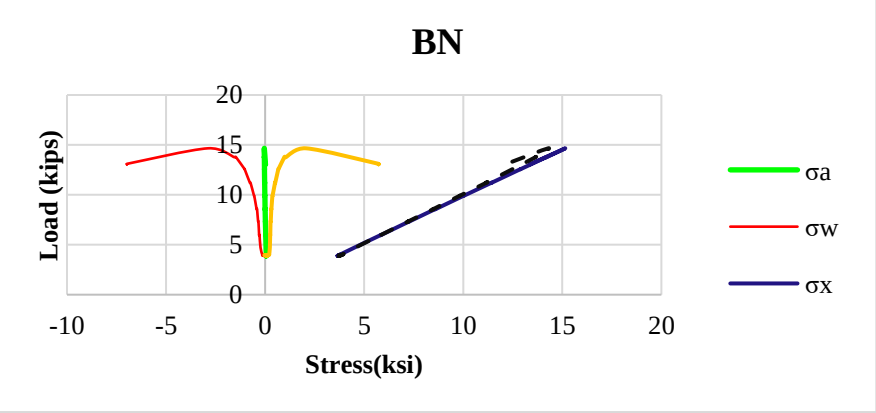

Figure 3-15: Stress components, Loc. 3 BN, Test Run #1

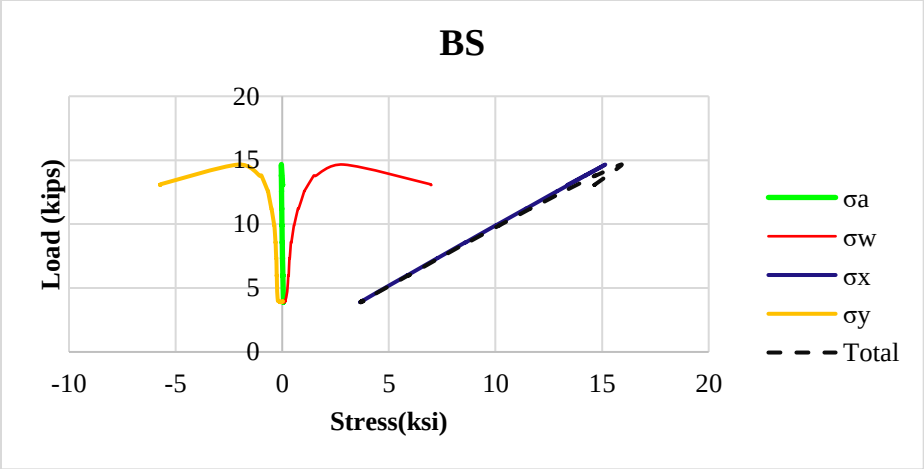

Figure 3-16: Stress components, Loc. 3 BS, Test Run #1

3.3 Finite Element Analyses

Finite element analysis (FEA) simulated the stringer's behavior while accounting for various parameters, including geometric imperfections, various bracing configurations, rigid and flexible interior supports, other loading conditions, etc. FEA was completed using ANSYS R19 [72]. A combination of static, linear Eigenvalue buckling, and non-linear buckling analyses were performed. The FEA model includes three lines of stringers, end diaphragms, and the floorbeam and non-composite concrete deck (see **Figure 3-17**).

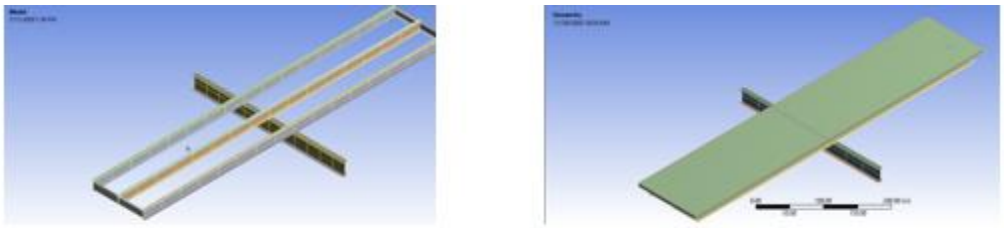

(a) Model without deck (b) Model with non-composite deck

Figure 3-17: FEA models

3.3.1 Element Type

SHELL181 elements were used for the stringers, end and intermediate diaphragms, and floorbeam. This shell element is a first-order element with 4 external nodes and no internal nodes and six degrees of freedom at each node: translations in and rotations about the x, y, and z axes.

The concrete deck in the linear analysis was modeled using SOLID185 elements. This is a linear 3D eight-node element with only three (translational) degrees of freedom. The deck has three layers of elements across the thickness and the element size in the transverse and longitudinal directions is 4 in. In the nonlinear analysis, the SOLID185 are substituted for CPT215 elements because SOLID185 elements are not compatible in non-linear analyses. CPT215 is a coupled physics 3D eight-node suitable for the microplane model used to capture the nonlinear behavior of the concrete. The element has temperature, pressure, and nonlocal field values degrees of freedom in addition to three translations at each node.

LINK180 elements were used to represent the reinforcing steel bars in the concrete deck for both linear and nonlinear analyses. The element is a linear 3D spar with two nodes and only translation degrees of freedom suitable for uniaxial tension or compression. Similarly, this element was employed for the wood bracing at the top flanges and at appropriate tests because it best represented the test data compared to BEAM188, which resists load in bending.

3.3.2 Material

The selected structural steel stress-strain diagram is shown in **Figure 3-18**. The elastic modulus of steel is assumed to be 29,000 ksi. The stringers and floorbeam were

Grade 50 steel, and the diaphragms Grade 36 steel. The concrete strength considered to be 5,000 psi (f'_c).

Linear elastic concrete properties were used for the linear analysis and the parameters were chosen to obtain the best imperfection for the stringers. A micro plane model with coupled damage-plasticity was employed for the nonlinear analysis. This material model accounts for the elasticity, plasticity, damage, and nonlocal interaction of the concrete.

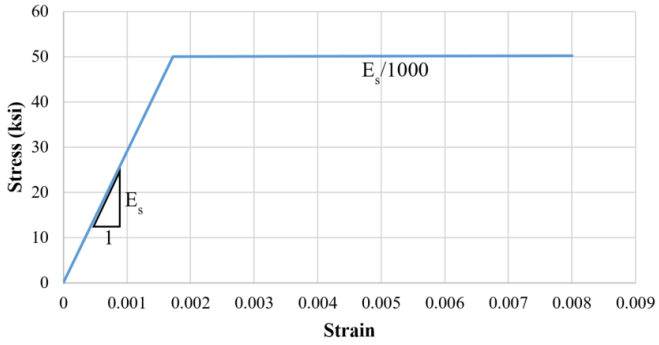

Figure 3-18: Selected stress-strain diagram for structural steel

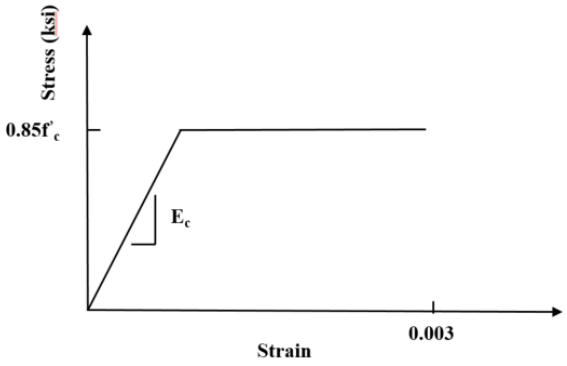

Figure 3-19: Selected stress-strain diagram for concrete

3.3.3 Mesh

Each stringer flange consists of 4 elements along its width while the stringer web is divided into 8 equal elements. A typical mesh of the stringer section is shown in

Figure 3-20. The element size along the length of the stringer at each span is 2 in. A convergence study was performed to validate the mesh for both linear and nonlinear analyses. **Figure 3-21** shows a comparison among three mesh types (fine, finer, and finest meshes) for Test Run #3 and indicates that the fine mesh type is sufficient to capture the stringer's behavior.

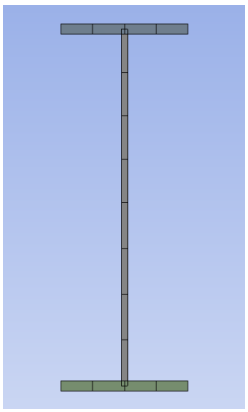

Figure 3-20: Typical meshes in the model

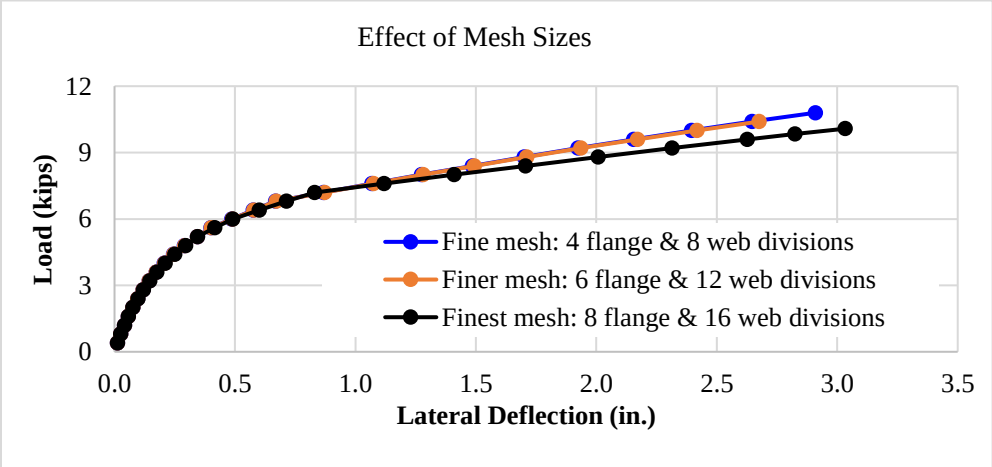

Figure 3-21: Model mesh sensitivity study

3.3.4 Boundary Conditions

Boundary conditions of the models at various supports are illustrated in **Figure 3-22**. Ends of the stringers were connected with the steel diaphragms using the node merge option in ANSYS. The floorbeam served as the interior supports (rigid or flexible supports) for the stringers. For the case of the flexible floorbeam, the floorbeam was laterally braced at every 3 ft. to ensure that the floorbeam could reach the plastic moment without failing before the stringers fail. In Group IV, the non-composite deck is applied.

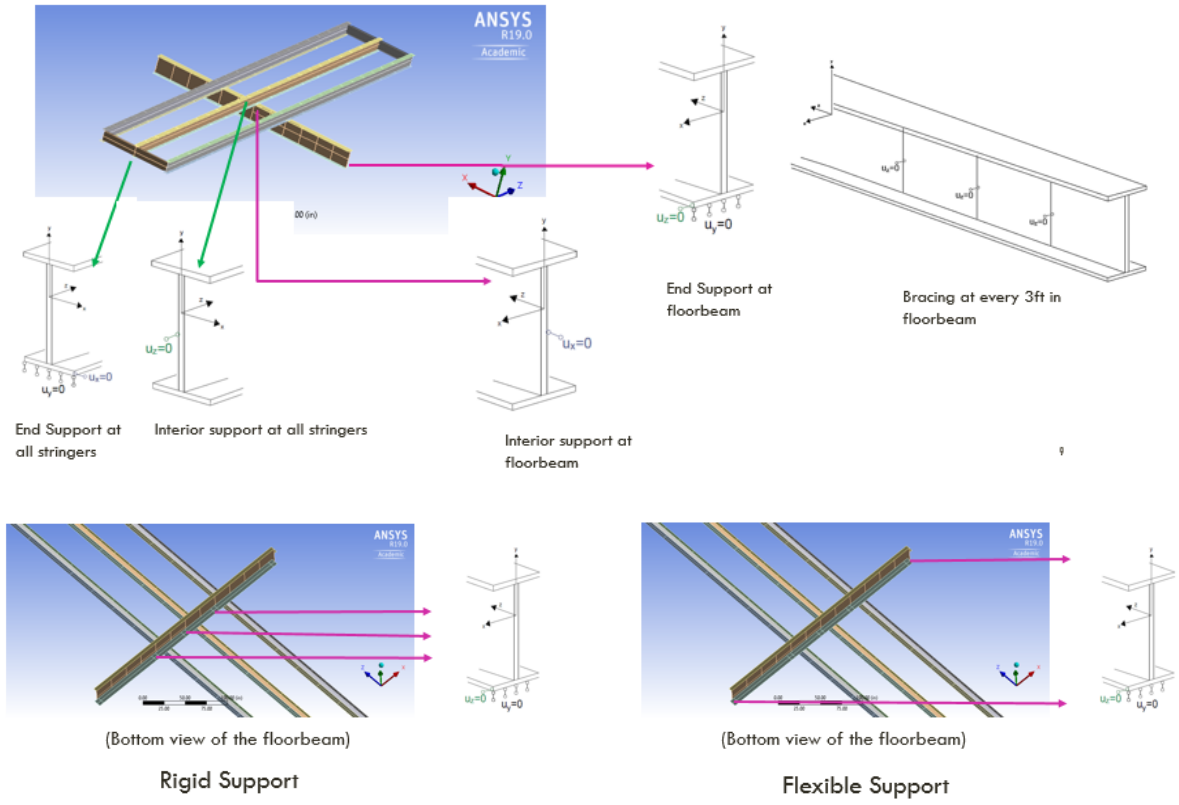

Figure 3-22: Boundary conditions at the stringers and floorbeam

3.3.5 Load Cases

As shown in **Figure 3-23**, the interior stringer was loaded at either one span or both spans. An area load (6 in. diameter) was applied at the mid-span matching the test setup.

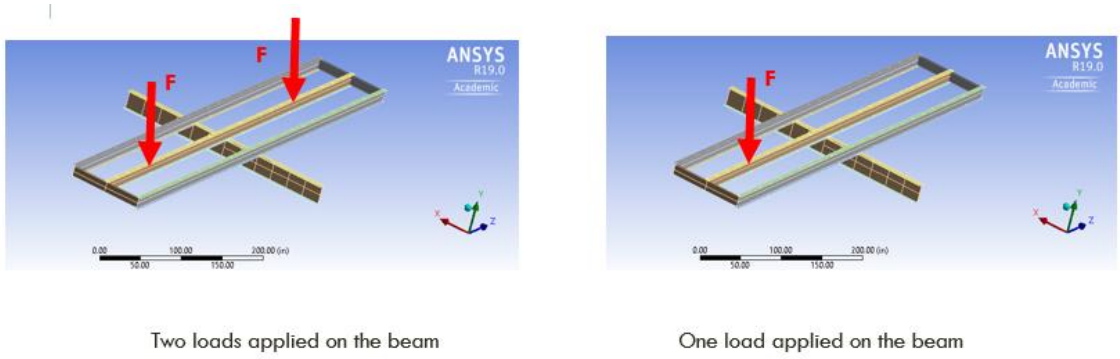

Figure 3-23: Load cases

3.3.6 Stringer Models

A combination of static, linear Eigenvalue buckling, and non-linear buckling analyses were performed. **Figure 3-24** presents a flow chart of the FEA modeling in ANSYS. **Figure 3-25** shows the procedure of developing the FEA models in ANSYS corresponding to Group III's test setups.

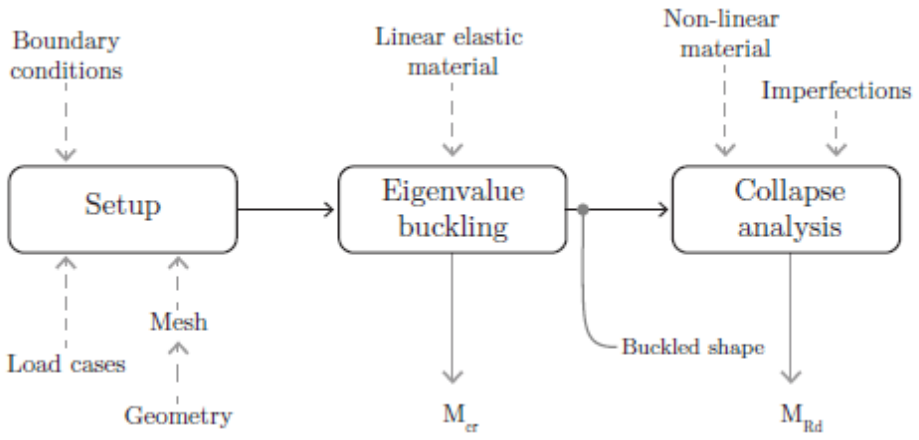

Figure 3-24: Flow chart of FEA modeling in ANSYS [73]

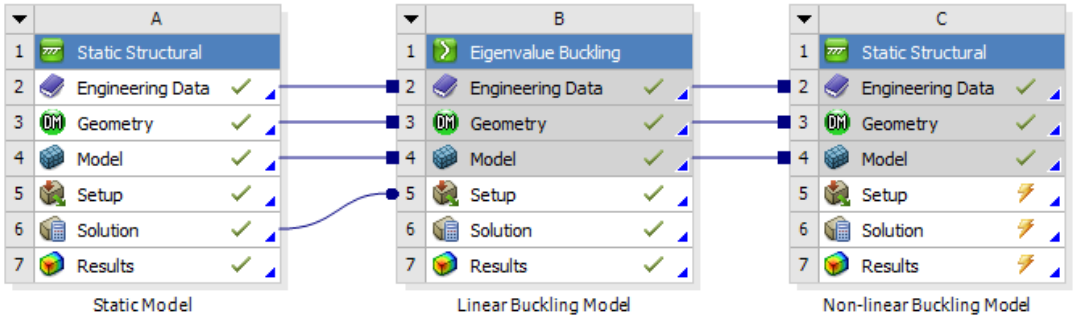

Figure 3-25: Stringer model development using ANSYS

3.3.7 Non-composite Concrete Deck

Regarding the connection between the deck and stringers, initial model trials assumed no friction between them along any direction while the stringer's top flanges were laterally braced by the deck at discrete points along the stringer's length. After calibrating the models with the test results, a frictional interface with a coefficient of 0.1 was selected along both transverse and longitudinal directions because it best matched the testing data.

SOLID185 was tried initially for the deck, but it was incompatible in the non-linear buckling analysis. Hence, CPT 215 element was adopted to maintain the same mesh as the static analysis. Linear buckling and non-linear buckling models were not connected because they used two different material elements. (See **Figure 3-26**) Instead, linear buckling results were extracted using commands. ANSYS commands that helped to attribute these elements and to implement non-linear behavior are shown in Appendix.

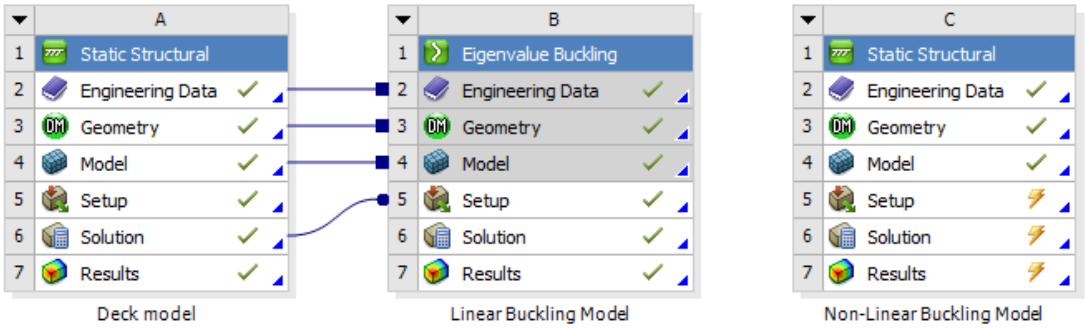

Figure 3-26: Deck model setup using ANSYS

3.3.8 Parametric Study

Lateral Stiffness at the Loading Frame

After numerous FEA model trials, use of a lateral spring with a stiffness of 1.0 kip/in. at the loading location best represent the load assembly's lateral stiffness and provide comparable results with the test data. The spring connected to midpoint of the top flange, and explicitly constrained in a vertical direction (using a constraint equation), so that stringer and spring have the same vertical movement (See **Figure 3-27**). Observed lateral stiffness is attributable to friction between the load bearing plate and the interior stringer, and lateral stiffness of the loading assembly largely provided by the two threaded rods used to support the spreader beam in the lab tests. **Figure 3-28** shows the effect of the spring's stiffness for a simple supported beam.

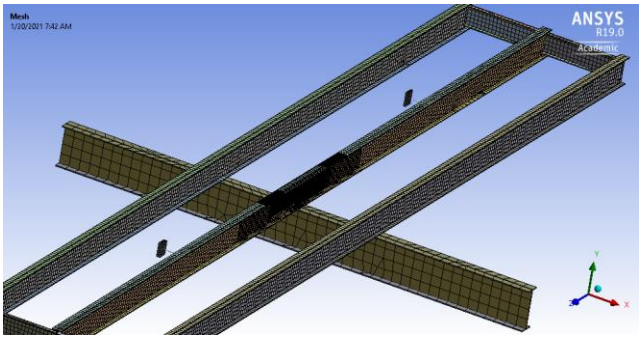

Figure 3-27: Spring placement in Test Run #3

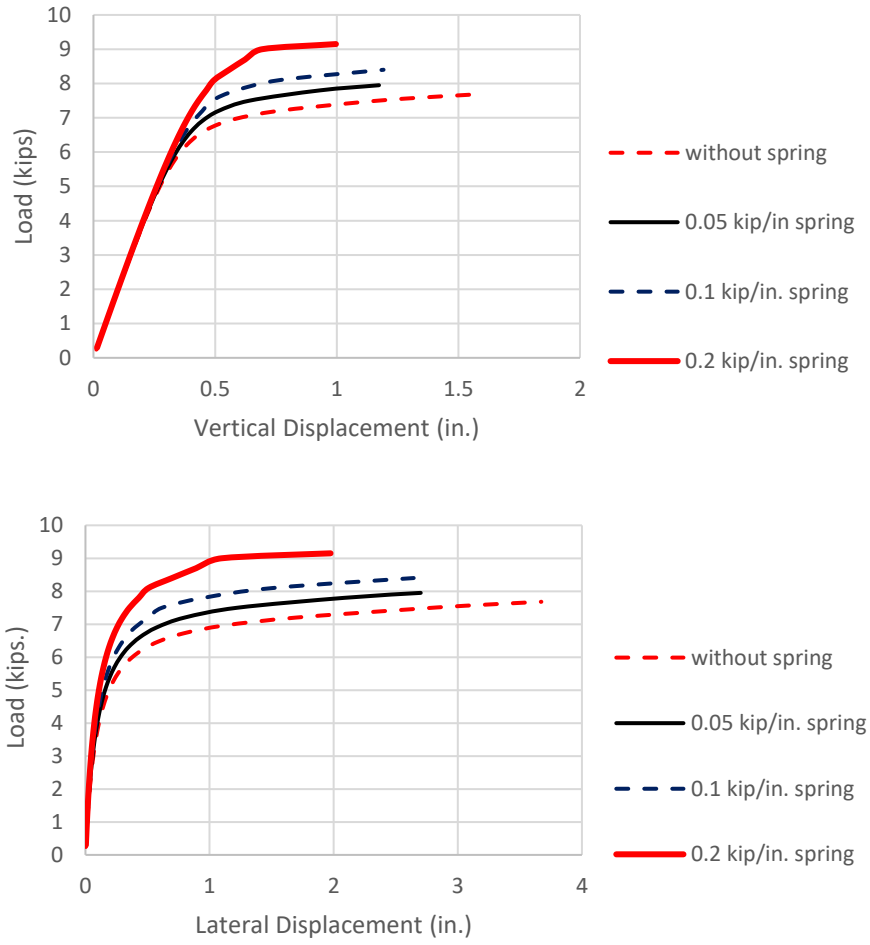

Figure 3-28: Effect of spring stiffness for a simply supported beam

Geometry Imperfections

Stringer geometry measurements were collected using laser scans prior to the lab tests. An initial imperfection for the interior stringer, approximately $L/1{,}500$ (L = span), was accounted for in the non-linear analysis following the critical buckling mode. **Figure 3-29** shows the lateral and vertical deflection variation in LTB due to imperfections.

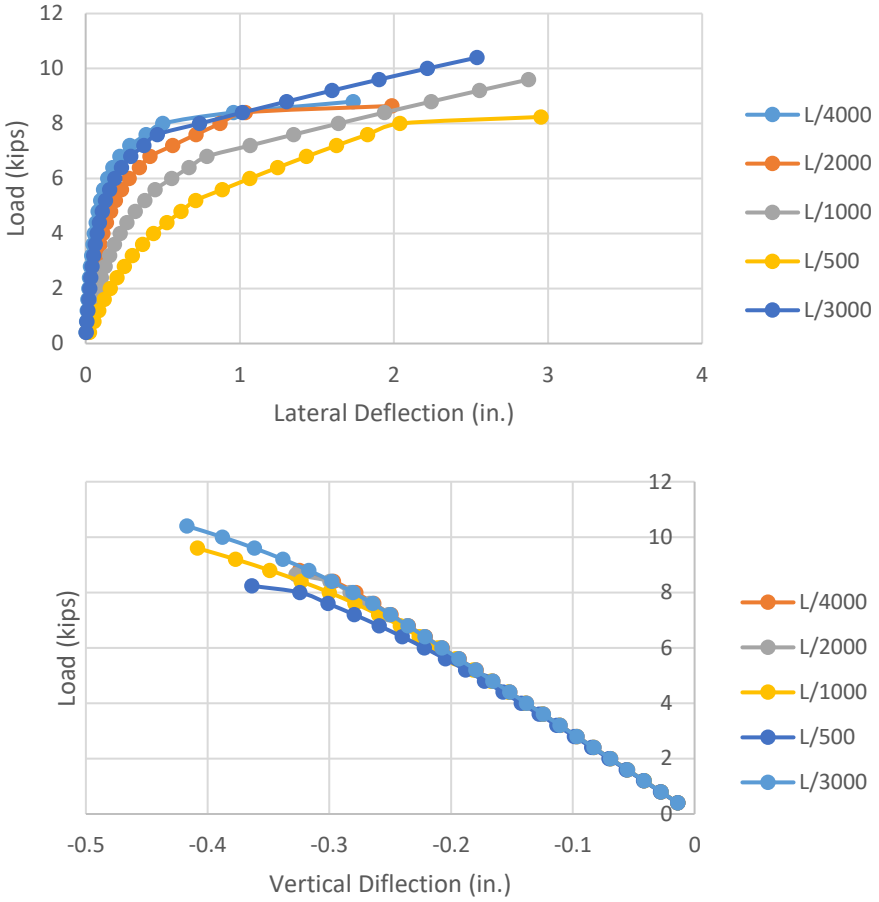

Figure 3-29: Effect of geometry imperfections on LTB

Friction between the Stringers and Floorbeam

In the test runs without bolt connection between the stringers and the floorbeam, friction was assumed at the interface. Friction coefficient of 0.05, 0.1, 0.2, and 0.4 were accounted for, and the interior stringer lateral movement at the floorbeam is shown in **Figure 3-30**. After comparing the test results, the friction coefficient of 0.2 was chosen for the models.

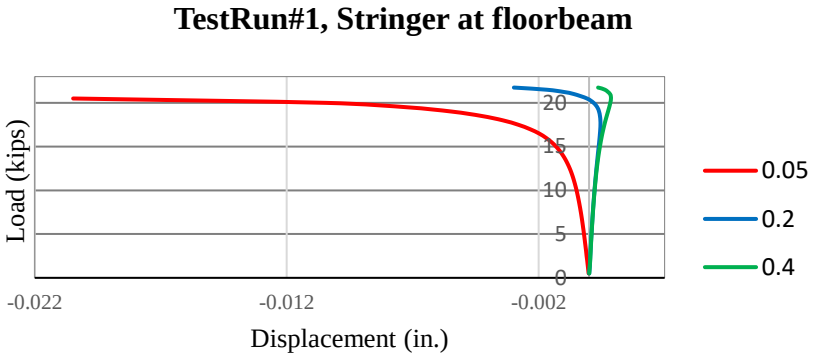

Figure 3-30: Interior stringer displacement at floorbeam location

Connections between the Stringer Ends and Diaphragms

End diaphragms were modeled using either truss elements (LINK180) for shear connection, or beam elements (BEAM188) for moment connection. However, both types of connection demonstrated comparable results. This result is acceptable because at the end of the stringer, moments are close to zero, and therefore, use of moment or shear connection does not make much of a difference.

3.4 Group I Results

Test Run #3 was selected for discussion purpose. This test run had a rigid support at the floorbeam and used a bolted connection between the stringers and the floorbeam. It was only loaded at one span (1 ft. away from the critical Location 3). **Figure 3-31** and **Figure 3-32** show the lateral deflection and element normal stress contours, respectively. **Figure 3-33** to **Figure 3-36** present analysis results compared with the test data at the mid-span of both spans (Locations 3 and 10). Analysis results were generally comparable to the test data. **Figure 3-37** shows the buckled shape when the stringer was loaded at both spans.

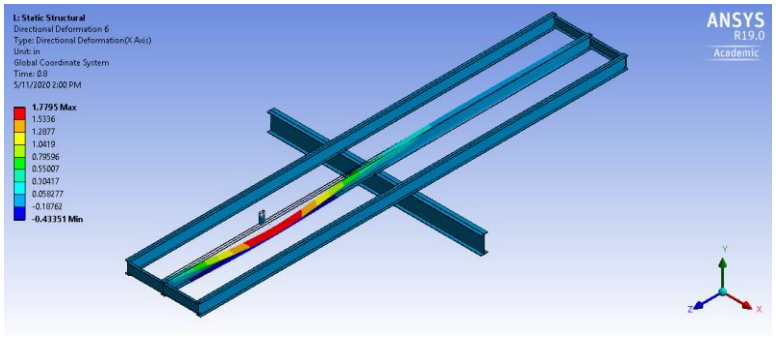

Figure 3-31: Lateral deflection contour, Test Run #3

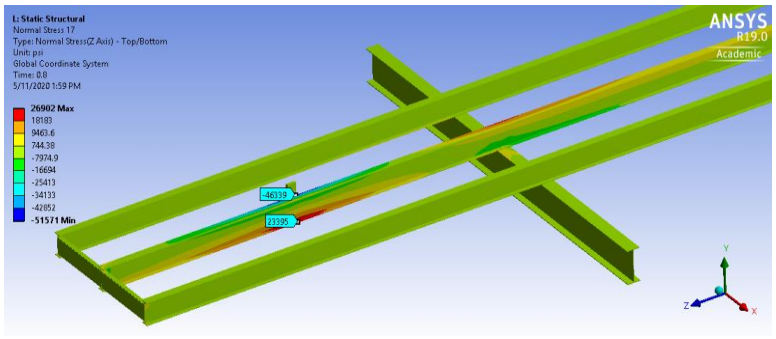

Figure 3-32: Normal stress contour, Test Run #3

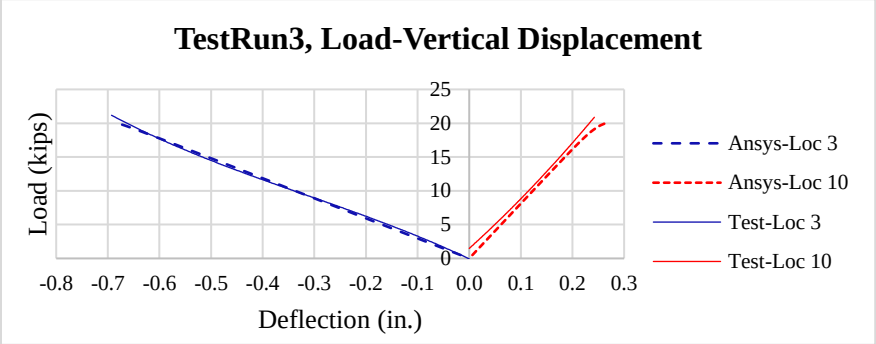

Figure 3-33: Comparison of FEA and measured vertical deflections, Test Run #3

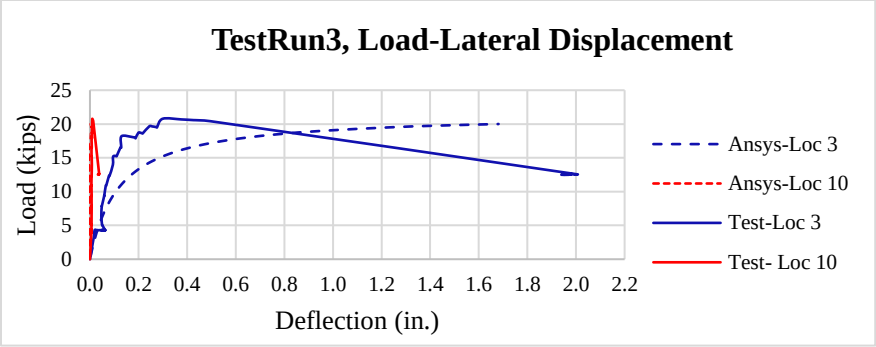

Figure 3-34: Comparison of FEA and measured deflections, Test Run #3

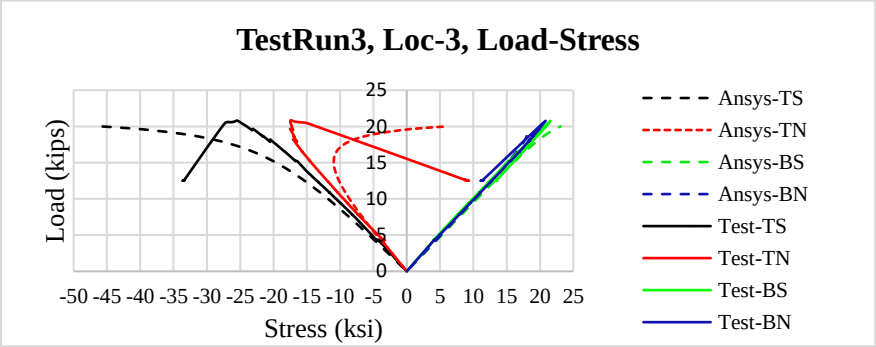

Figure 3-35: Comparison of Loc. 3 normal stresses between analysis and test data, Test Run #3

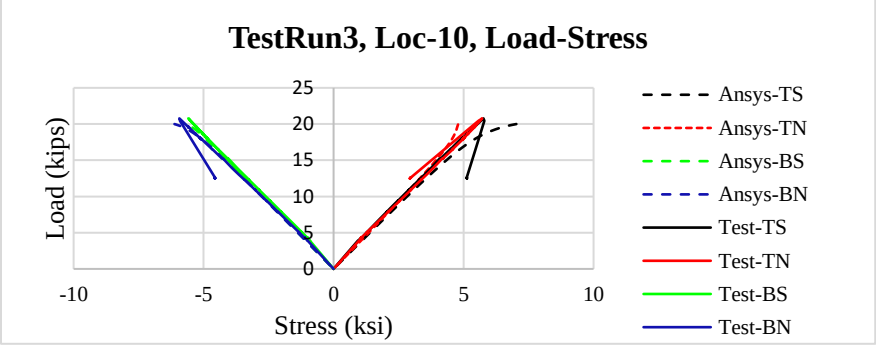

Figure 3-36: Comparison of Loc. 10 normal stresses between analysis and test data, Test Run #3

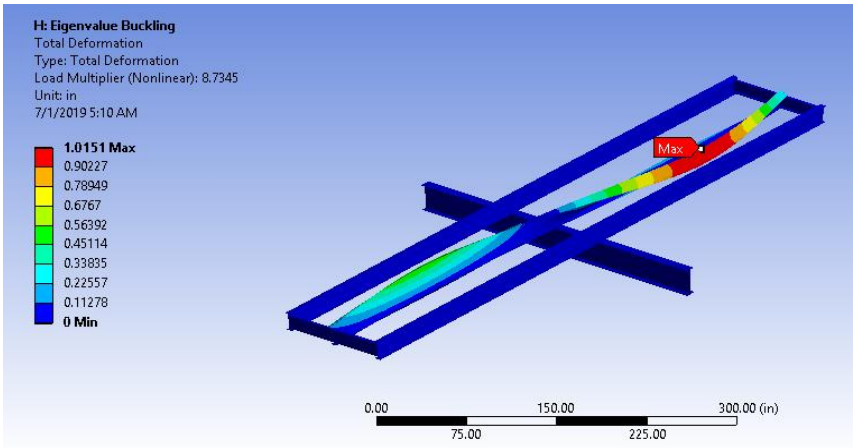

Figure 3-37: Total deformation contour, both spans loaded

3.5 Group II Results

Figure 3-38 shows the buckled shapes of the interior stringer due to various unbraced lengths when intermediate steel diaphragms were provided at L/2, 3L/8, L/4, and L/8 subject to a load at one span. **Figure 3-39** presents the buckled shapes for two span load cases. Test Run #15 was selected as an example to show the comparison between the FEA and test results. It had a rigid floorbeam and used no bolted connection between the stringer and the floorbeam. Steel diaphragms were provided at a quarter span from the interior supports. The analysis results were compared with the test data, including the vertical and lateral deflections, and the stresses at Locations 3 and 10 (see **Figure 3-40** to **Figure 3-43**). The analysis results were generally comparable with the test data.

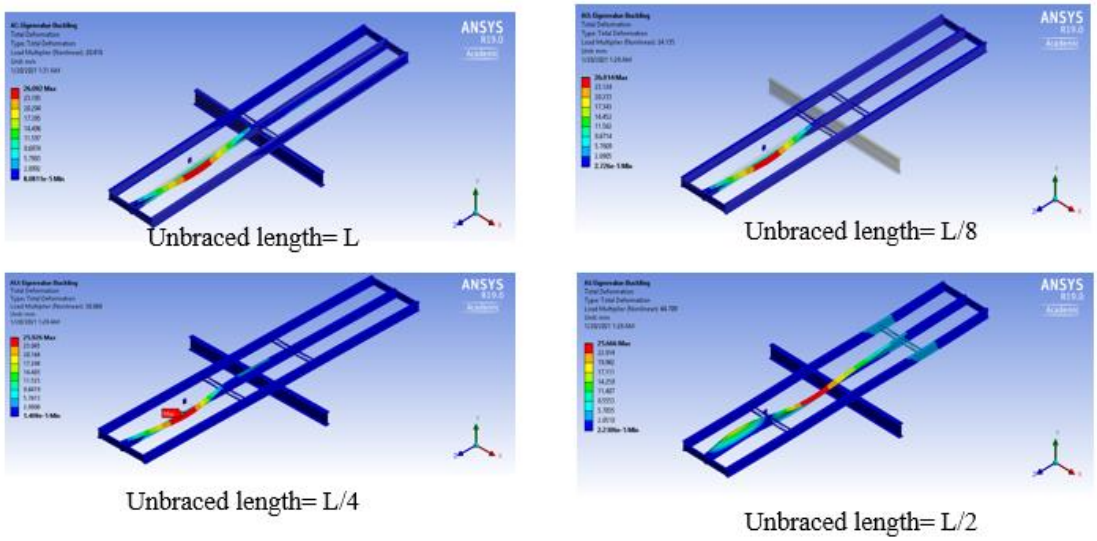

Figure 3-38: Buckled shapes of the interior stringer for Group II tests when one span is loaded

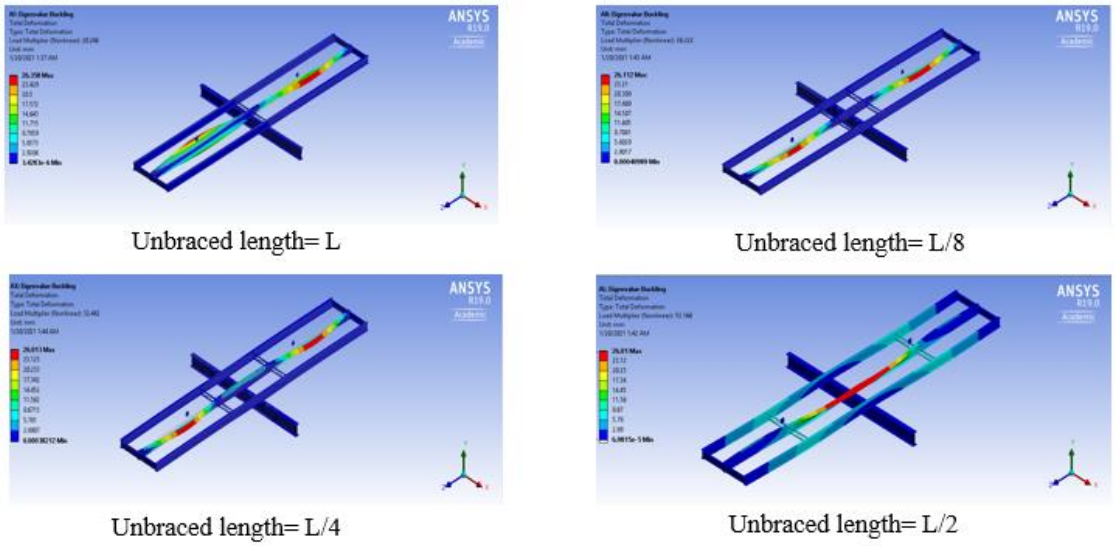

Figure 3-39: Buckled shapes of the interior stringer for Group II tests when both spans are loaded

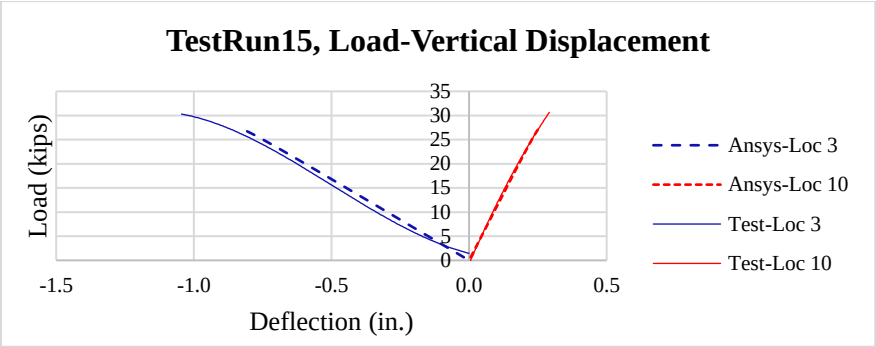

Figure 3-40: Comparison of FEA and measured vertical deflections, Test Run #15

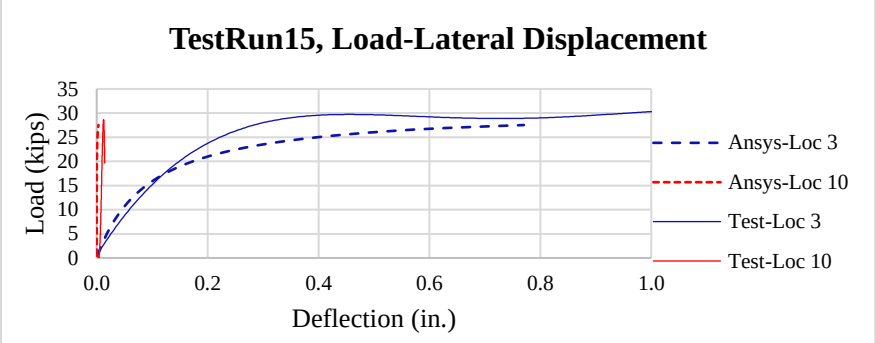

Figure 3-41: Comparison of FEA and measured lateral deflections, Test Run #15

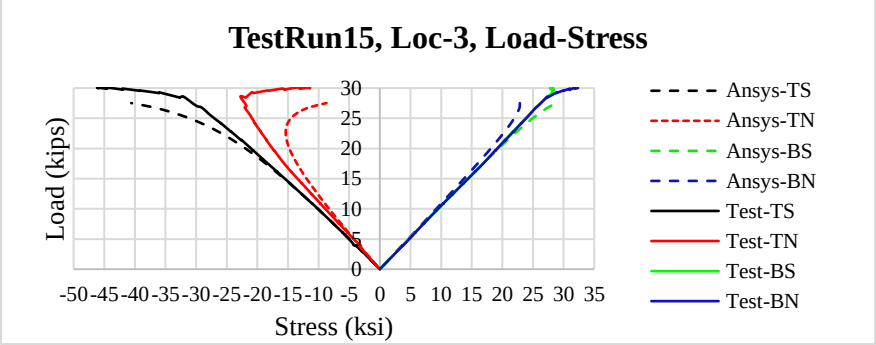

Figure 3-42: Comparison of Loc. 3 stresses between analysis and test data, Test Run #15

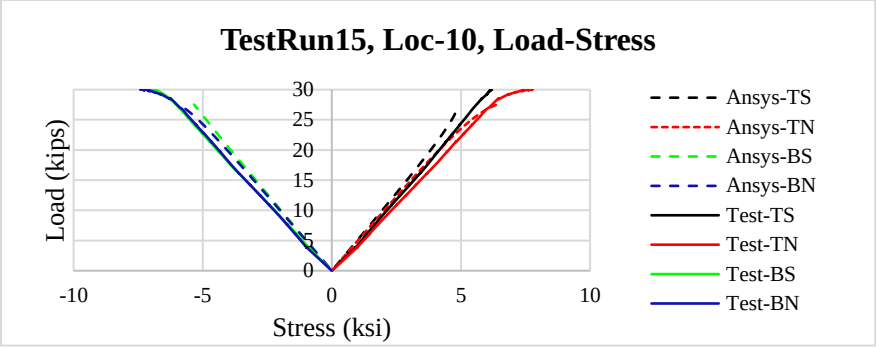

Figure 3-43: Comparison of Loc. 10 stresses between analysis and test data, Test Run #15

3.6 Group III Results

Figure 3-44 presents a model that has timber bracings at the top flange. Initially, timber struts were modeled as truss elements (LINK180 elements). However, BEAM188 elements (that can handle bending) with an elastic modulus of 110 ksi appeared to result in comparable results with the test data. **Figure 3-45** shows the buckled shapes of the stringers in Group III test runs. These tests were loaded at both spans.

Test Run #33 was selected as an example to show the comparison between the FEA and test results. It used a rigid floorbeam and a bolted connection between the stringer and the floorbeam. The stringer top flanges were braced by timber ties and C-clamps at the mid-spans and over the floorbeam. **Figure 3-46** and **Figure 3-47** present the contours of the vertical and lateral deflections, respectively. The analysis results were compared with the test data, including the vertical and lateral deflections, and stresses at Locs. 3 and 10 (**Figure 3-48** and **Figure 3-51**). The analysis results were generally comparable with the testing data.

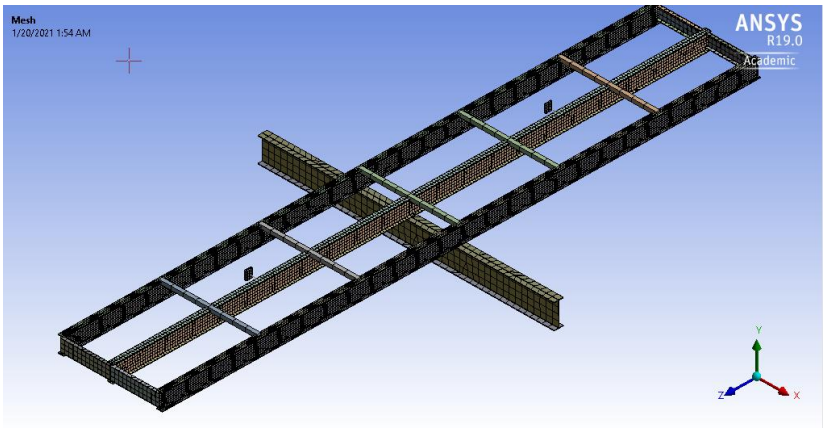

Figure 3-44: Group III ANSYS model

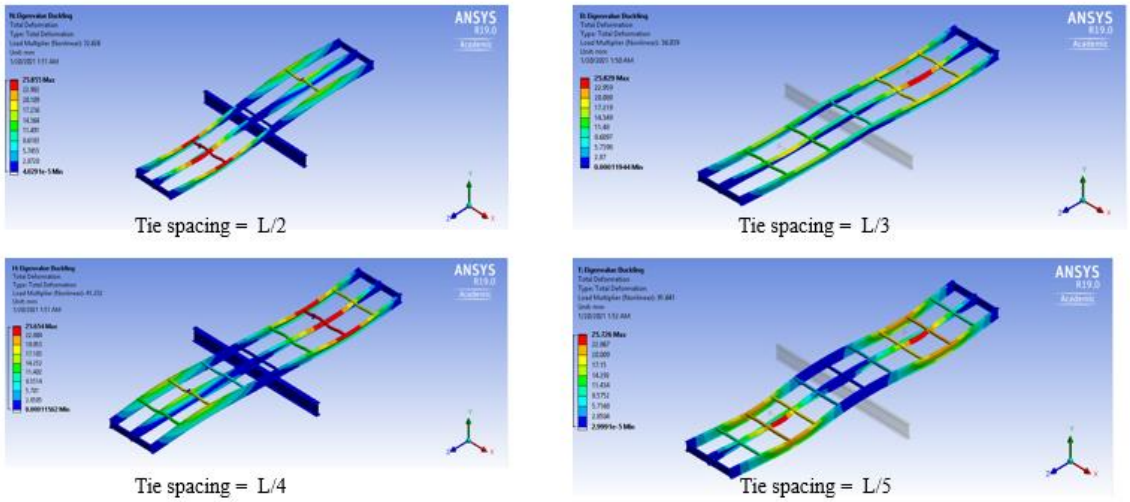

Figure 3-45: LTB of Group III subjected to two-span loading

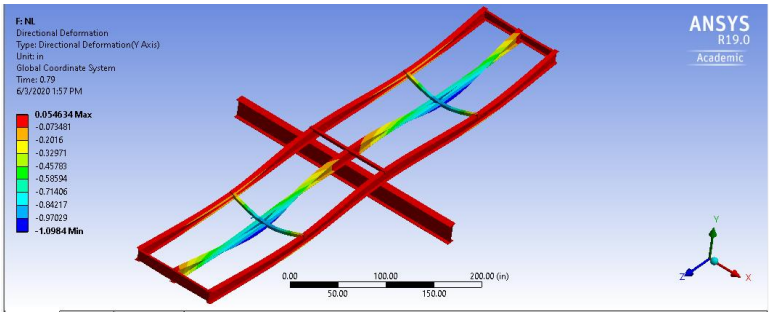

Figure 3-46: Vertical deflection contour, Test Run #33

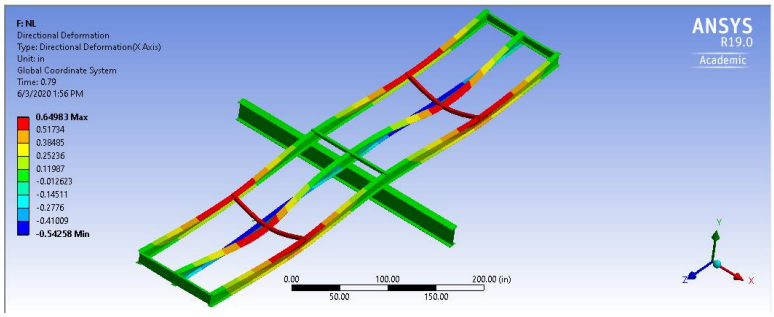

Figure 3-47. Lateral deflection contour, Test Run #33

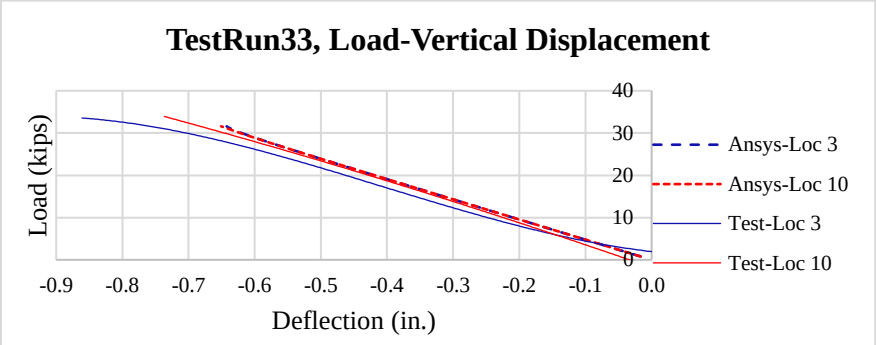

Figure 3-48: Comparison of FEA and measured vertical deflections, Test Run #33

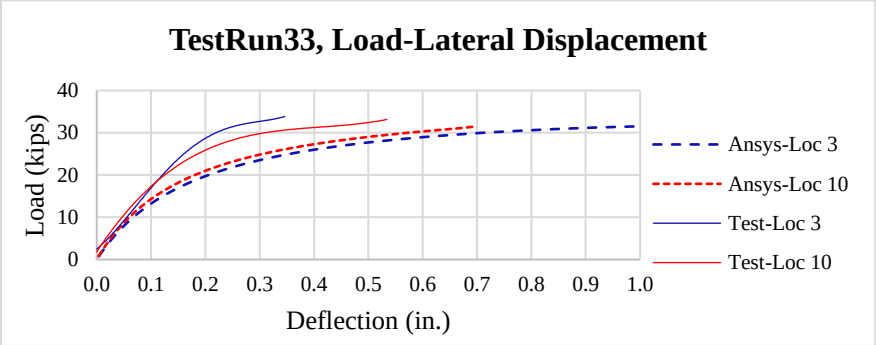

Figure 3-49: Comparison of FEA and measured lateral deflections, Test Run #33

Figure 3-50: Comparison of Loc. 3 normal stresses between analysis and test data, Test Run #33

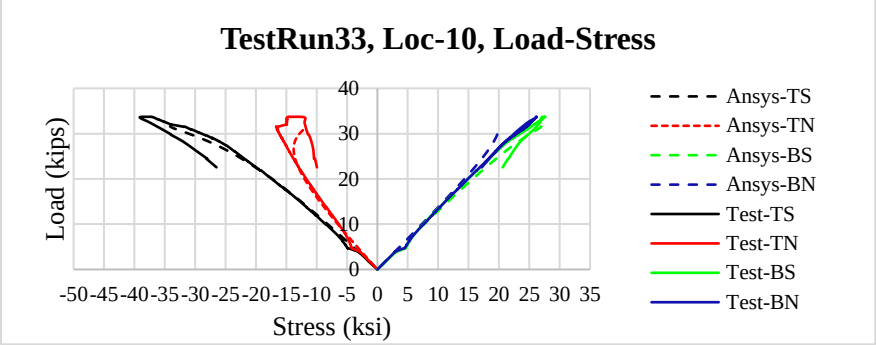

Figure 3-51: Comparison of Loc. 10 normal stresses between analysis and test data, Test Run #33

3.7 Group IV Results

3.7.1 One Span Loaded Case

For discussion purposes, Test Run #45 Failure 3 (load at Loc.10) is presented. The FEA model included the non-composite deck and accounted for concrete cracking and crushing. The FEA model was calibrated against measured test results when a frictional coefficient of 0.1 was assumed between the stringer and the deck. The FEA results agreed reasonably well with the test data. **Figure 3-52** and **Figure 3-53** show the vertical deflection contours subject to a peak load of 128.1 kips in the stringers and the deck, respectively. **Figure 3-54** shows the lateral deflection contours, and **Figure 3-55**,

and **Figure 3-56** present the longitudinal stress contours in the stringers and the deck. Comparisons between the analysis and test results are provided in **Figure 3-57** to **Figure 3-61**. Comparisons showed that the peak load predicted by the FEA model was slightly lower than that from the test, indicating that the FEA model can conservatively simulate the stringers' overall behavior.

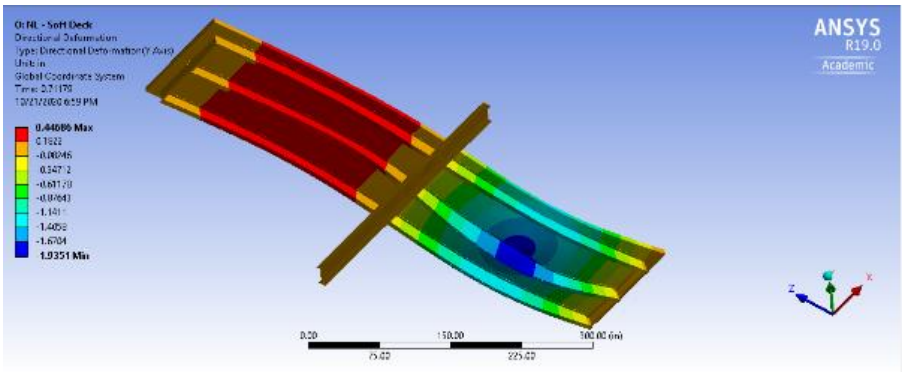

Figure 3-52: Stringer vertical deflection contour, Test Run #45 Failure 3

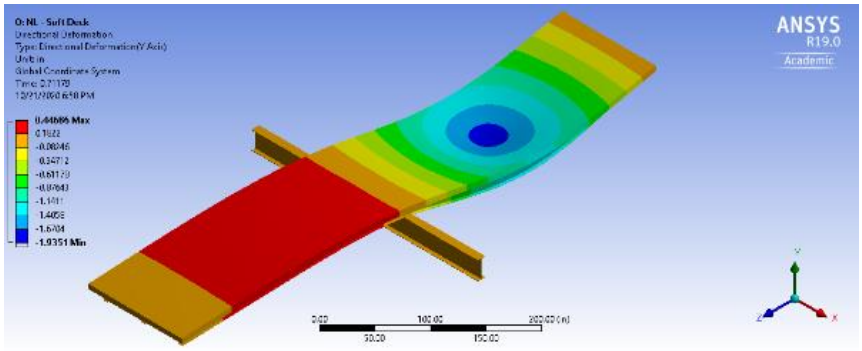

Figure 3-53: Deck vertical deflection contour, Test Run #45 Failure 3

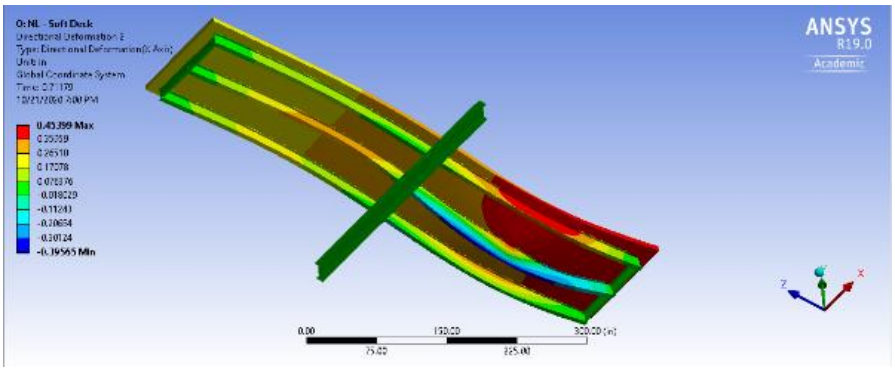

Figure 3-54: Lateral deflection contour, Test Run #45 Failure 3

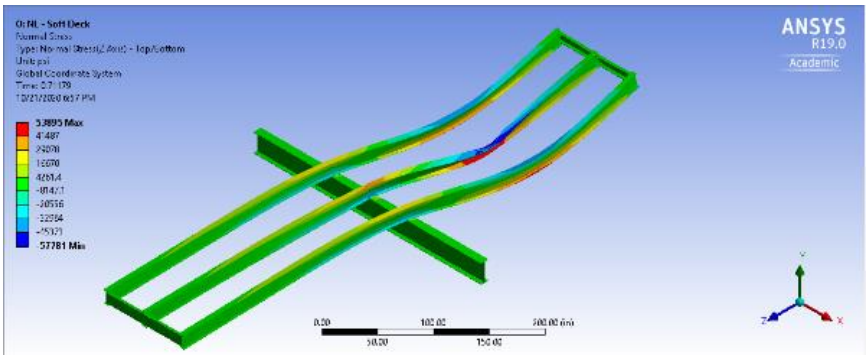

Figure 3-55: Stringer longitudinal normal stress contour, Test Run #45 Failure 3

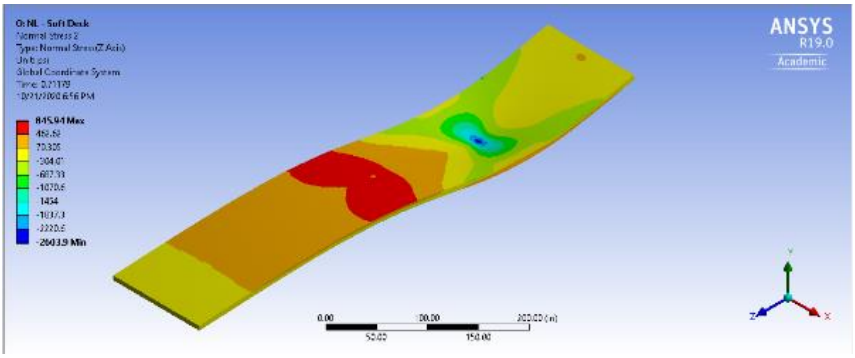

Figure 3-56: Deck longitudinal normal stress contour, Test Run #45 Failure 3

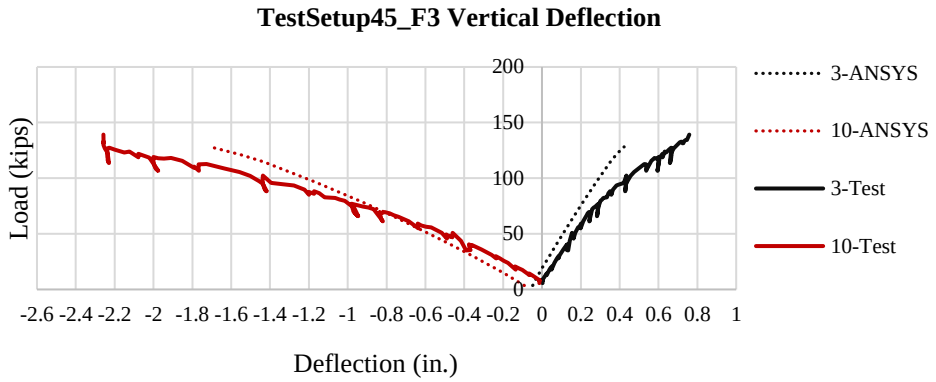

Figure 3-57: Comparison of FEA and measured vertical deflections, Test Run #45 Failure 3

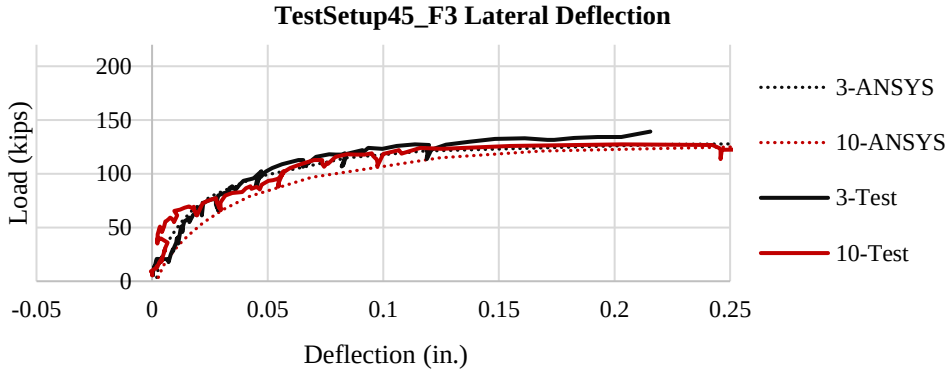

Figure 3-58: Comparison of FEA and measured lateral deflections, Test Run #45 Failure 3

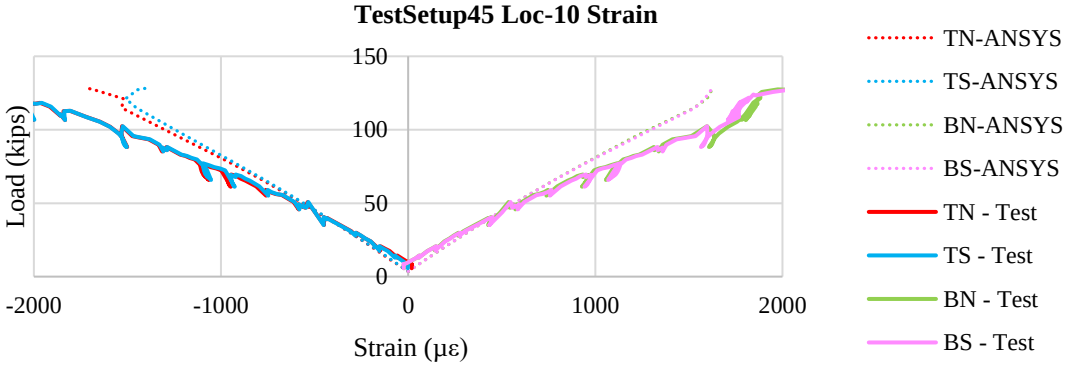

Figure 3-59: Comparison of FEA and measured axial strains, Loc. 10, Test Run #45 Failure 3

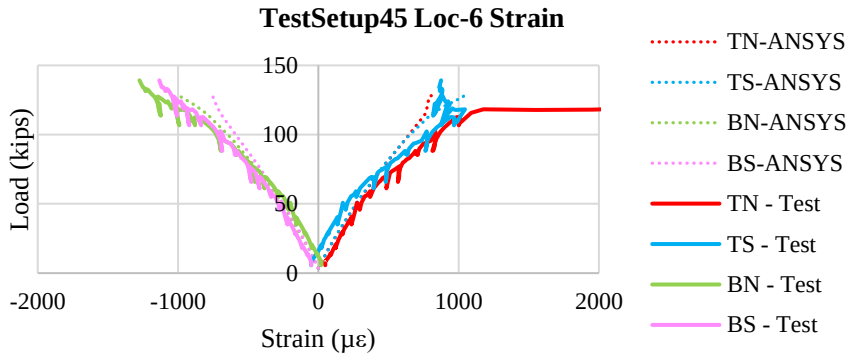

Figure 3-60: Comparison of FEA and measured axial strains, Loc. 6, Test Run #45 Failure 3

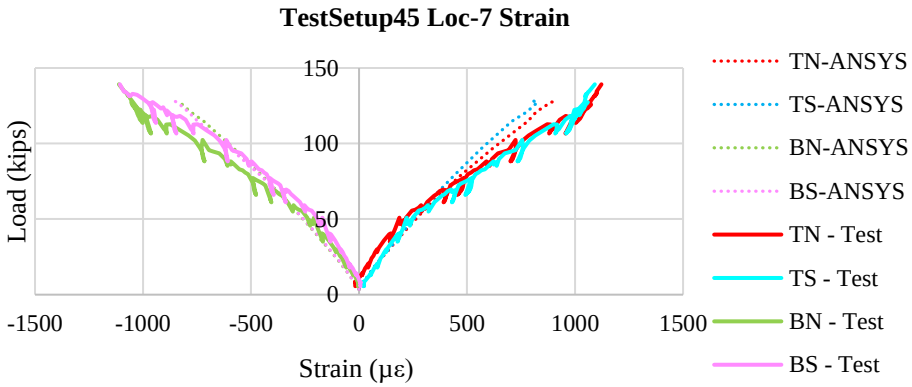

Figure 3-61: Comparison of FEA and measured axial strains, Loc. 7, Test Run #45 Failure 3

3.7.2 Two Spans Loaded Case

FEA results agreed reasonably well with the test data. **Figure 3-62** and **Figure 3-63** are FEA vertical deflection contours subject to a peak load of 122.8 kips in the stringers and the deck, respectively. **Figure 3-64** shows the FEA lateral deflection contours, and **Figure 3-65** and **Figure 3-66** present longitudinal FEA stress contours in the stringers and the deck. The test results are provided in **Figure 3-67** to **Figure 3-73**. The FEA results are generally comparable with the test data and allowed to predict the stringer flexural strength.

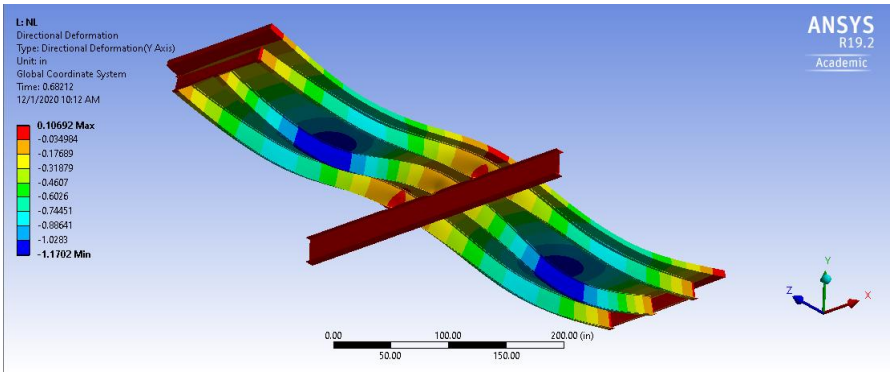

Figure 3-62: Stringer vertical deflection contour, Test Run #46

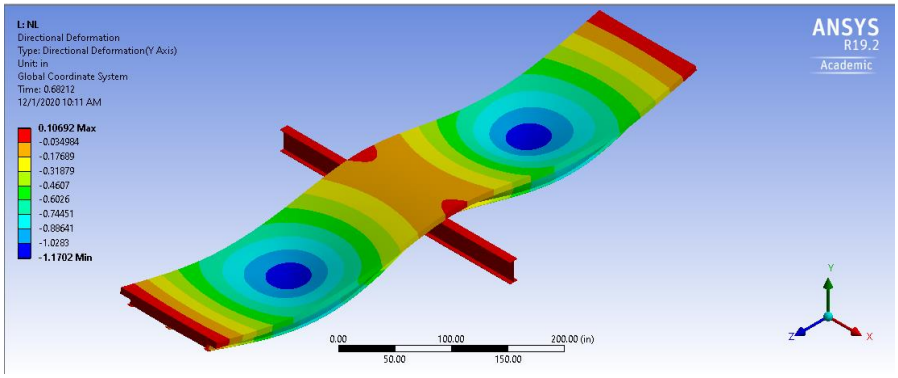

Figure 3-63: Deck vertical deflection contour, Test Run #46

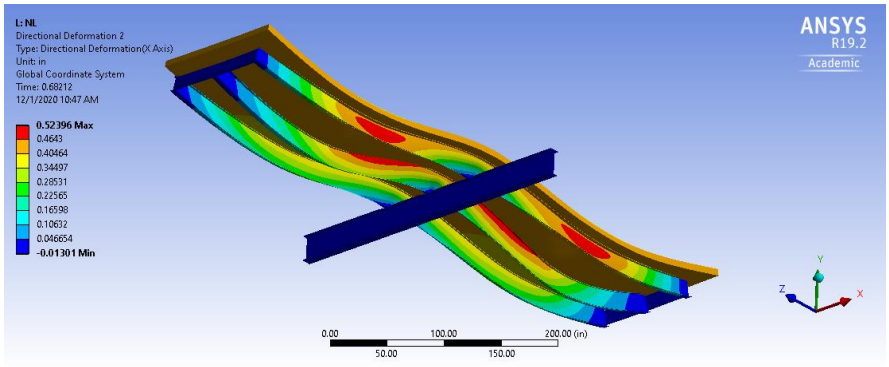

Figure 3-64: Lateral deflection contour, Test Run #46

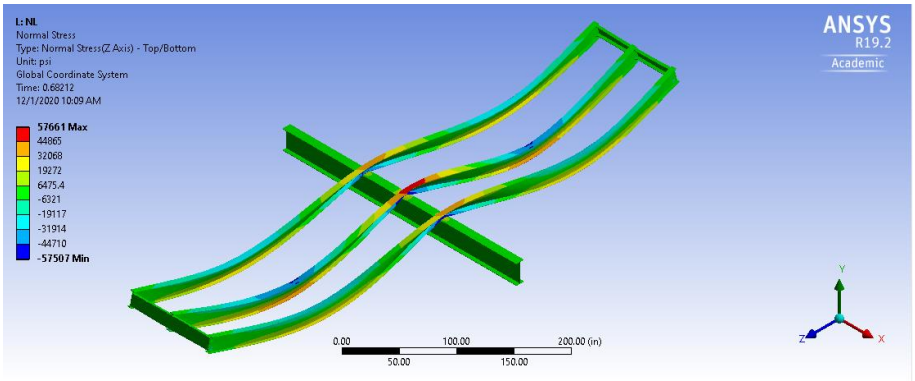

Figure 3-65: Stringer longitudinal normal stress contour, Test Run #46

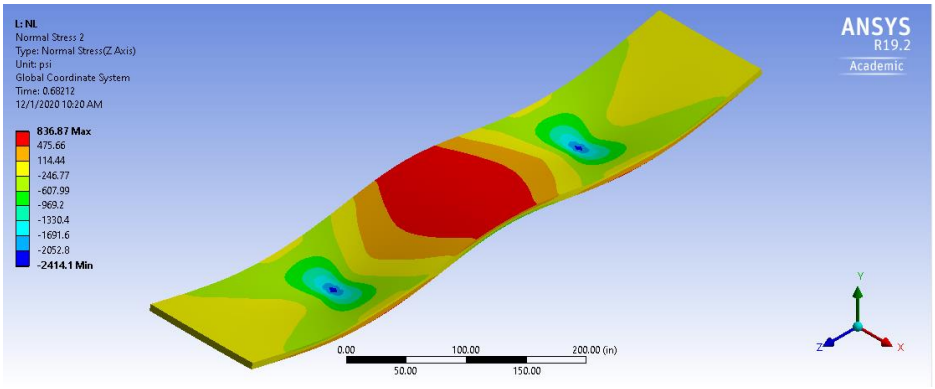

Figure 3-66: Deck longitudinal normal stress contour, Test Run #46

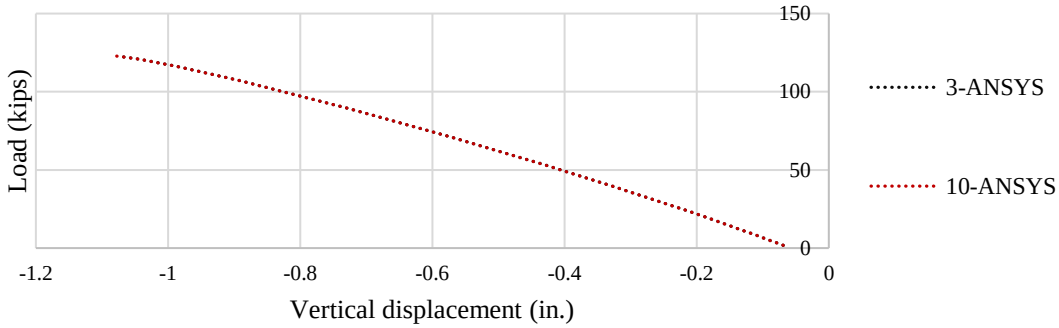

Figure 3-67: ANSYS vertical deflection results, Test Run #46

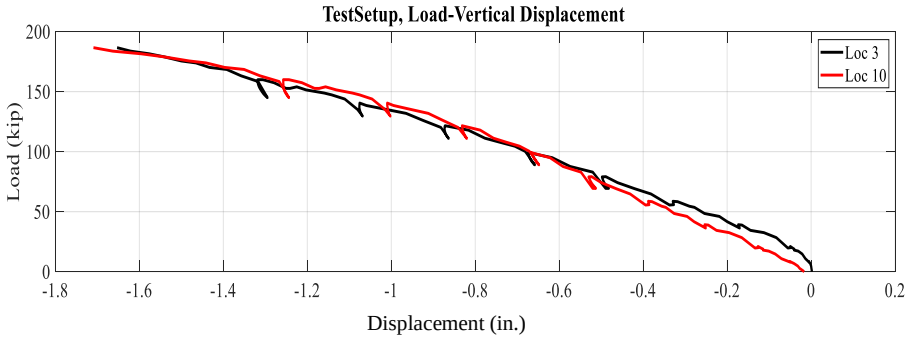

Figure 3-68: Lab test vertical deflection results, Test Run #46

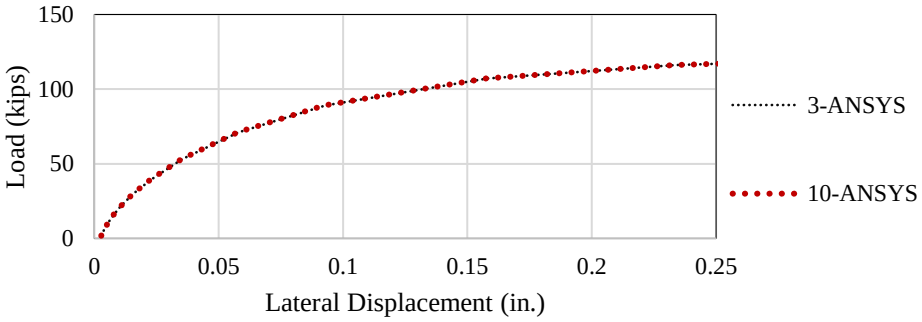

Figure 3-69: ANSYS lateral deflection results, Test Run #46

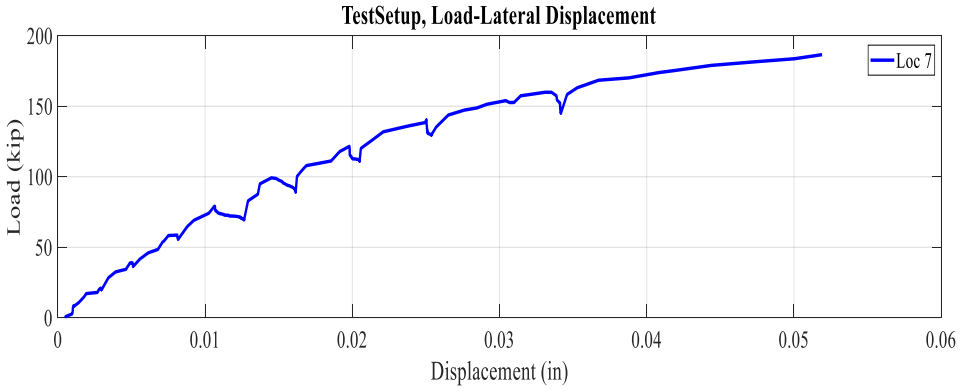

Figure 3-70: Lab test lateral deflection results, Test Run #46

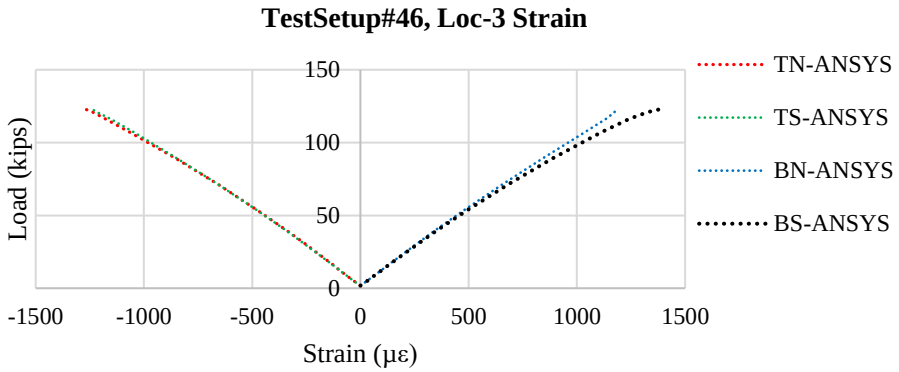

Figure 3-71: ANSYS applied load versus measured longitudinal strains results, Test Run #46

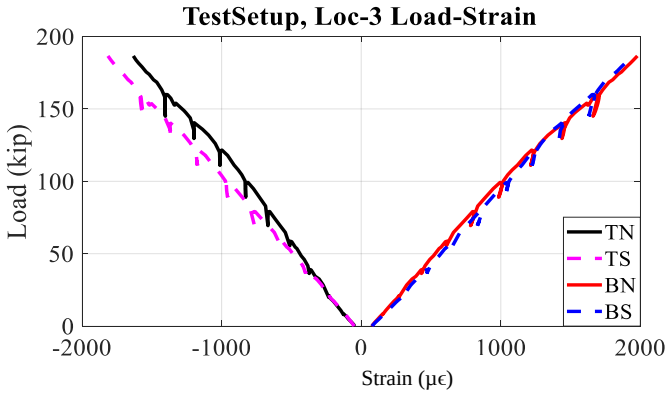

Figure 3-72: Lab test applied load versus measured longitudinal strains results, Test Run #46

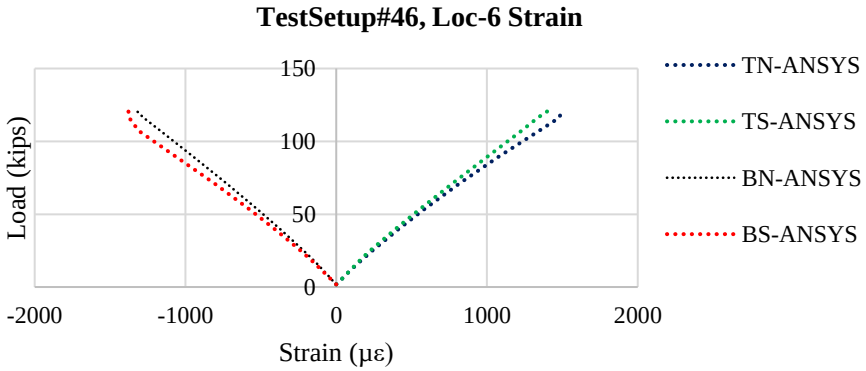

Figure 3-73: ANSYS applied load versus measured longitudinal strains, Test Run #46

CHAPTER 4

LAB TESTING FINDINGS

For discussion purpose, **Table 4-1** is extracted from **Table 3-1** by showing Group I tests only. The tests accounted for both rigid and flexible interior supports. The stringer's top flanges were unbraced and the stringer's bottom flanges were either unbraced or braced at the floorbeam. The loads were applied at one span or both spans [74].

Table 4-1: Group I test matrix

Test setup	NC or C	Description of boundary conditions				
		Interior support at center beam	Top flange of stringer	Bottom flange of stringer	*Test Runs*	*Test Count*
No. 1	NC	Rigid	Unbraced	Unbraced	*1 point* load	*1*
					2 point load	*2*
No. 1A				Braced laterally by bolts	*1 point* load	*3*
					2 point load	*4*
No. 1B		Flexible		Unbraced	*1 point* load	*5*
					2 point load	*6*
No. 1C				Braced laterally by bolts	*1 point* load	*7*
					2 point load	*8*

4.1.1 Effect of Connections between the Stringer and Floorbeam

Figure 4-1 illustrates the effect of the stringer to floorbeam's fixity for Test Runs #1 to 8. As expected, when the stringer's bottom flanges were braced with the floorbeam, the stringers exhibited higher buckling loads as compared to those unbraced cases.

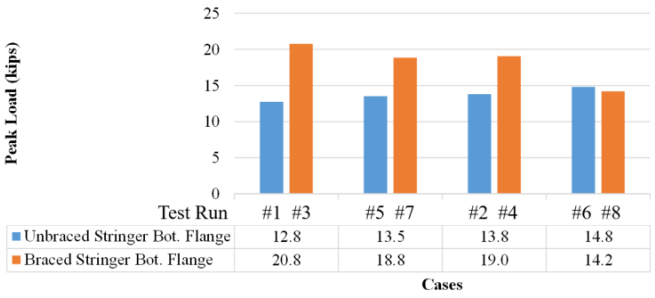

Figure 4-1: Effect of stringer to floorbeam fixity on loading capacity

4.1.2 Effect of Floorbeam Stiffness

Figure 4-2 illustrates the effect of the floorbeam's relative stiffness on the observed response for Test Runs #1 to 8. A flexible floorbeam results in approximately 10% difference for LTB resistance for most cases and increases the maximum vertical displacement.

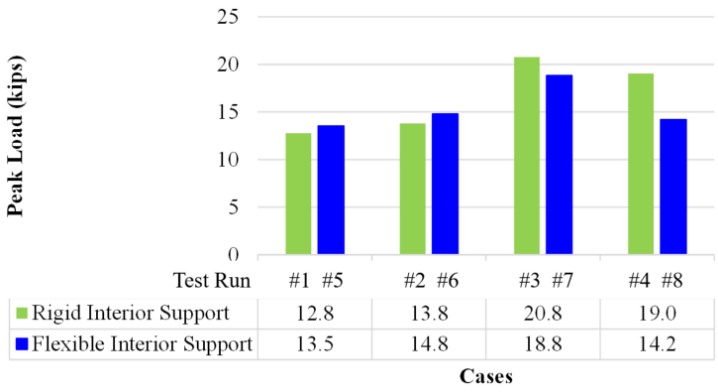

Figure 4-2: Effect of floorbeam's relative stiffness on loading capacity

4.1.3 Bracing Effect of Intermediate Steel Diaphragms

Intermediate steel diaphragms were installed at various locations in Group II test setups to study their effect on LTB resistance. **Figure 4-3** illustrates the buckling load capacities for unbraced lengths between 12 and 24 ft. The interior stringer is loaded at

mid-span of one or both spans and the stringer is bolted to the floorbeam. **Figure 4-4** is similar in comparison when the stringer's bottom flange is not bolted to the floorbeam. Both figures confirm that larger unbraced lengths correspond to reduced buckling loads as expected.

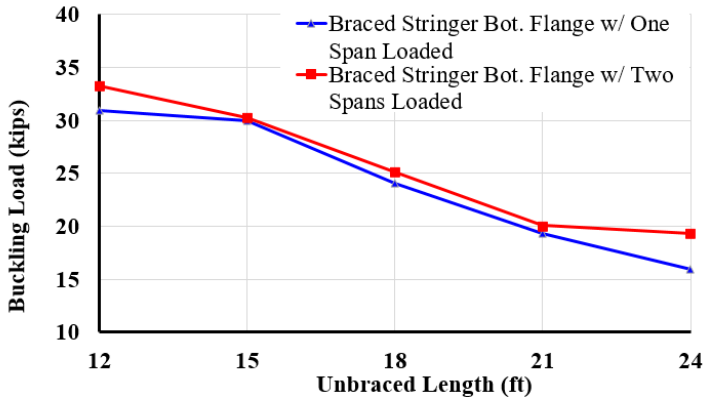

Figure 4-3: Intermediate steel diaphragm effect on LTB, stringer bolted to floorbeam

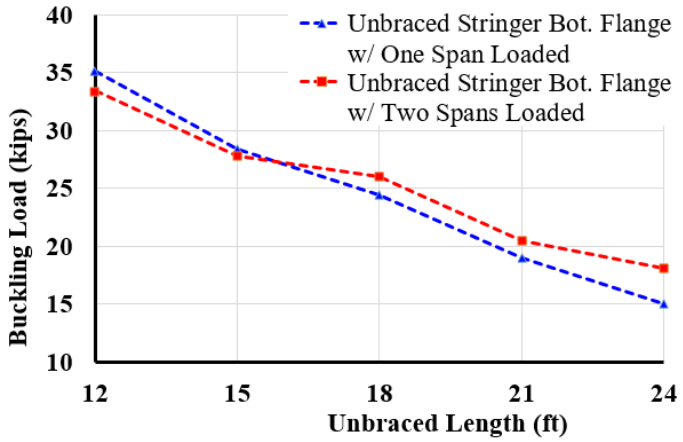

Figure 4-4: Intermediate steel diaphragm effect on LTB, stringer unbolted to floorbeam

4.1.4 Bracing Effect of Timber Ties

Group III tests were of the grillage system braced by timber ties (4" x 4") and installed on the stringer's top flanges using C-clamps. **Table 4-2** lists the descriptions of

Test Run (TR) Nos. 2, and 29 to 32 that are subject to loading at both spans. **Figure 4-5** and **Figure 4-6** show the load-vertical and load-lateral deflection plots. Use of timber ties at the mid-span (TR #29) can nearly double the loading capacity as compared to the baseline (TR #2). When the stringer is braced at its mid-span (TR #29), the bracing effect is more effective as compared to TR #30 (ties spaced at L/3). The bracing effects of the ties in TRs #31 (ties spaced at L/4) and #32 (ties spaced at L/5) are nearly the same.

Table 4-2: Descriptions of Test Run Nos. 2, and 29 to 32 that are subject to loading at both spans

A.1 Test Run No.	Description of boundary conditions			
	Floorbeam relative stiffness	**Stringer top flange bracing**		**Stinger bottom flange bracing**
2	Rigid	Unbraced		Unbraced
29	Rigid	Timber ties (4"x4"), connected using C-clamps	Spaced at L/2	Unbraced
30	Rigid		Spaced at L/3	Unbraced
31	Rigid		Spaced at L/4	Unbraced
32	Rigid		Spaced at L/5	Unbraced

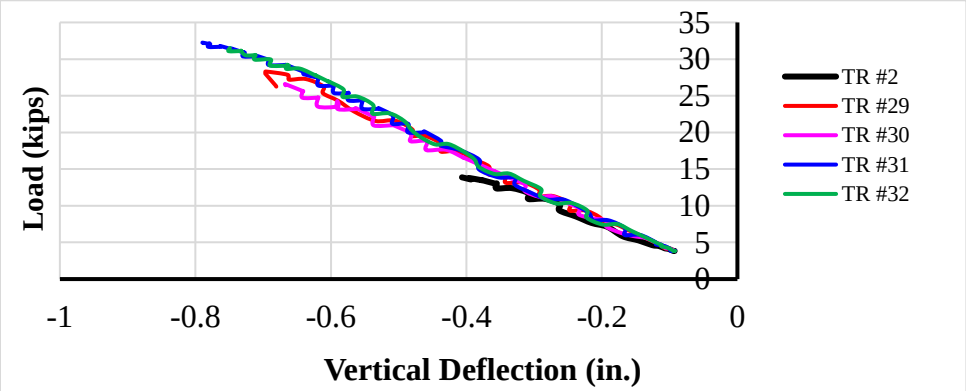

Figure 4-5: Load-vertical deflection plot

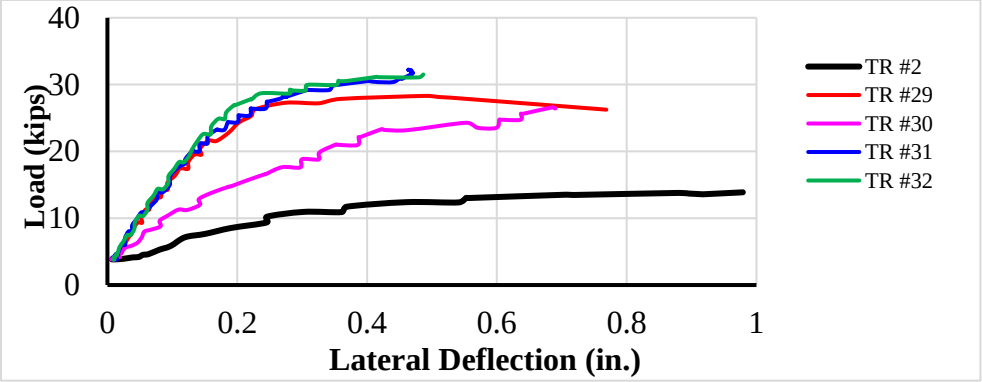

Figure 4-6: Load-lateral deflection plot

The bracing effect of the timber ties is evaluated for a number of test runs involving either rigid or flexible interior supports, as shown in **Figure 4-7** and **Figure 4-8**. These figures plot the buckling loads versus timber tie spacing. Group III test results show that the LTB resistance can be increased significantly using minimal lateral stiffness provided by 4 in. by 4 in. timber ties and C-clamps. For example, buckling load increased by approximately 70% for all tests when timber ties were provided only at the mid-span.

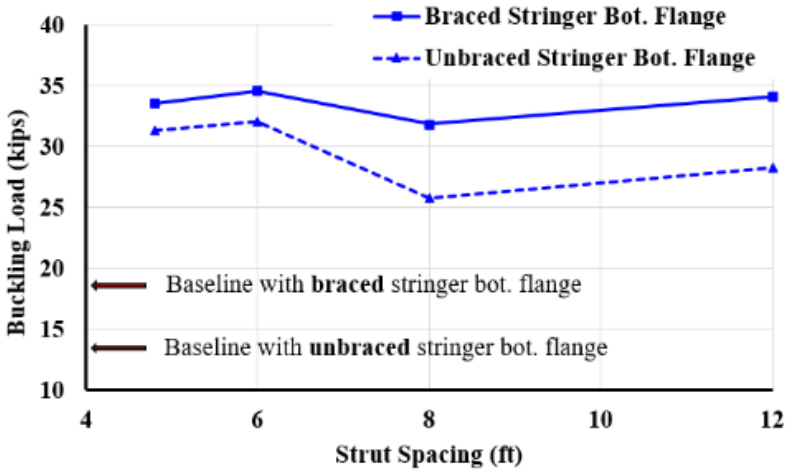

Figure 4-7: Bracing effect of timber ties with rigid interior support

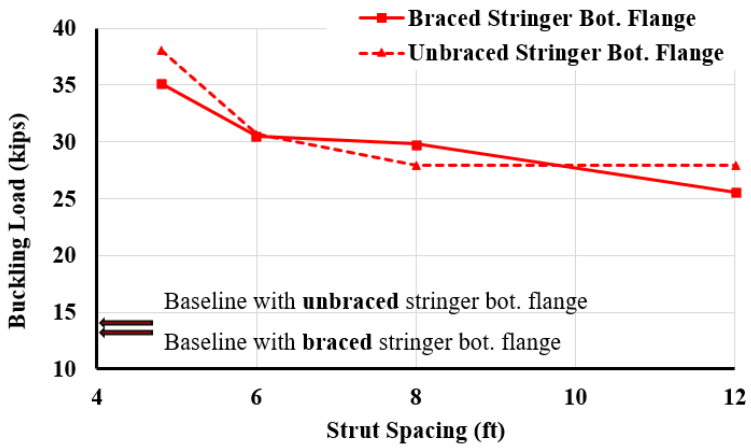

Figure 4-8: Bracing effect of timber ties with flexible interior support

4.1.5 Bracing Effect of Non-composite Concrete Deck

Test Runs #57, 45, 81, and 69 were loaded at Loc. 3 and accounted for various floorbeam's relative stiffness and stringer to the floorbeam's connection conditions as shown in **Table 4-3.** Load-vertical deflection and load-lateral deflection at critical locations were compared for these test runs to an applied load of approximately 80 kips. These comparisons are conducted to study the effects due to the floorbeam's relative stiffness and stringer to the floorbeam's connection conditions (**Figure 4-9** and **Figure 4-10**). As predicted, the maximum vertical deflections increased substantially with a flexible floorbeam. Tests where stringers were not bolted to the floorbeam produced slightly increased maximum vertical deflections when compared to the bolted cases, irrespective of the floorbeam's relative stiffness. **Figure 4-11** to **Figure 4-13** provide the strain diagrams at interior stringer Locations, 3, 6, and 7 at a load of around 80 kips. It can be observed that neutral axis's locations remain constant for the tests. Strains at the stringer's top and bottom flanges are not entirely the same, indicating the existence of small axial strains as a result of possible friction between the stringers and the deck.

Table 4-3: Test Run #57, 45, 81, and 69

Test Run No.	Floorbeam relative stiffness	Stringer to floorbeam connection
57	Rigid	Bolted
45		Unbolted
81	Flexible	Bolted
69		Unbolted

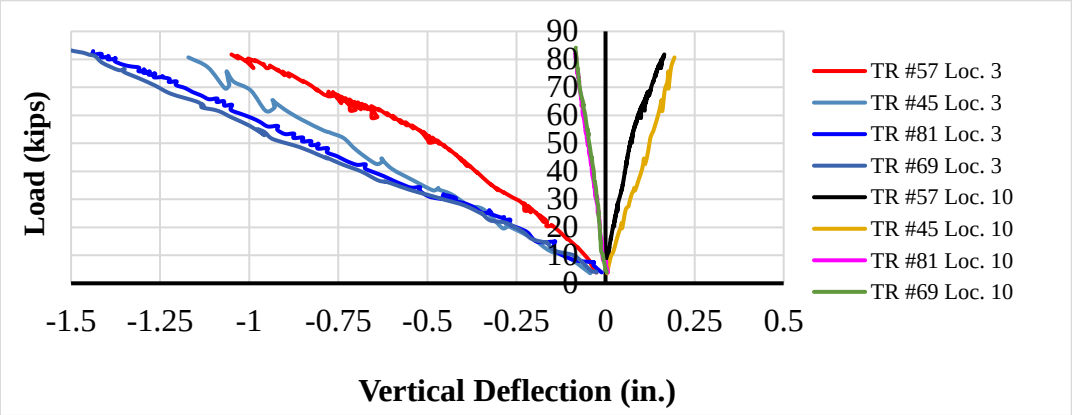

Figure 4-9: Vertical displacement at Loc.3 in Group IV tests

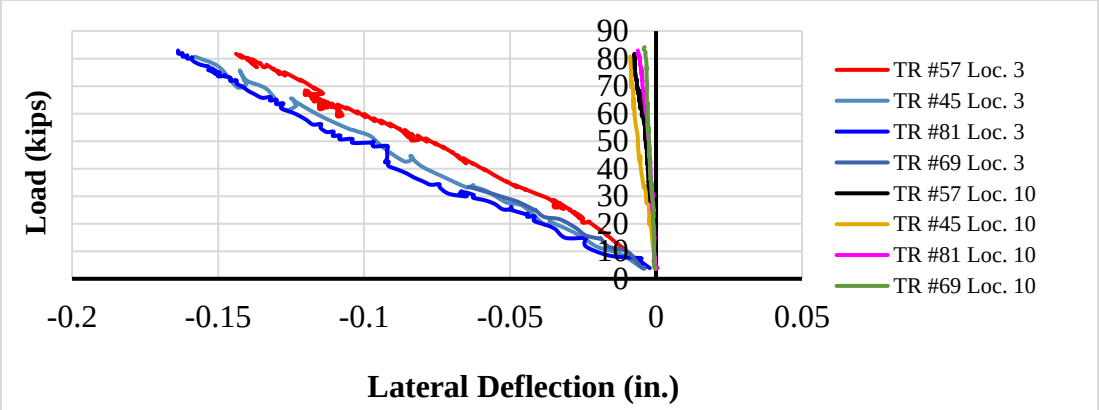

Figure 4-10: Lateral displacement at Loc. 3 in Group IV tests

Note: Lateral deflection of TR #69 at Loc. 3 not recorded after load exceeded 33.4 kips, LVDT slipped.

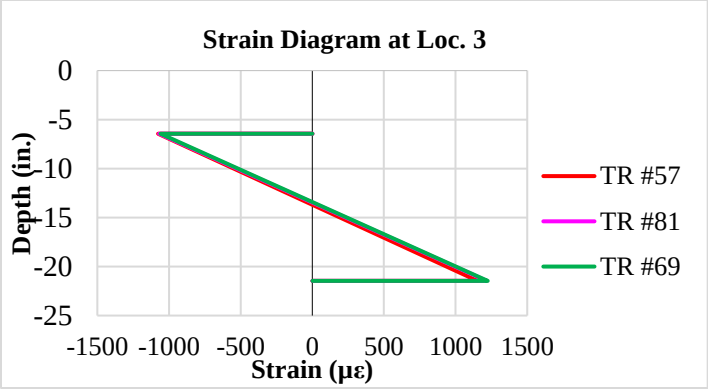

Figure 4-11: Strain diagrams at Loc. 3 due to 82 kips

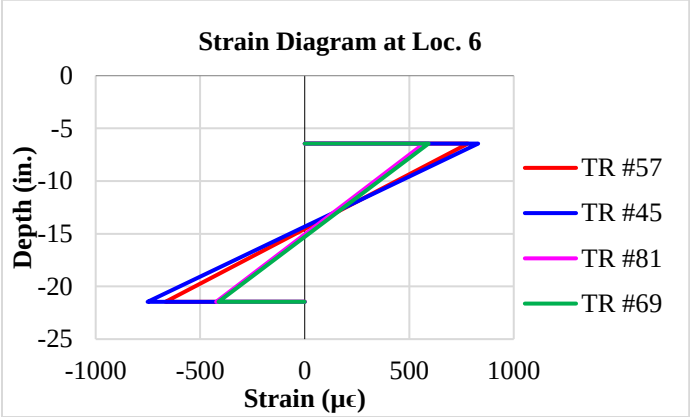

Figure 4-12: Strain diagrams at Loc. 6 due to 82 kips (Load at Loc. 3)

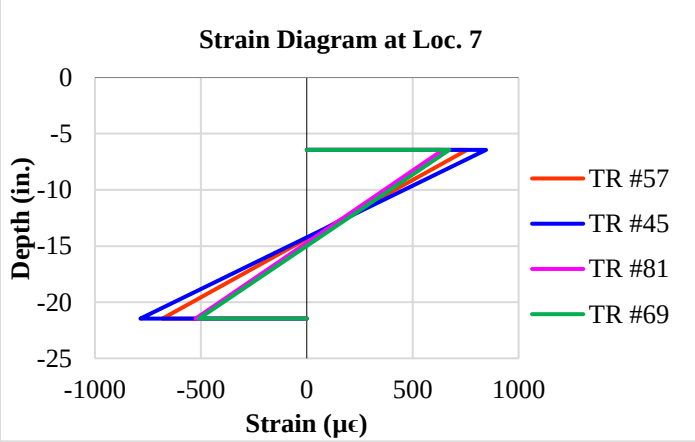

Figure 4-13: Strain diagrams at Loc. 10 due to 82 kips (Load at Loc. 3)

A diagram of the primary bending moment, M_x, including the deck and spreader beam weights, is plotted at an applied load of 82 kips in **Figure 4-14**. The primary bending moments, M_x, at the interior stringer were determined from measured strains at critical sections and compared to an elastic analysis from RISA-3D. These comparisons were performed to study the effect of the floorbeam's relative stiffness and stringer to the floorbeam's connection conditions. Findings indicate that analysis results mostly matched the measured values:

1. Strains and M_x in Test Run #45 are noticeably larger than Test Run #57.
2. Strains and M_x in Test Run #69 (flexible/unbraced) are slightly larger than Test Run #81 (flexible/braced) under the same loading.
3. Maximum positive M_x in Test Run #81 (flexible/braced) is larger than Test Run #57 (rigid/braced) under the same loading. Similarly, maximum negative M_x in Test Run #81 (flexible/braced) is smaller than Test Run #57 (rigid/braced) under the same loading.
4. Nearly same M_x is observed in Test Run #81 (flexible/braced) and Test Run #69 (flexible/unbraced).

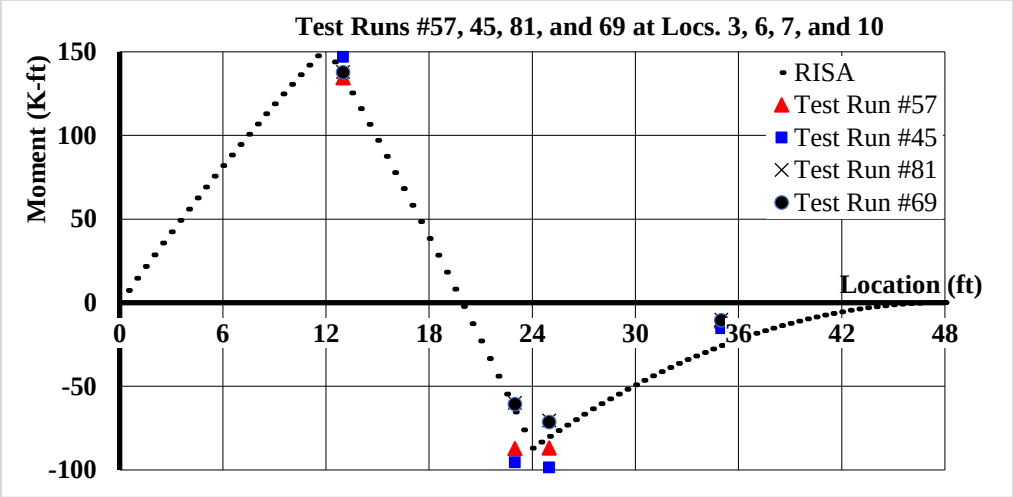

Figure 4-14: Measured and modeled interior stringer M_x diagrams at an applied load of 82 kips

4.1.6 Moment Gradient Factor

One Span Loaded Case

When *AASHTO LRFD Bridge Design Specifications* (2020) are followed for an unbraced length of 24 ft. and using a moment gradient factor of 1.0, the flexural resistance of the stringer is 45.1 kip-ft. **Figure 4-15** compares the primary bending moments, M_x, from the elastic analysis and test data at an applied load of 118.2 kips. Loc. 6 exhibited LTB at 118.2 kips, which resulted in a flexural strength of 122.9 kip-ft. The ratio of these flexural strengths is 2.73, which corresponds to C_b. From total of three test runs that was performed for Test Run #45, it was concluded that C_b varies from 2.34 to 2.73 [1].

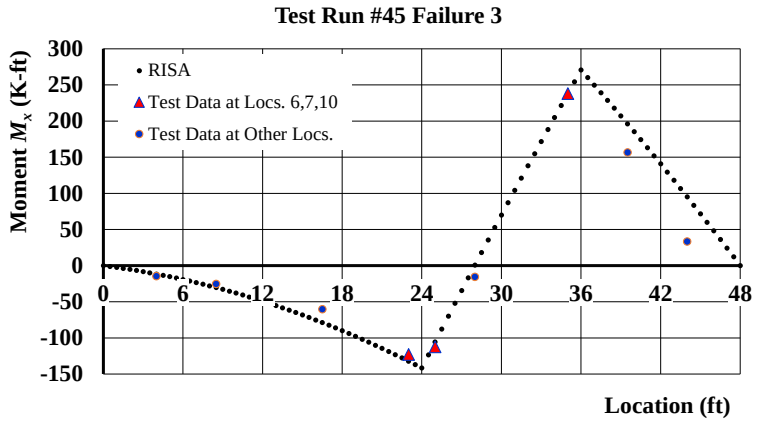

Figure 4-15: Measured and modeled interior stringer M_x diagrams at an applied of 118.2 kips

Two Spans Loaded Case

Figure 4-16 and **Figure 4-17** show the strain diagrams at Loc. 3 and 10 subject to the maximum load of 186.6 kips. Both sections had comparable strain readings and their strains at the flange top and bottom reached the yield strain.

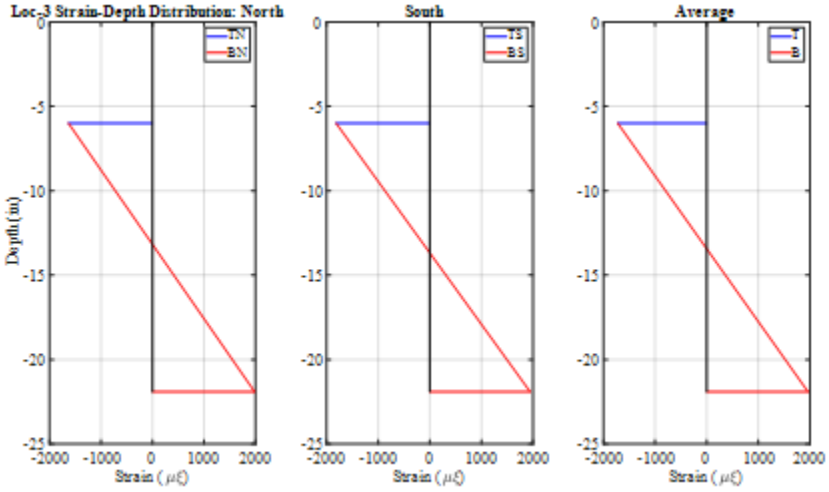

Figure 4-16: Strain diagrams, Loc. 3, maximum load of 186.6 kips at each span

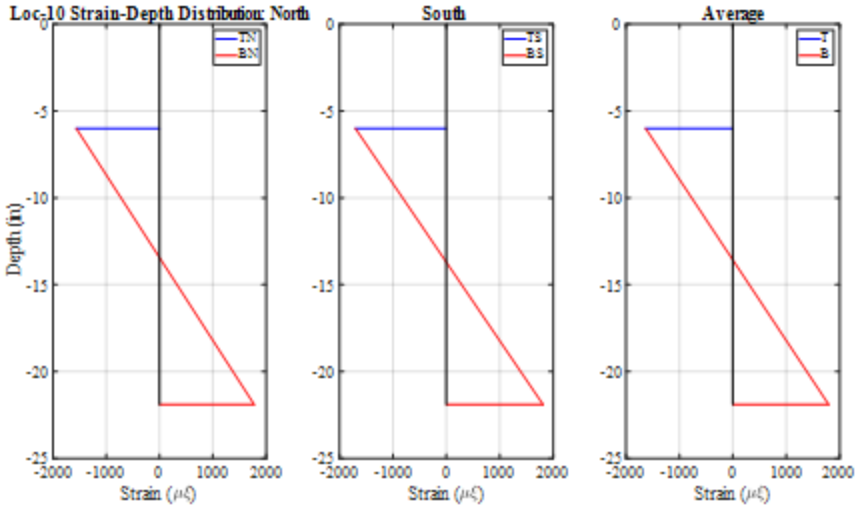

Figure 4-17: Strain diagrams, Loc. 10, maximum load of 186.6 kips at each span

Figure 4-18 presents a M_x diagram based on an elastic analysis of the whole structure subject to 100 kips at each span. The load of 100 kips was selected for discussion purpose. It shows that the critical positive moment is about 22% higher than the moment at Loc. 3. Similarly, the critical negative moment is approximately 18% higher than the moment at Loc. 6. Also, the critical negative moment is about 20% larger than the critical positive moment. **Figure 4-16** shows that Loc. 3 reached the yield moment subject to the peak load, indicating that the critical positive moment section reached plastic moment.

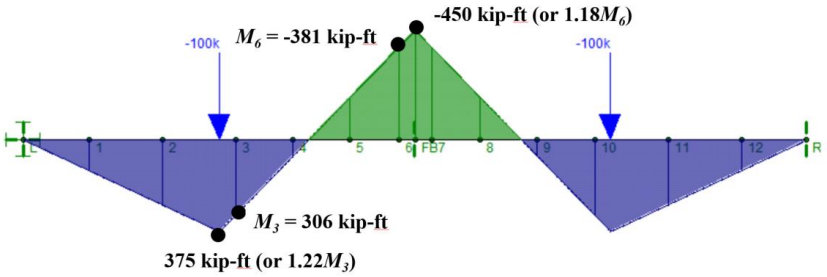

Figure 4-18: M_x diagram, 100 kips at each span

Figure 4-19, shows that Loc. 6 has not reached yielding at maximum load of 186.6 kips and indicate a flexural strength of 159.7 kip-ft. Flexural strength at critical negative moment section is 188.4 kip-ft corresponding to C_b of 4.17.

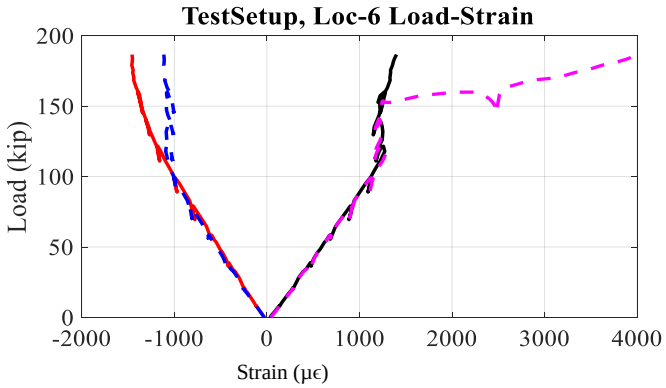

Figure 4-19: Lab test results - Applied load versus measured longitudinal strains, Test Run #46

CHAPTER 5

CONCLUSIONS

Finite difference method was used to obtain a theoretical solution for continuous stringers without any bracings. Finite element models were created and calibrated to match the lab test results to examine the LTB resistance of a two-span structure. Various types and locations of bracings were studied on their effects on the LTB resistance, including the steel diaphragms, timber ties, and non-composite concrete deck. Also, both braced and unbraced (bolted and unbolted) conditions were investigated at the stringer's bottom flange on the floorbeam. In addition, both rigid and flexible floorbeam conditions were evaluated. The following conclusions are drawn:

1. The concrete deck braces the positive moment section of a stringer; therefore, the non-composite plastic moment may be used for the stringer's nominal strength in load rating. The negative moment section, however, should account for the LTB resistance subject to either one or two span load case. Comparisons between the measured flexural strength and predicted strength from the *AASHTO LRFD Bridge Design Specifications* were completed to identify the moment gradient factor. The moment gradient factor can be

determined using the following equation proposed by Yura and Helwig (2010) and included in the Commentary C-F1-5 of the AISC (2017):

$$C_b = 3.0 - \frac{2}{3}\left(\frac{M_1}{M_0}\right) - \frac{8}{3}\left[\frac{M_{CL}}{(M_1 + M_0)}\right] \qquad \textbf{Eq. 1-17}$$

The equation above results in comparable moment gradient factors with the lab testing data and FEA results. The bracing effect of deck is significant in increasing the LTB resistance of the stringer, which results in a moment gradient factor appreciably larger than 1.0.

2. In comparison with the test runs using a rigid interior support, the test setups including a flexible interior support resulted in a larger positive moment and a smaller negative moment at the critical sections. Therefore, when the floorbeam is flexible, it is conservative to calculate C_b assuming a rigid interior support.

3. Nearly the same primary bending moment is observed in flexible test runs, irrespective of stringer to floorbeam connection fixity. Hence, it is recommended to use the full span length as the unbraced length in both braced and unbraced cases at interior support.

4. Compared to no top bracing test runs, timber bracing increased the flexural strength by approximately 70% when located at midspan, and non-composite deck increased by approximately by 300%.

5. Use of the proposed moment gradient factor allows to increasing the load ratings of continuous stringers substantially. Implementation of the recommended method is

demonstrated using one representative bridge, which shows the benefits of using an increased moment gradient factor (See **Appendix A**).

APPENDIX A

IMPLEMENTATION

One of the representative bridges was taken as an example to show how the proposed moment gradient factor can be implemented in load rating. A four-span unit of the bridge superstructure was selected in the analysis and an interior stringer, a W21 x 68, was load rated for HL-93 (Inventory rating). Floorbeams are spaced at approximately 24 ft. – 8 5/8 in. and the stringers are spaced at 7 ft. – 6 in. A36 steel is used. (See **Figure A-1** and **Figure A-2**).

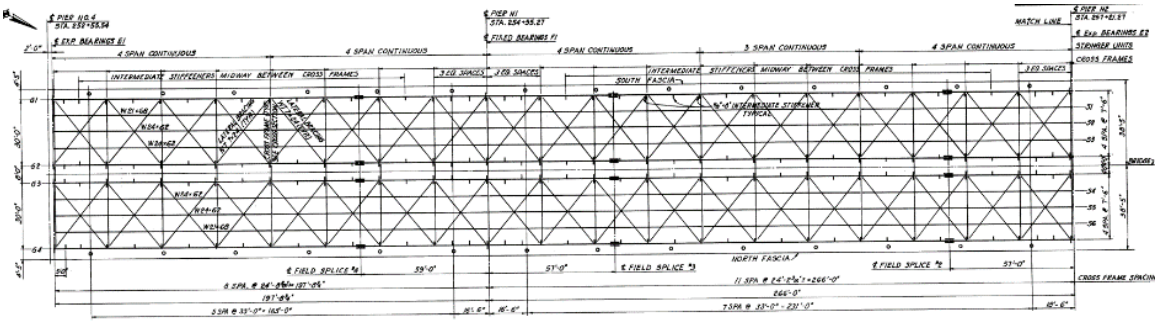

Figure A-1: Framing plan, Bridge No. 610065

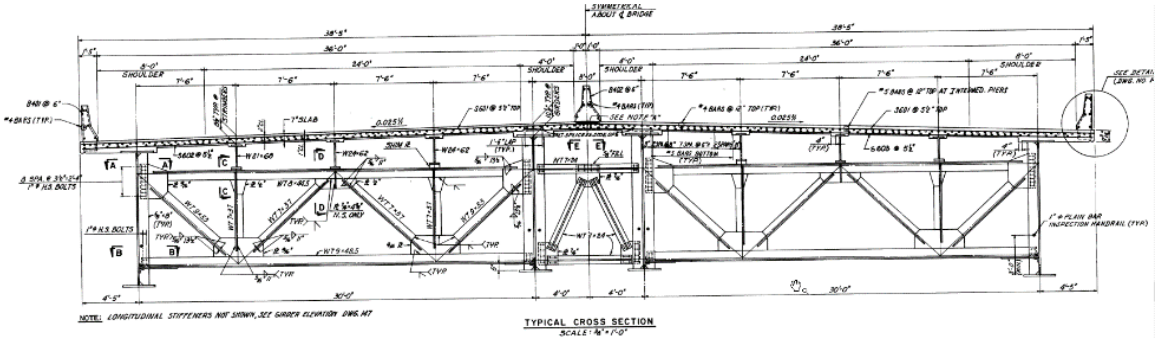

Figure A-2: Cross section, Bridge No. 610065

C_b and Flexural Resistance in Accordance with the AASHTO LRFR

The AASHTO LRFD Specifications Art. A6.3.3 was followed to determine the flexural strength of the stringers when AASHTOWare BrR [75] was used for load rating. Excel spreadsheets were developed to perform the rating using the proposed C_b.

Both moment envelope and concurrent moment approaches were examined for live load analysis. **Figure A-3** shows the unfactored moment envelope due to HL-93, in which a pair of design tandems and a design lane load controlled over other live loads. The maximum negative moment at the first interior floor stringer is -181.5 Kip-ft. **Figure A-4** plots the concurrent moment under HL-93 matching the maximum negative moment in **Figure A-3**. As a result, both moment envelope and concurrent moment approaches were used to determine moment gradient coefficients and corresponding load rating factors. Inventory load rating factors under HL-93 are determined using AASHTOWare BrR and Excel spreadsheets assuming the full stringer span as the unbraced length. **Table A-1** and **Table A-2** were created using factored dead load, and live loads. **Table A-3** presents C_b calculation for the recommended Yura and Helwig (2010) equation.

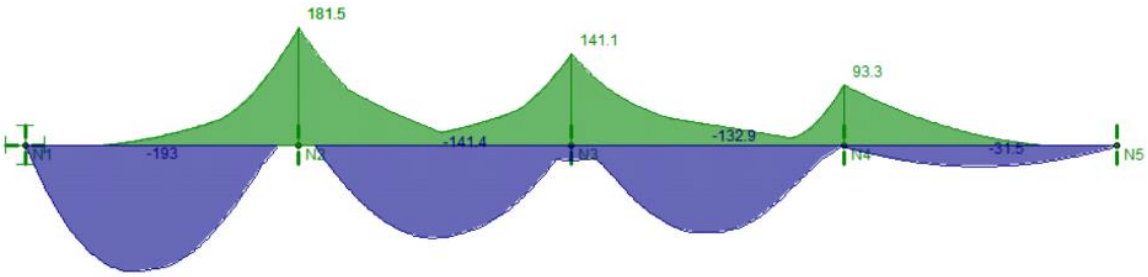

Figure A-3: Unfactored moment envelope due to HL-93 (unit in Kip-ft.)

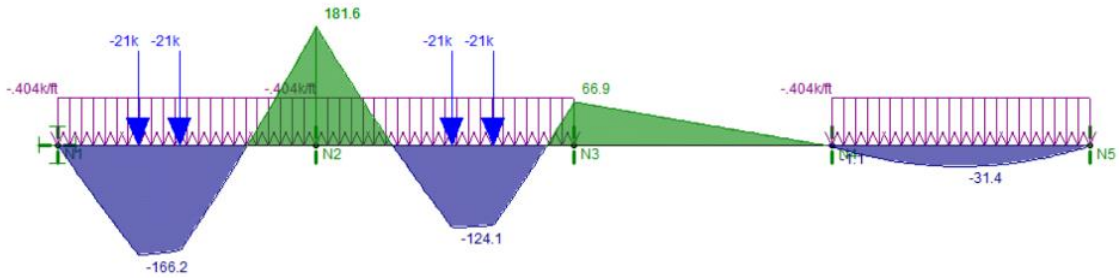

Figure A-4: Unfactored concurrent moment due to HL-93 (unit in Kip-ft.)

Table A-1: List of moment from BrR using moment envelope approach

		End span		Interior span	
		Unfactored	Factored	Unfactored	Factored
M_0	DL	-48.7	-60.9	-48.7	-60.9
	LL	-176.8	-309.4	-176.8	-309.4
	Total		-370.3		-370.3
M_{CL}	DL	32.5	40.6	16.2	20.3
	LL	0.0	0.0	0.0	0.0
	Total		40.6		20.3
M_1	DL			-32.5	-40.6
	LL			-158.2	-276.9
	Total		0.0		-317.5

Table A-2: List of moment from RISA using concurrent moment approach

		End span		Interior span	
		Unfactored	Factored	Unfactored	Factored
M_0	DL	-48.7	-60.9	-48.8	-60.9
	LL	-176.6	-309.1	-176.6	-309.1
	Total	0.0	-370.0		-370.0
M_{CL}	DL	32.5	40.6	16.2	20.3
	LL	142.8	249.9	105.0	183.8
	Total		290.5		204.1
M_1	DL			-32.5	-40.6
	LL			-65.3	-114.3
	Total		0.0		-154.9

Table A-3: C_b calculations using Yura and Helwig (2010)

		Moment Envelope $L_b = L$				Concurrent Moment $L_b = L$	
		End Span	Interior Span			End Span	Interior Span
M_0		-370.3	-370.3	M_0		-370.0	-370.0
M_1		0.0	-317.5	M_1		0.0	-154.9
M_{CL}		40.6	20.3	M_{CL}		290.5	204.1
$M_1 + M_0$		-370.3	-687.8	$M_1 + M_0$		-370.0	-524.9
Yura and Helwig	C_b	3.3	2.5	Yura and Helwig	C_b	5.1	3.8

Table A-4 lists moment gradient factors using moment envelope and concurrent moment approaches, which follow either the AASHTO LRFD Specifications Art. A6.3.3, or the proposed approach similar to Yura and Helwig (2010). As shown in, the moment gradient factor is increased when the proposed C_b is used and the load rating factor is increased accordingly. Furthermore, the concurrent moment approach allows for an increased C_b as compared to the moment envelope approach.

Table A-4: Moment gradient and load rating factors

	Follow LRFD Art. A6.3.3		Yura and Helwig (2010)	
	Moment Envelope	Concurrent moment	Moment Envelope	Concurrent moment
C_b	1.12*	1.36	2.51	3.76
Rating Factor	0.37*	0.49	1.06	1.26

Note: 1.12* and 0.37* from AASHTOWARE BrR software

APPENDIX B

THEORETICAL SOLUTION

One Span Loaded

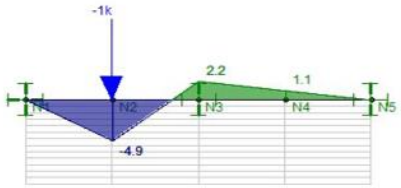

C_b Calculation - AISC

$$C_b = \frac{12.5M_{max}}{2.5M_{max} + 3M_1 + 4M_2 + 3M_3}$$

LHS Span		RHS Span	
M_max =	4.9 k-ft	M_max =	2.2 k-ft
M1 =	2.45 k-ft	M1 =	1.65 k-ft
M2 =	4.9 k-ft	M2 =	1.1 k-ft
M3 =	1.35 k-ft	M3 =	0.55 k-ft
C_b =	**1.42**	C_b =	**1.67**

Two Spans Loaded

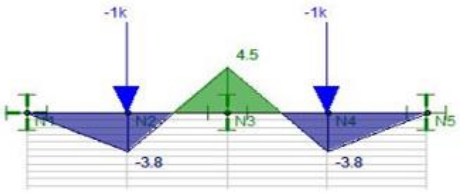

M_max =	4.5 k-ft
M1 =	1.9 k-ft
M2 =	3.8 k-ft
M3 =	0.35 k-ft
C_b =	**1.69** (similar for both spans)

	When a load is applied at the top flange:		
	y/h	-0.5	
	1.4*(2y/h)	0.714	
	Mn for uniform M case (Cb=	45.1	k-ft
	LAB TESTING (Load Applied at Top Flange)		
	TB #19		
	Max. P =	15.67	K
	Mn	**76.8**	k-ft
	Cb	**1.70**	
	TB #20		
	Max. P =	19.17	K
	Mn	**72.8**	k-ft
	Cb	**1.62**	
	FDM (Load Applied at Shear Center)		
	One span loaded		
at shear	Mn	**122.6**	k-ft
	Cb	**1.94**	
at top	Mn	87.536	
	Two spans loaded		
at shear	Mn	**89.0**	k-ft
	Cb	**1.41**	
at top	Mn	63.571	

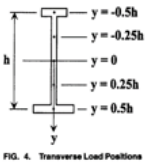

FIG. 4. Transverse Load Positions

be applicable to singly symmetric sections, the method from the SSRC *Guide* (1988) was modified as follows:

$$C_7 = B^{3m}C_s \quad (5)$$

Helwig (1997)

Matrix C =

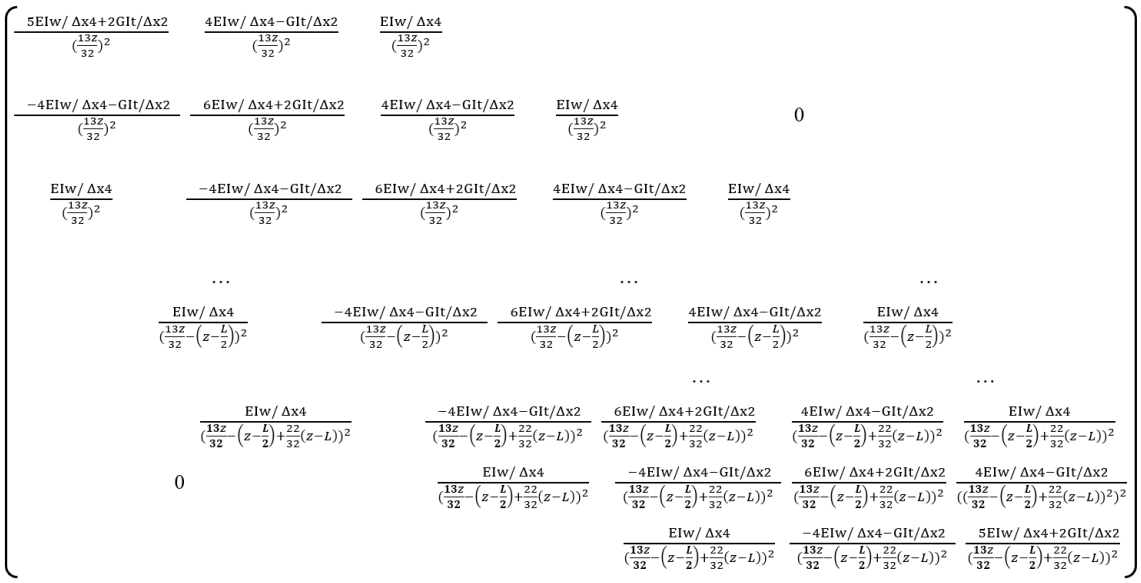

MatLab Codes

Continuous moment

```
%parameters
E = 29000; %modulus elasticity
Iw = 739; %warping constant
G = 11154; %Shear modulus
It = 0.461; %torsional constant
Iy = 12.4; %Minor axis inertia
L=180; %unbraced length
N =100; %dimension of matrix
D=L/(N-1);
a= 6*E*Iw+ 2*G*It*D^2;
b= -4*E*Iw-G*It*D^2;
c = E*Iw;

A = zeros(N,N);

for i = 3:N-2
    A(i,i) = a;
    A(i, i+1) = b;
    A(i, i+2) = c;
    A(i,i-1) = b;
    A(i, i-2) = c;
end

A(1,1) = 5*E*Iw+ 2*G*It*D^2;
A(1,2) = b;
A(1,3) =c;
A(2,1) = b;
A(2,2) = a;
A(2,3) = b;
```

```
A(2,4) =c;
A(N-1,N-3) = c;
A(N-1,N-2) = b;
A(N-1,N-1) = a;
A(N-1,N) = b;
A(N,N-2) = c;
A(N,N-1) = b;
A(N,N) = (5*E*Iw+ 2*G*It*D^2);

[Eigen_vec, Eigen_val] = eig(A);
[val, idx] = sort(diag(Eigen_val));

i = 1;
while i<=length(val)
    if val(i)> 0
        break
    end
    i = i+1;
end
eigval = val(i);
Mcr=sqrt(eigval*E*Iy)/(D^2)

plot(Eigen_vec(:,idx(i)))
hold on
plot(Eigen_vec(:,idx(i+1)))
plot(Eigen_vec(:,idx(i+2)))
plot(Eigen_vec(:,idx(i+3)))
%plot(Eigen_vec(:,idx(i+4)))
%eigval = min(eig(A));

%M= sqrt (eigval*E*Iy)/D^2

%Mcr=sqrt(eigval*E*Iy)/(D^2)
Mocr=pi/L*sqrt(E*Iy*G*It+(pi*E/L)^2*Iy*Iw)
```

Simple span- Point loaded

```
E = 29000; %modulus elasticity
Iw = 739; %warping constant
G = 11154; %Shear modulus
It = 0.461; %torsional constant
Iy = 12.4; %Minor axis inertia
L= 288; %unbraced length
N = 100; %dimension of matrix
%n= 5;
D= L/(N-1);
a= 6*E*Iw/D^4+ 2*G*It/D^2;
b= -4*E*Iw/D^4-G*It/D^2;
c = E*Iw/D^4;

A = zeros(N,N);

for i = 3:N/2
    A(i,i) = a/(i*D*13/32)^2;
    A(i, i+1) = b/(i*D*13/32)^2;
    A(i, i+2) = c/(i*D*13/32)^2;
```

```
    A(i,i-1) = b/(i*D*13/32)^2;
    A(i, i-2) = c/(i*D*13/32)^2;
end

for i=(N/2)+1:N-2
    A(i,i) = a/((13*D*i-16*L)/32)^2;
    A(i, i+1) = b/((13*D*i-16*L)/32)^2;
    A(i, i+2) = c/((13*D*i-16*L)/32)^2;
    A(i,i-1) = b/((13*D*i-16*L)/32)^2;
    A(i, i-2) = c/((13*D*i-16*L)/32)^2;
end
A(1,1) = (5*E*Iw/D^4+ 2*G*It/D^2);
A(1,2) = b;
A(1,3) =c;
A(2,1) = b/(2*D*13/32)^2;
A(2,2) = a/(2*D*13/32)^2;
A(2,3) = b/(2*D*13/32)^2;
A(2,4) =c/(2*D*13/32)^2;
A(N-1,N-3) = c/((13*D*(N-1)-16*L)/32)^2;
A(N-1,N-2) = b/((13*D*(N-1)-16*L)/32)^2;
A(N-1,N-1) = a/((13*D*(N-1)-16*L)/32)^2;
A(N-1,N) = b/((13*D*(N-1)-16*L)/32)^2;
A(N,N-2) = c;
A(N,N-1) = b;
A(N,N) = (7*E*Iw/D^4+ 2*G*It/D^2);

[Eigen_vec, Eigen_val] = eig(A);
[val, idx] = sort(diag(Eigen_val));

i = 1;
while i<=length(val)
    if val(i)> 0
        break
    end
    i = i+1;
end
eigval = val(i);
Pcr=sqrt(eigval*E*Iy*4)

plot(Eigen_vec(:,idx(i)))
hold on
plot(Eigen_vec(:,idx(i+1)))
plot(Eigen_vec(:,idx(i+2)))


Mocr=pi/L*sqrt(E*Iy*G*It+(pi*E/L)^2*Iy*Iw)
```

APPENDIX C

COMMANDS USED IN ANSYS

Link elements

```
!   Commands inserted into this file will be executed just after material
definitions in /PREP7.
!   The material number for this body is equal to the parameter "matid".

!   Active UNIT system in Workbench when this object was created:  Metric (mm, kg,
N, s, mV, mA)
!   NOTE:  Any data that requires units (such as mass) is assumed to be in the
consistent solver unit system.
!                See Solving Units in the help system for more information.


/com,
/com,
/com,
*get, myarea, SECP, MATID, PROP, Area
ET, MATID, 180
KEYOPT, MATID,2,0
KEYOPT, MATID,3,0
KEYOPT, MATID,12,0

MP,EX,MATID,199947.9615
MP,PRXY,MATID,0.3


TB,BISO,MATID,1,2
TBDATA,,4.2E+2,199.9479615


SECTYPE, MATID, LINK
SECDATA, myarea
/com,
/com,
       /com,
```

Shell elements

```
!DENS_ = 7850.0
!EX_ = 2.1E5
EX_ = 199947.9615
NUXY_=0.3

!MP,DENS,MAT_ID,DENS_,
MP,EX,MATID,EX_,
MP,NUXY,MATID,NUXY_,

Yield_strength=3.4474E+2
Tangent_modulus=199.9479615

!TB,BKIN,MAT_ID,1,,0
```

```
TB, BISO, MATID

TBDATA,1,Yield_strength
TBDATA,2,Tangent_modulus
```

Deck

Solid 185

```
EX_ = 2E+4
!X_ = 2E+1
NUXY_=0.2

!MP,DENS,MATID,DENS_,
MP,EX,MATID,EX_,
MP,NUXY,MATID,NUXY_,

ET,MATID, 185
KEYOPT, MATID,2,0
KEYOPT, MATID,3,0
KEYOPT, MATID,6,0
```

CPT 215

```
ET,MATID, 215
KEYOPT, MATID,18,2
```

Microplane

```
!   Commands inserted into this file will be executed just after material
definitions in /PREP7.
!   The material number for this body is equal to the parameter "matid".

!   Active UNIT system in Workbench when this object was created:  Metric (mm, kg,
N, s, mV, mA)
!   NOTE:  Any data that requires units (such as mass) is assumed to be in the
consistent solver unit system.
!                See Solving Units in the help system for more information.


EX_ = 2E+4
NUXY_=0.2

!MP,DENS,MATID,DENS_,
MP,EX,MATID,EX_,
MP,NUXY,MATID,NUXY_,


f_uc = 22.12
f_bc = 25.4384
f_ut = 2.1

r_t = 1
D = 4e4
sigma_c_v = -35
R = 2
gamma_t0 = 0
gamma_c0 = 2e-5
beta_t = 3000
beta_c = 2000
c = 1600
m = 2.5
```

```
TB, MPLA, MATID,,,DPC

tbdata,1,f_uc
tbdata,2,f_bc
tbdata,3,f_ut
tbdata,4,r_t
tbdata,5,D
tbdata,6,sigma_c_v
tbdata,7,R,gamma_t0,gamma_c0,beta_t,beta_c

TB, MPLA, MATID,,,NLOCAL
tbdata,1,c,m
```

Rebar- concrete connection

```
fini
/prep7

!UPGEOM,5,1,1,..\..\buckling2005,rst
!ALLSEL,ALL

CMSEL,S,Deck,ELEM
CMSEL,A,Bar,ELEM
NSLE,S,ALL
CPINTF,ALL,50

ALLSEL,ALL

fini
/solu
```

Extract solution from Eigenvalue buckling

```
/copy,file,rst,,..\..\buckling1000,rst
```

Import solution from Eigenvalue buckling to non-linear analyses

```
fini
/prep7
upgeom,0.1252,1,1,..\..\buckling326,rst     ! Multiplies "factor" by mode 1
displacement
fini
/solu
```

ACRONYMS, ABBREVIATIONS, AND SYMBOLS

Term	Description
AASHTO	American Association of State Highway and Transportation Officials
ft.	foot (feet)
in.	inch(es)
LADOTD	Louisiana Department of Transportation and Development
LTRC	Louisiana Transportation Research Center
LTB	Lateral torsional buckling
C_b	Moment gradient factor
L	Length of span
L_b	Unbraced length
RF	Rating factor
LRFD	Load and resistance factor design
MBE	Manual of bridge evaluation
DC	Dead load effect due to structural components and attachments
DW	Dead load effect due to wearing surface and utilities
LL	Live load effect
γ_{DW}	LRFD load factor for wearing surfaces and utilities
γ_P	LRFD load factor for permanent loads other than dead loads
γ_{LL}	Evaluation live load factor
R_n	Nominal member resistance
LADV	Louisiana Design Vehicle Live Load
F_{max}	Maximum potential compression-flange flexural resistance
F_{yr}	Compression-flange stress at the onset of nominal yielding within the cross section
F_{yc}	Specified minimum yield strength of a compression flange
L_r	Limiting unbraced length to achieve the onset of nominal yielding in either flange under uniform bending

Term	Description
L_p	Limiting unbraced length to achieve the nominal flexural resistance M_p under uniform bending
R_b	Web load-shedding factor
R_h	Hybrid factor
M_{max}	Maximum potential flexural resistance based on the compression flange
HL-93	LRFD design live load
F_{nc}	Nominal flexural resistance of a member
NRL	Notional Rating Load
F_y	Specified minimum yield strength of steel
FLB	Flange lateral buckling
f_1	stress without consideration of lateral bending at the brace point opposite to the one corresponding to f_2, calculated as the intercept of the most critical assumed linear stress variation passing through f_2 and either f_{mid} or f_0, whichever produces the smaller value of C_b
f_2	Largest compressive stress without consideration of lateral bending at either end of the unbraced length of the flange under consideration, calculated from the critical moment envelope value
f_0	Stress due to the factored loads without consideration of flange lateral bending at a brace point opposite to the one corresponding to f_2
M_A	Absolute value of moment at quarter point of the unbraced segment
M_B	Absolute value of moment at center of the unbraced segment
M_C	Absolute value of moment at three-quarter point of the unbraced segment
Mp	Plastic moment
Mu	Moment due to the factored loads
Mr	Factored flexural resistance
E_s	Elastic modulus of steel
E_c	Elastic modulus of concrete
Iy	Moment of inertia about the minor principal axis of the cross section
Ix	Moment of inertia about the major principal axis of the cross section

REFERENCES

1. AASHTO, 2020. *AASHTO LRFD Bridge Design Specifications*, Ninth Edition. Washington, D.C.

2. Ravindra, M.K. and Galambos, T.V., 1978. Load and Resistance Factor Design for Steel. *Journal of the Structural Division,* 104(9), pp.1337-1353.

3. Salvadori, M.G., 1955. Lateral Buckling of I-Beams. *Transactions of the American Society of Civil Engineers*, 120(1), pp. 1165-1177.

4. AISC, 2017. *Steel Construction Manual*, Fifteenth Edition. Chicago, IL.

5. Kirby, P.A. and Nethercot, D.A., 1979. *Design for Structural Stability*. Halsted Press.

6. CSA Canadian Standards Association, 2014. *Canadian Highway Bridge Design Code S6-14*.

7. Standards Australia (SA), 1998. *AS4100 Steel Structures*. Standards Australia, Sydney, Australia.

8. British Standards Institution (BSI), 2000. *BS5950-1 Structural Use of Steelwork in Buildings – Part1,* Code of Practice for Design Rolled and Welded Sections. England.

9. López, A., Yong, D.J. and Serna, M.A., 2006. Lateral-Torsional Buckling of Steel Beams: A General Expression for the Moment Gradient Factor. In *Stability and Ductility of Steel Structures.* (pp. 6-8).

10. Subramanian, L. and White, D.W., 2016. Reassessment of the Lateral Torsional Buckling Resistance of Rolled I-Section Members: Moment Gradient Tests. *Journal of Structural Engineering*, 143(4), pp. 04016203.

11. White, D.W., 2008. Unified Flexural Resistance Equations for Stability Design of Steel I-Section Members: Overview. *Journal of Structural Engineering*, 134(9), pp. 1405-1424.

12. White, D.W. and Jung, S.K., 2008. Unified Flexural Resistance Equations for Stability Design of Steel I-Section Members: Uniform Bending Tests. *Journal of Structural Engineering*, 134(9), pp. 1450-1470.

13. White, D.W. and Duk Kim, Y., 2008. Unified Flexural Resistance Equations for Stability Design of Steel I-Section Members: Moment Gradient Tests. *Journal of Structural Engineering*, 134(9), pp. 1471-1486.

14. Helwig, T.A., Frank, K.H. and Yura, J.A., 1997. Lateral-Torsional Buckling of Singly Symmetric I-Beams. *Journal of Structural Engineering*, 123(9), pp. 1172-1179.

15. Salvadori, M.G., 1956. Lateral Buckling of Eccentrically Loaded I-Columns. *Transactions of the American Society of Civil Engineers*, 121(1), pp. 1163-1178.

16. Wong, E. and Driver, R.G., 2010. Critical Evaluation of Equivalent Moment Factor Procedures for Laterally Unsupported Beams. *Engineering Journal*, 47(1), pp. 1.

17. Yura, J.A., 1995. Bracing for Stability—State-of-the-Art. In *Restructuring: America and Beyond*. (pp. 88-103). ASCE.

18. Yura, J.A. and Helwig, T.A., 2010. Buckling of Beams with Inflection Points. In *Proceedings, Annual Stability Conference 2010*.

19. Japan Society of Civil Engineers (JSCE), 2007. *Standard Specifications for Steel and Composite Structures*. Tokyo: JSCE.

20. Aydin, R., Gunaydin, A. and Kirac, N., 2015. On the Evaluation of Critical Lateral Buckling Loads of Prismatic Steel Beams. *Steel and Composite Structures*, 18(3), pp. 603-621.

21. Cheng, J.J.R., Yura, J.A. and Johnson, C.P., 1998. Lateral Buckling of Coped Steel Beams. *Journal of Structural Engineering*, 114(1), pp. 1-15.

22. Da Silva, L.S., Rebelo, C., Nethercot, D., Marques, L., Simões, R. and Real, P.V., 2009. Statistical Evaluation of the Lateral–Torsional Buckling Resistance of Steel I-Beams, Part 2: Variability of Steel Properties. *Journal of Constructional Steel Research*, 65(4), pp. 832-849.

23. Bui, H.C., 2009. Buckling Analysis of Thin-Walled Sections under General Loading Conditions. *Thin-Walled Structures*, 47(6), pp. 730-739.

24. Galambos, T.V., 1993. *Inelastic Rating Procedures for Steel Beam and Girder Bridges*, (Vol. 352). Transportation Research Board.

25. Galambos, T.V., 1998. *Guide to Stability Design Criteria for Metal Structures*. John Wiley & Sons.

26. Galambos, T.V. and Surovek, A.E., 2008. *Structural Stability of Steel: Concepts and Applications for Structural Engineers* (pp. 236-289). New York: John Wiley & Sons.

27. Geng-Shu, T. and Shao-Fan, C., 1988. Buckling of Laterally and Torsionally Braced Beams. *Journal of Constructional Steel Research*, 11(1), pp. 41-55.

28. Greiner, R., Ofner, R. and Salzgeber, G., 1999. Lateral Torsional Buckling of Beam–Columns: Theoretical Background. *ECCS-Validation Group, Report 5.*

29. Greiner, R. and Lindner, J., 1999. Proposal for Buckling Resistance of Members: Flexural and Lateral Torsional Buckling. *ECCS-Validation Group, Report 6.*

30. Gupta, P., Wang, S.T. and Blandford, G.E., 1996. Lateral-Torsional Buckling of Nonprismatic I-Beams. *Journal of Structural Engineering*, 122(7), pp. 748-755.

31. Kala, Z., Valeš, J. and Martinásek, J., 2017. Inelastic Finite Element Analysis of Lateral Buckling for Beam Structures. *Procedia Engineering*, 172, pp. 481-488.

32. Kitipornchai, S., Wang, C.M. and Trahair, N.S., 1986. Buckling of Monosymmetric I-Beams under Moment Gradient. *Journal of Structural Engineering*, 112(4), pp. 781-799.

33. Kubo, M. and Fukumoto, Y., 1988. Lateral-Torsional Buckling of Thin-Walled I-Beams. *Journal of Structural Engineering*, 114(4), pp. 841-855.

34. Kucukler, M., Gardner, L. and Macorini, L., (2015). Lateral–Torsional Buckling Assessment of Steel Beams through a Stiffness Reduction Method. *Journal of Constructional Steel Research*, 109, pp. 87-100.

35. Kucukler, M., Gardner, L. and Macorini, L., 2015. Flexural–Torsional Buckling Assessment of Steel Beam–Columns through a Stiffness Reduction Method. *Engineering Structures*, 101, pp. 662-676.

36. Kurniawan, C.W. and Mahendran, M., 2009. Lateral Buckling Strength of Simply Supported Litesteel Beams Subject to Moment Gradient Effects. *Journal of Structural Engineering*, 135(9), pp. 1058-1067.

37. Larue, B., Khelil, A. and Gueury, M., 2007. Elastic Flexural–Torsional Buckling of Steel Beams with Rigid and Continuous Lateral Restraints. *Journal of Constructional Steel Research*, 63(5), pp. 692-708.

38. Lim, N.H., Park, N.H., Kang, Y.J. and Sung, I.H., 2003. Elastic Buckling of I-Beams under Linear Moment Gradient. *International Journal of Solids and Structures*, 40(21), pp. 5635-5647.

39. Naderian, H.R. and Ronagh, H.R., 2015. Buckling Analysis of Thin-Walled Cold-Formed Steel Structural Members Using Complex Finite Strip Method. *Thin-Walled Structures*, 90, pp. 74-83.

40. Nguyen, N.D., Han, S.R., Lee, G.S. and Kang, Y.J., 2011. Moment Modification Factor of I-Girder with Trapezoidal-Web-Corrugations Considering Concentrated Load Height Effects. *Journal of Constructional Steel Research*, 67(11), pp. 1773-1787.

41. Park, J.S. and Kang, Y.J., 2003. Lateral Buckling of Beams with Top Bracing. *Structural Engineering and Mechanics*, 16(5), 2003, pp. 613-625.

42. Park, J.S., Stallings, J.M. and Kang, Y.J., 2004. Lateral–Torsional Buckling of Prismatic Beams with Continuous Top-Flange Bracing. *Journal of Constructional Steel Research*, 60(2), pp. 147-160.

43. Park, N.H., Kang, Y.J., Jo, Y.M. and Lim, N.H., 2007. Modification of C-Equation in the SSRC Guide for Buckling of Monosymmetric I-Beams under Transverse Loads. *Engineering Structures*, 29(12), pp. 3293-3300.

44. Ronagh, H.R. and Bradford, M.A., 1994. Some Notes on Finite Element Buckling Formulations for Beams. *Computers & Structures*, 52(6), pp. 1119-1126.

45. Serna, M.A., López, A., Puente, I. and Yong, D.J., 2006. Equivalent Uniform Moment Factors for Lateral–Torsional Buckling of Steel Members. *Journal of Constructional Steel Research*, 62(6), pp. 566-580.

46. Subramanian, L. and White, D.W., 2016. Reassessment of the Lateral Torsional Buckling Resistance of I-Section Members Uniform-Moment Studies. Journal of Structural Engineering, 143(3), pp. 04016194.

47. Subramanian, L., Jeong, W.Y., Yellepeddi, R. and White, D.W., 2018. Assessment of I-Section Member LTB Resistances Considering Experimental Test Data and Practical Inelastic Buckling Design Calculations. *Engineering Journal-American Institute of Steel Construction*, 55(1), pp. 15-44.

48. Suryoatmono, B. and Ho, D., 2002. The Moment–Gradient Factor in Lateral–Torsional Buckling on Wide Flange Steel Sections. *Journal of Constructional Steel Research*, 58(9), pp. 1247-1264.

49. Trahair, N.S., 1996. Laterally Unsupported Beams. *Engineering Structures*, 18(10), pp. 759-768.

50. Trahair, N.S. and Hancock, G.J., 2004. Steel Member Strength by Inelastic Lateral Buckling. *Journal of Structural Engineering*, 130(1), pp. 64-69.

51. White, D.W., Jeong, W.Y. and Toğay, O., 2016. Comprehensive Stability Design of Planar Steel Members and Framing Systems via Inelastic Buckling Analysis. *International Journal of Steel Structures*, 16(4), pp. 1029-1042.

52. Yura, J.A. and Widianto, J.A., 2005, April. Lateral buckling and bracing of beams—A Re-evaluation after the Marcy Bridge Collapse. In *Structural Stability Research Council-2005 Annual Stability Conference, Apr 6-9 2005* (pp. 277-294).

53. Yura, J., Helwig, T., Herman, R. and Zhou, C., 2008. Global Lateral Buckling of I-Shaped Girder Systems. *Journal of Structural Engineering*, 134(9), pp. 1487-1494.

54. Yura, J.A., Phillips, B., Raju, S. and Webb, S., 1992. *Bracing of Steel Beams in Bridges*. Interior for Transportation Research. The University of Texas at Austin.

55. Yura, J.A., 2001. Fundamentals of Beam Bracing. *Engineering Journal-American Institute of Steel Construction*, 38(1). pp. 11-26.

56. Vegesna, S. and Yura, J.A., 1992. *An Ultimate Load Test to Study Bracing Effects of Bridge Decks*. Interior for Transportation Research, University of Texas.

57. Kissane, R.J., 1985. *Lateral Restraint of Non-composite Beams*. New York State Department of Transportation, Engineering Research and Development Bureau.

58. Linzell, D., Nevling, D., Kollias, A. and Laman, J., 2002. Experimental and Numerical Response of a 1915 Riveted Through-Girder Bridge. *Transportation Research Record: Journal of the Transportation Research Board*, 1814, pp. 127-134.

59. Ziemian, R.D., 2010. *Guide to Stability Design Criteria for Metal Structures*. 6th Edition. John Wiley & Sons.

60. Timoshenko, S.P. and Gere, J.M., 1961.*Theory of Elastic Stability*. McGraw Hill, Newyork.

61. Mottram, J.T., 1992. Lateral-Torsional Buckling of Thin-Walled Composite I-Beams by the Finite Difference Method. *Composites Engineering*, 2(2), pp.91-104.

62. Suryoatmono, B. and Ho, D., 2002. The Moment–Gradient Factor in Lateral–Torsional Buckling on Wide Flange Steel Sections. *Journal of Constructional Steel Research*, 58(9), pp.1247-1264.

63. Chen, W.F. and Lui, E.M., 1987. *Structural Stability: Theory and Implementation*. Elscvier Science Publishing Co. Inc, Newyork.

64. Nethercot, D.A., K. C. Rockey K.C., 1971. A Unified Approach to the Elastic Lateral Buckling of Beams. *The Structural Engineer*, 49(7).

65. Kamiński, M. and Supeł, Ł., 2016. Elastic Critical Moment for Bisymmetric Steel Profiles and its Sensitivity by the Finite Difference Method. *International Journal of Applied Mechanics and Engineering*, 21(1).

66. MatLab R2019a, MathWorks Inc, Las Vegas, NV.

67. Sun C., Linzell D., Puckett J., 2020. *Load Rating of Existing Continuous Stringers on Louisiana's Bridges*. (No. FHWA/LA.19/XXX) United States. Federal Highway Administration.

68. Khelil, A. and Larue, B., 2008. Simple Solutions for the Flexural-Torsional Buckling of Laterally Restrained I-Beams. *Engineering structures*, 30(10), pp.2923-2934.

69. Durant, N.J., 1944. XCVII. An Application of the Method of Finite Difference Equations to A Problem of Bending Moments.(Continuous Beam of N Equal Spans under Uniform Loading.). *The London, Edinburgh, And Dublin Philosophical Magazine and Journal of Science*, 35(251), pp.848-850.

70. Wirianto, F., 1979. *Finite Difference Analysis of Two-span Continuous Composite Beams* (Doctoral Dissertation). McMaster University.

71. Balázs, I. and Melcher, J., 2015. Stability of Thin-Walled Beams with Lateral Continuous Restraint. *Transactions of the VŠB–Technical University of Ostrava, Civil Engineering Series*., 15(1), pp.1-10.

72. Ansys R19, Ansys Inc, Canonsburg, PA.

73. Ekström, C.M. and Wesley, D., 2017. *Lateral-torsional Buckling of Steel Channel Beams* (Master's Thesis). Chalmers University of Technology.

74. Sun C., Linzell D., Puckett J, Rageh, A., Babarinde, T., Kuruppuarachchi, D., 2021. Experimental Study of Stringer Lateral Torsional Resistance Using A Grillage System. In *SSRC Annual Stability Conference 2021*.

75. AASHTOWare Bridge Rating (BrR) 6.8.4.3001, Washington, DC.